Chapter 14
Conformal Field Theory Applied to Loop Models

Jesper Lykke Jacobsen

14.1 Introduction

The application of methods of quantum field theory to problems of statistical mechanics can in some sense be traced back to Onsager's 1944 solution [1] of the two-dimensional Ising model. It does however appear fair to state that the 1970's witnessed a real gain of momentum for this approach, when Wilson's ideas on scale invariance [2] were applied to study critical phenomena, in the form of the celebrated renormalisation group [3]. In particular, the so-called ε expansion permitted the systematic calculation of critical exponents [4], as formal power series in the space dimensionality d, below the upper critical dimension d_c. An important lesson of these efforts was that critical exponents often do not depend on the precise details of the microscopic interactions, leading to the notion of a restricted number of distinct universality classes.

Meanwhile, further exact knowledge on two-dimensional models had appeared with Lieb's 1967 solution [5] of the six-vertex model and Baxter's subsequent 1971 generalisation [6] to the eight-vertex model. These solutions challenged the notion of universality class, since they provided examples of situations where the critical exponents depend continuously on the parameters of the underlying lattice model. On the other hand, the techniques of integrability used relied crucially on certain exact microscopic conservation laws, thus placing important restrictions on the models which could be thus solved.

An important break-through occurred in 1984 when Belavin, Polyakov and Zamolodchikov [7] applied ideas of conformal invariance to classify the possible types of critical behaviour in two dimensions. These ideas had emerged earlier in string theory and mathematics, and in fact go back to earlier (1970) work of Polyakov [8] in which global conformal invariance is used to constrain the form of correlation functions in d-dimensional theories. It is however only by imposing

Jesper Lykke Jacobsen
Laboratoire de Physique Théorique, École Normale Supérieure (LPTENS), 24 rue Lhomond, 75231 Paris Cedex 05, France, e-mail: jesper.jacobsen@ens.fr

local conformal invariance in $d = 2$ that this approach becomes really powerful. In particular, it immediately permitted a full classification of an infinite family of conformally invariant theories (the so-called "minimal models") having a finite number of fundamental ("primary") fields, and the exact computation of the corresponding critical exponents. In the aftermath of these developments, conformal field theory (CFT) became for some years one of the most hectic research fields of theoretical physics, and indeed has remained a very active area up to this date.

Despite the amazing classification powers of CFT, it remains a tricky question to make the link between a given critical lattice model and the corresponding CFT. This is particularly true for geometrically defined models, such as percolation and self-avoiding polygons (SAP) and walks (SAW), since then typically the usual assumptions of minimality and unitarity (roughly speaking, positive definite Boltzmann weights) fail. Such models are however well treated by the so-called Coulomb gas (CG) approach, in which the geometric degrees of freedom are directly identified with the level lines of one or more free bosonic "height" fields. This approach preceded [9, 10, 11] the break-through of CFT, but shortly thereafter it was used (in a more formal and less geometrically inspired form) for the extensive computation of correlation functions in minimal models by Dotsenko and Fateev [12, 13]. A large number of applications in polymer physics was developed by Duplantier and Saleur [14].

The goal of this chapter is to present the application of CFT—with special emphasis on the CG approach—to two-dimensional models of self-avoiding loops, each loop occurring with a fugacity n. Self-avoiding polygons and walks then appear as special cases in the limit $n \to 0$. In section 14.2 we outline the key concepts of CFT. The aim is to make the presentation self-contained while remaining rather brief; the reader interested in more details should turn to the comprehensive textbook [15] or the Les Houches volume [16]. The geometric CG approach is introduced in section 14.3, and is shown to lead to a CFT of the Liouville type. The presence of screening charges is linked to a marginality requirement [17, 18] that ensures the exact solvability of the model.

The CG approach is subsequently applied in section 14.4 to the computation of bulk critical properties of SAP's and SAW's. It should be emphasised that most of the material is presented within the general framework of loop models, taking the SAP limit ($n \to 0$) only at the end of the computations. SAW's are then obtained by inserting appropriate defects before taking the limit. There are good reasons for this manner of presentation: first, more general results are obtained at no extra expense; second, a number of general concepts emerge more clearly; and third, the example of the Θ-point collapse transition [19] shows that also $n \neq 0$ is of relevance to polymer problems. In fact, loop models furnish a nice illustration of most of the key concepts of two-dimensional CFT.

While section 14.3 focuses on loop models with a scalar height field, equivalent to the standard O(n) and Q-state Potts models (with $n = \sqrt{Q}$), a new class of loop models with vectorial target spaces is introduced in section 14.5. In these models, first solved by Kondev and collaborators [20, 17, 21], the loops are fully packed on the lattice, and become Hamiltonian circuits or walks in the $n \to 0$ limit.

In sections 14.6–14.7 we illustrate the importance of the topology of the space in which the loops are embedded. The preceding discussion in fact pertained to the geometry of the (punctured) plane. In contrast, section 14.6 is devoted to the half-plane geometry, in which the loops undergo specific interactions with the surface. The appropriate theoretical setup is that of boundary CFT, a subject pioneered by Cardy [22]. Finally, in section 14.7 the loops are embedded in a torus and the fundamental requirement of modular invariance [23] is exploited to write down modular invariant partition functions in the continuum limit. Using a similar approach, exact continuum limit partition functions are written down in the annulus geometry as well.

14.2 Basic Concepts of CFT

14.2.1 Global Conformal Invariance

A conformal transformation in d dimensions is an invertible mapping $\mathbf{x} \to \mathbf{x}'$ which multiplies the metric tensor $g_{\mu\nu}(\mathbf{x})$ by a space-dependent scale factor:

$$g'_{\mu\nu}(\mathbf{x}') = \Lambda(\mathbf{x}) g_{\mu\nu}(\mathbf{x}). \tag{14.1}$$

Note that such a mapping preserves angles. Therefore, just as Wilson [2] suggested using *global* scale invariance as the starting point for investigating a system at its critical point, Polyakov [8] proposed imposing the *local* scale invariance (14.1) as the fundamental requirement for studying a critical system in which the microscopic interactions are short ranged. A priori, a geometrical model of self-avoiding objects such as SAP's and SAW's does not seem to be governed by short-range interactions; that this is nevertheless true will be shown in section 14.3.2 where we shall make explicit the locality of such models.

The group of conformal transformations is easily shown to be generated by translations, dilations, rotations, and the so-called special conformal transformations (which are just the composition of an inversion $x^\mu \to x^\mu/\mathbf{x}^2$, a translation, and another inversion). Writing down the commutation rules of the generators, one establishes that the conformal group is isomorphic to the pseudo-orthogonal group $\mathrm{SO}(d+1,1)$ with $\frac{1}{2}(d+1)(d+2)$ real parameters.

The connection between a statistical mechanics model and quantum field theory is made as usual by writing the partition function and correlation functions of the former as functional integrals in the latter:

$$\begin{aligned} Z &= \int \mathscr{D}\boldsymbol{\Phi}\, \mathrm{e}^{-S[\boldsymbol{\Phi}]} \\ \langle \phi_1(\mathbf{x}_1) \dots \phi_k(\mathbf{x}_k) \rangle &= Z^{-1} \int \mathscr{D}\boldsymbol{\Phi}\, \phi_1(\mathbf{x}_1) \dots \phi_k(\mathbf{x}_k) \mathrm{e}^{-S[\boldsymbol{\Phi}]} \end{aligned} \tag{14.2}$$

Here $S[\Phi]$ is the euclidean action, Φ the collection of fields, and $\phi_i \in \Phi$. In other words, $Z^{-1}\mathrm{e}^{-S[\Phi]}\mathscr{D}\Phi$ is the Gibbs measure in the continuum limit. Paradoxically, in many cases the hypothesis of conformal invariance may permit one to classify and precisely characterise the possible continuum theories without ever having to write down explicitly the action $S[\Phi]$.

A field $\phi(\mathbf{x})$, here supposed spinless for simplicity, is called *quasi-primary* provided it transforms covariantly under the conformal transformation (14.1):

$$\phi(\mathbf{x}) \to \phi'(\mathbf{x}') = \left|\frac{\partial \mathbf{x}'}{\partial \mathbf{x}}\right|^{-\Delta/d} \phi(\mathbf{x}). \tag{14.3}$$

The number $\Delta = \Delta_\phi$ is a property of the field and is called its *scaling dimension*. Using this, conformal invariance completely fixes [8] the form of the two- and three-point correlation functions:

$$\langle \phi_1(\mathbf{x}_1)\phi_2(\mathbf{x}_2)\rangle = \frac{\delta_{\Delta_1,\Delta_2}}{x_{12}^{2\Delta_1}}, \tag{14.4}$$

$$\langle \phi_1(\mathbf{x}_1)\phi_2(\mathbf{x}_2)\phi_3(\mathbf{x}_3)\rangle = \frac{C_{123}}{x_{12}^{\Delta_1+\Delta_2-\Delta_3} x_{23}^{\Delta_2+\Delta_3-\Delta_1} x_{31}^{\Delta_3+\Delta_1-\Delta_2}} \tag{14.5}$$

where we have introduced $x_{ij} = |\mathbf{x}_i - \mathbf{x}_j|$. The fields have here been normalised so that the coefficient in (14.4) is unity. The structure constants C_{123} appearing in (14.5) are then fundamental dynamical quantities characterising the theory at hand. With four or more points, the correlation functions are no longer completely fixed, due to the existence of conformally invariant functions of four points, $\eta = x_{12}x_{34}/x_{13}x_{24}$, the so-called *anharmonic ratios*.

14.2.2 Two Dimensions and Local Conformal Invariance

Conformal invariance is especially powerful in two dimensions for reasons that we shall expose presently. For the moment, we work in the geometry of the Riemann sphere, i.e., the plane with a point at infinity, and we shall write the coordinates as $\mathbf{x} = (x^1, x^2)$. Under a general coordinate transformation $x^\mu \to x'^\mu = w^\mu(x^1, x^2)$ application of (14.1) implies the Cauchy-Riemann equations, $\partial w^2/\partial x^1 = \pm\partial w^1/\partial x^2$ and $\partial w^1/\partial x^1 = \mp\partial w^2/\partial x^2$, i.e., $\mathbf{w}(\mathbf{x})$ is either a holomorphic or an antiholomorphic function. Important simplifications will therefore result upon introducing the complex coordinates $z \equiv x^1 + ix^2$ and $\bar{z} \equiv x^1 - ix^2$. A conformal mapping then reads simply $z \to z' = w(z)$.

The identification of two-dimensional conformal transformations with analytic maps $w(z)$ could have been anticipated from the well-known fact that the latter are angle-preserving. It should be noted that an analytic map is defined (via its Laurent series) by an *infinite* number of parameters. This does not contradict the result of section 14.2.1 that the set of global conformal transformations is defined by only

$\frac{1}{2}(d+1)(d+2) = 6$ real parameters, since analytic maps are not necessarily invertible and defined in the whole complex plane. Global conformal transformations in $d = 2$ take the form of the projective transformations

$$w(z) = \frac{a_{11}z + a_{12}}{a_{21}z + a_{22}} \tag{14.6}$$

with $a_{ij} \in \mathbb{C}$ and the constraint $\det a_{ij} = 1$, i.e., they form the group $\mathrm{SL}(2,\mathbb{C}) \simeq \mathrm{SO}(3,1)$.

In complex coordinates, the transformation law (14.3) becomes

$$\phi'(w,\bar{w}) = \left(\frac{\mathrm{d}w}{\mathrm{d}z}\right)^{-h} \left(\frac{\mathrm{d}\bar{w}}{\mathrm{d}\bar{z}}\right)^{-\bar{h}} \phi(z,\bar{z}) \tag{14.7}$$

where the *real* parameters $(h,\bar{h})$ are called the *conformal weights*. The combinations $\Delta = h + \bar{h}$ and $s = h - \bar{h}$ are called respectively the scaling dimension and the spin of ϕ. A field ϕ satisfying (14.7) for any projective transformation (resp. any analytic map) $w(z)$ is called quasi-primary (resp. primary). An example of a quasi-primary field which is not primary is furnished by the stress tensor (see below).

The expressions (14.4)–(14.5) for the two- and three-point correlation functions still hold true with the obvious modification that the dependence in $z_{ij} \equiv z_i - z_j$ (resp. in $\bar{z}_{ij}$) goes with the conformal weights h (resp. $\bar{h}$).

14.2.3 Stress Tensor and Ward Identities

The stress tensor $T^{\mu\nu}$ is the conserved Noether current associated with the conformal symmetry. It can be defined[1] as the response of the partition function to a local change in the metric:

$$T^{\mu\nu}(\mathbf{x}) = -\frac{1}{2\pi} \frac{\delta \log Z}{\delta g_{\mu\nu}(\mathbf{x})} \tag{14.8}$$

Translational and rotational invariances imply the conservation law $\partial_\mu T^{\mu\nu} = 0$ as well as the symmetry $T^{\mu\nu} = T^{\nu\mu}$. Scale invariance further implies the tracelessness $T^{\mu}_{\mu} = 0$; in general the trace would be proportional to the beta function, which vanishes at a renormalisation group fixed point.

Rewriting this in complex coordinates, one finds that $T_{z\bar{z}} = T_{\bar{z}z} = 0$, while the conservation law takes the form $\partial_{\bar{z}} T(z) = \partial_z \bar{T}(\bar{z})$, where we have defined $T(z) \equiv T_{zz}$ and $\bar{T}(\bar{z}) \equiv T_{\bar{z}\bar{z}}$. So $T(z)$ is analytic, while $\bar{T}(\bar{z})$ is antianalytic. This is a very important element in the solvability of two-dimensional CFT. Following Fateev and Zamolodchikov [24] it is even possible to go (much) further: CFT's in which the conformal symmetry is enhanced with other, so-called extended, symmetries (superconformal, parafermionic, W algebra,...) can be constructed by requiring more

[1] Note the analogy with the theory of integrable systems, where the conserved charges are obtained as derivatives of the transfer matrix with respect to the anisotropy (spectral parameter).

analytic currents and making them coexist with $T(z)$ by imposing certain associativity requirements.

Consider now the change in the metric induced by an infinitesimal conformal transformation $z' = z + \varepsilon(z)$. Its effects on an arbitrary product of primary fields $X = \prod_j \phi_j(z_j, \bar{z}_j)$ can be written in terms of $T(z)$ as

$$\oint_C \langle T(z)X \rangle \varepsilon(z)\, \mathrm{d}z = \sum_j \left(h_j \varepsilon'(z_j) + \varepsilon(z_j)\partial_{z_j} \right) \langle X \rangle, \tag{14.9}$$

where C is any counterclockwise contour encircling $\{z_j\}$. This is called the *conformal Ward identity*. By the Cauchy theorem, this is equivalent to

$$T(z)\phi_j(z_j,\bar{z}_j) = \frac{h_j}{(z-z_j)^2}\phi_j(z_j,\bar{z}_j) + \frac{1}{z-z_j}\,\partial_{z_j}\phi(z_j,\bar{z}_j) + \mathscr{O}(1)\,. \tag{14.10}$$

This is our first example of an *operator product expansion* (OPE), i.e., a formal power series in the coordinate difference that expresses the effect of bringing close together two operators. Several remarks are in order. First, it is tacitly understood that OPE's only have a sense when placed between the brackets $\langle \cdots \rangle$ of a correlation function. Second, we generically expect singularities to arise when approaching two local operators in a quantum field theory; in particular the average of a field over some small volume will have a variance that diverges when that volume is taken to zero. Third, an OPE should be considered an exact identity rather than an approximation, provided the formal expansion is written out to arbitrarily high order. In our example, (14.9) only determines the first two terms in the OPE (14.10). Fourth, contracting any field ϕ with $T(z)$ and comparing with (14.10) is actually a useful practical means of determining its primarity and its conformal dimension h_ϕ.

It is not difficult to see from (14.8) that on dimensional grounds T itself is a quasi-primary field of conformal dimension $h = 2$. However, the average $\langle T(z_1)T(z_2)\rangle \sim (z_1 - z_2)^{-4}$ has no reason to vanish, and so the OPE of T with itself takes the form

$$T(z_1)T(z_2) = \frac{c/2}{(z_1-z_2)^4} + \frac{2T(z_2)}{(z_1-z_2)^2} + \frac{\partial T(z_2)}{z_1-z_2} + \mathscr{O}(1). \tag{14.11}$$

In particular, T is *not* primary. The constant c appearing in (14.11) is called the *central charge*. Considering two non-interacting CFT's as a whole, one has from (14.8) that their stress tensors, and hence their central charges, add up, and so c can be considered as a measure of the number of quantum degrees of liberty in the CFT. It is straightforward to establish that $c = 1/2$ for a free fermion and $c = 1$ for a free boson. We shall see later that standard SAP's have $c = 0$.

As T is not primary, it cannot transform like (14.7) under a finite conformal transformation $z \to w(z)$. We can always write the modified transformation law as

$$T'(w) = \left(\frac{\mathrm{d}w}{\mathrm{d}z}\right)^{-2} \left[T(z) - \frac{c}{12}\{w;z\} \right]. \tag{14.12}$$

To determine what $\{w;z\}$ represents, we use the constraint due to two successive applications of (14.12) and the fact that $\{w;z\} = 0$ for projective conformal transformations, since T is quasi-primary. The result is that $\{w;z\}$ is the Schwarzian derivative

$$\{w;z\} = \frac{\mathrm{d}^3 w/\mathrm{d}z^3}{\mathrm{d}w/\mathrm{d}z} - \frac{3}{2}\left(\frac{\mathrm{d}^2 w/\mathrm{d}z^2}{\mathrm{d}w/\mathrm{d}z}\right)^2. \tag{14.13}$$

14.2.4 Finite-Size Scaling on a Cylinder

The central charge c is ubiquitous in situations where the CFT is placed in a finite geometry, i.e., interacts with some boundary condition. An important example is furnished by conformally mapping the plane to a cylinder of circumference L by means of the transformation

$$w(z) = \frac{L}{2\pi}\log z. \tag{14.14}$$

This transformation can be visualised by viewing the cylinder in perspective, with one rim contracting to the origin and the other expanding to form the point at infinity. Taking the expectation value of (14.12), and using the fact that $\langle T(z)\rangle = 0$ in the plane on symmetry grounds, one finds that $\langle T(w)\rangle = -\pi^2 c/6L^2$ on the cylinder. Applying (14.8) then implies that the free energy per unit area $f_0(L)$ satisfies [25]

$$f_0(L) = f_0(\infty) - \frac{\pi c}{6L^2} + o(L^{-2}). \tag{14.15}$$

This is a very useful result for obtaining c for a concrete statistical model, since $f(L)$ can usually be determined from the corresponding transfer matrix, either numerically for small L by using exact diagonalisation techniques, or analytically in the Bethe Ansatz context by using the Euler-McLauren formula.

It is also of interest to study such finite-size effects on the level of the two-point correlation function of a primary field ϕ. Again using the mapping (14.14), the covariance property (14.7) and the form (14.4) of the correlator in the plane can be used to deduce its form on the cylinder. Assuming for simplicity $h = \bar{h} = \Delta/2$, and writing the coordinates on the cylinder as $w = t + ix$, with $t \in \mathbb{R}$ and $x \in [0,L)$, one arrives at

$$\langle \phi(t_1,x_1)\phi(t_2,x_2)\rangle = \left(\frac{2\pi}{L}\right)^{2\Delta}\left[2\cosh\left(\frac{2\pi t_{12}}{L}\right) - 2\cos\left(\frac{2\pi x_{12}}{L}\right)\right]^{-\Delta}, \tag{14.16}$$

where $t_{12} = t_1 - t_2$ and $x_{12} = x_1 - x_2$. In the limit of a large separation of the fields, $t_{12} \to \infty$, this decays like $\mathrm{e}^{-t_{12}/\xi}$ with correlation length $\xi = L/2\pi\Delta$. But this decay can also be written $(\Lambda_\phi/\Lambda_0)^{-t_{12}}$, where Λ_0 is the largest eigenvalue of the transfer matrix, and Λ_ϕ is the largest eigenvalue compatible with the constraint that an operator ϕ has been inserted at each extremity $t = \pm\infty$ of the cylinder. Denoting the corresponding free energies per unit area $f(L) = -L^{-1}\log\Lambda$, we conclude that [26]

$$f_\phi(L) - f_0(L) = \frac{2\pi\Delta}{L^2} + o(L^{-2})\,. \tag{14.17}$$

This is as useful as (14.15) in (numerical or analytical) transfer matrix studies, since the constraint imposed by ϕ can usually be related explicitly to properties of the transfer matrix spectrum.

14.2.5 Virasoro Algebra and Its Representation Theory

Up to this point, we have worked in a setup where the fields were seen as functionals of the complex coordinates z, $\bar{z}$. To obtain an operator formalism, one must impose a quantisation scheme, i.e., single out a time and a space direction. The transfer matrix then propagates the system from one time slice to the following and is written as the exponential of the Hamiltonian $\mathscr{H}$, i.e., the energy operator on a fixed-time surface. In the continuum limit, one may freely choose the time direction. In CFT this is most conveniently done by giving full honours to the scale invariance of the theory, viz., by using for $\mathscr{H}$ the dilatation operator (to be precise, $\mathscr{H} = (2\pi/L)(L_0 + \bar{L}_0 - c/12)$)

$$\mathscr{D} = \frac{1}{2\pi i}\oint_C z\,T(z)\,\mathrm{d}z - \frac{1}{2\pi i}\oint_C \bar{z}\,\bar{T}(\bar{z})\,\mathrm{d}\bar{z} = L_0 + \bar{L}_0\,, \tag{14.18}$$

where C is a counterclockwise contour enclosing the origin. This is called the *radial quantisation* scheme: the constant-time surfaces are concentric circles around the origin. Under the map (14.14) the time becomes simply the coordinate along the cylinder axis. The usual time ordering of operators then becomes a prescription of radial ordering.

In (14.18) we have anticipated the definition of the mode operators

$$L_n = \frac{1}{2\pi i}\oint_C z^{n+1}T(z)\,\mathrm{d}z, \qquad \bar{L}_n = \frac{1}{2\pi i}\oint_C \bar{z}^{n+1}\bar{T}(\bar{z})\,\mathrm{d}\bar{z}. \tag{14.19}$$

Using the radial ordering, the OPE (14.11) becomes, after a deformation of contours, the commutation relations

$$[L_n, L_m] = (n-m)L_{n+m} + \frac{c}{12}n(n^2-1)\delta_{n+m,0} \tag{14.20}$$

with a similar expression for $[\bar{L}_n, \bar{L}_m]$, whereas $[L_n, \bar{L}_m] = 0$. The algebra defined by (14.20) is called the *Virasoro algebra*. Importantly, the decoupling into two isomorphic Virasoro algebras, one for L_n and another for $\bar{L}_n$, means that in the geometry chosen we can focus exclusively on L_n. It should be stressed that in the geometry of a torus, the two algebras couple non-trivially, in a way that is revealed by imposing modular invariance (see section 14.2.7 below).

We now describe the structure of the Hilbert space in radial quantisation. The vacuum state $|0\rangle$ must be invariant under projective transformations, whence $L_{\pm1}|0\rangle = 0$, and we fix the ground state energy by $L_0|0\rangle = 0$. Non-trivial eigenstates of $\mathscr{H}$ are

created by action with a primary field, $|h,\bar{h}\rangle = \phi(0,0)|0\rangle$. Translating (14.10) into operator language implies then in particular $L_0|h,\bar{h}\rangle = h|h,\bar{h}\rangle$. We must also impose the highest-weight condition $L_n|h,\bar{h}\rangle = \bar{L}_n|h,\bar{h}\rangle = 0$ for $n > 0$. Excited states with respect to the primary ϕ then read

$$\phi^{\{n,\bar{n}\}} \equiv L_{-n_1}L_{-n_2}\cdots L_{-n_k}\bar{L}_{-\bar{n}_1}\bar{L}_{-\bar{n}_2}\cdots\bar{L}_{-\bar{n}_{\bar{k}}}|h,\bar{h}\rangle \tag{14.21}$$

with $1 \le n_1 \le n_2 \le \cdots \le n_k$ and similarly for $\{\bar{n}\}$. These states are called the *descendents* of ϕ at level $\{N,\bar{N}\}$, where $N = \sum_{i=1}^{k} n_i$. A primary state and its descendents form a highest weight representation (or Verma module) of the Virasoro algebra.

Correlation functions of descendent fields can be obtained by acting with appropriate differential operators on the correlation functions of the corresponding primary fields. To see this, consider first for $n \ge 1$ the descendent $\big(L_{-n}\phi\big)(w)$ of the primary field $\phi(w)$, and let $X = \prod_j \phi_j(w_j)$ be an arbitrary product of other primaries as in the conformal Ward identity (14.9). Using (14.19) and (14.10) we have then

$$\begin{aligned}\big\langle \big(L_{-n}\phi\big)(w)X\big\rangle &= \frac{1}{2\pi i}\oint_z \mathrm{d}z\,(z-w)^{1-n}\,\langle T(z)\phi(w)X\rangle \qquad (14.22)\\ &= -\frac{1}{2\pi i}\oint_{\{w_j\}} \mathrm{d}z\,(z-w)^{1-n}\sum_j\left\{\frac{\partial_{w_j}}{z-w_j}+\frac{h_j}{(z-w_j)^2}\right\}\langle\phi(w)X\rangle\end{aligned}$$

where the minus sign comes from turning the integration contour inside out, so that it surrounds all the points $\{w_j\}$. In other words, a descendent in a correlation function may be replaced by the corresponding primary

$$\big\langle \big(L_{-n}\phi\big)(w)X\big\rangle = \mathscr{L}_{-n}\,\langle\phi(w)X\rangle \tag{14.23}$$

provided that we act instead on the correlator with the linear differential operator

$$\mathscr{L}_{-n} \equiv \sum_j\left\{\frac{(n-1)h_j}{(w_j-w)^n}-\frac{\partial_{w_j}}{(w_j-w)^{n-1}}\right\} \tag{14.24}$$

It is readily seen that a general descendent (14.21) is similarly dealt with by replacing each factor L_{-n_i} by the corresponding factor of $\mathscr{L}_{-n_i}$ in (14.23).

We can now write the general form of the OPE of two primary fields ϕ_1 and ϕ_2. It reads

$$\phi_1(z,\bar{z})\phi_2(0,0) = \sum_p C_{12p}\sum_{\{n,\bar{n}\}\cup\{\emptyset,\emptyset\}} C_{12p}^{\{n,\bar{n}\}}\,z^{h_p-h_1-h_2+N}\bar{z}^{\bar{h}_p-\bar{h}_1-\bar{h}_2+\bar{N}}\phi_p^{\{n,\bar{n}\}}(0,0)\,, \tag{14.25}$$

where the summation is over a certain set of primaries $\phi_p \equiv \phi_p^{\{\emptyset,\emptyset\}}$ as well as their descendents. The coefficients $C_{12p}^{\{n,\bar{n}\}}$ (we have set $C_{12p}^{\{\emptyset,\emptyset\}} = 1$) can be determined by acting with all combinations of positive-index mode operators on both sides of (14.25) and solving the resulting set of linear equations. In contradistinction, the coefficients C_{12p} are fundamental quantities, easily shown to coincide with those appearing in the three-point functions (14.5). They can be computed by the so-called

conformal bootstrap method, i.e., by assuming crossing symmetry of the four-point functions.

14.2.6 Minimal Models

Denote by $\mathscr{V}(c,h)$ the highest weight representation (Verma module) generated by the mode operators $\{L_n\}$ acting on a highest weight state $|h\rangle$ in a CFT of central charge c. The Hilbert space of the CFT can then be written

$$\bigoplus_{h,\bar{h}} n_{h,\bar{h}} \mathscr{V}(c,h) \otimes \mathscr{V}(c,\bar{h}) \tag{14.26}$$

where the multiplicities $n_{h,\bar{h}}$ indicate the number of distinct primaries of conformal weights $(h,\bar{h})$ that are present in the theory. A *minimal model* is a CFT for which the sum in (14.26) is finite.

The Hermitian conjugate of a mode operator is defined by $L_n^\dagger = L_{-n}$; this induces an inner product on the Verma module. The *character* $\chi_{(c,h)}$ of the module $\mathscr{V}(c,h)$ can then be defined as

$$\chi_{(c,h)}(\tau) = \mathrm{Tr}\, q^{L_0 - c/24}, \tag{14.27}$$

where $\tau \in \mathbb{C}$ is the so-called *modular parameter* (see section 14.2.7 below) and $q = \mathrm{e}^{2\pi i \tau}$. Since the number of descendents of $|h\rangle$ at level N is just the number $p(N)$ of integer partitions of N, cf. (14.21), we have simply

$$\chi_{(c,h)}(\tau) = \frac{q^{h-c/24}}{P(q)}, \tag{14.28}$$

where

$$\frac{1}{P(q)} \equiv \prod_{n=1}^{\infty} \frac{1}{1-q^n} = \sum_{n=0}^{\infty} p(n) q^n \tag{14.29}$$

is the generating function of partition numbers; this is also often expressed in terms of the Dedekind function

$$\eta(\tau) = q^{1/24} P(q). \tag{14.30}$$

However, the generic Verma module is not necessarily irreducible, so further work is needed.

For certain values of h, it may happen that a specific linear combination $|\chi\rangle$ of the descendents of $|h\rangle$ at level N is itself primary, i.e., $L_n|\chi\rangle = 0$ for $n > 0$. In other words, $|\chi\rangle$ is primary and descendent at the same time, and it generates its own Verma module $\mathscr{V}_\chi(c,h) \subset \mathscr{V}(c,h)$. One easily shows that the states in $\mathscr{V}_\chi(c,h)$ are orthogonal to those in $\mathscr{V}(c,h)$, and so in particular they have zero norm. A Verma module $\mathscr{V}(c,h)$ containing one or more such *null fields* $|\chi\rangle$ is called reducible, and can be turned into an irreducible Verma module $\mathscr{M}(c,h)$ by quotienting out the null fields, i.e., by setting $|\chi\rangle = 0$. The Hilbert space is then given by (14.26) with $\mathscr{V}$

replaced by $\mathscr{M}$; since it contains fewer states the corresponding characters (14.27) are *not* given by the simple result (14.28).

The concept of null states is instrumental in constructing *unitary* representations of the Virasoro algebra (14.20), i.e., representations in which no state of *negative* norm occurs. An important first step is the calculation of the Kac determinant $\det M^{(N)}$ of inner products between descendents at level N. Its roots can be expressed through the following parameterisation:

$$\begin{aligned} c(m) &= 1 - \frac{6}{m(m+1)} \\ h(m) &= h_{r,s}(m) \equiv \frac{[(m+1)r - ms]^2 - 1}{4m(m+1)} \end{aligned} \tag{14.31}$$

where $r,s \geq 1$ are integers with $rs \leq N$. The condition for unitarity of models with $c < 1$, first found by Friedan, Qiu and Shenker [27] reads: $m,r,s \in \mathbb{Z}$ with $m \geq 2$, and (r,s) must satisfy $1 \leq r < m$ and $1 \leq s \leq m$.

According to (14.23) the presence of a descendent field in a correlation function can be replaced by the action of a differential operator (14.24). Now let

$$\chi(w) = \sum_{Y,|Y|=N} \alpha_Y L_{-Y} \phi(w) \tag{14.32}$$

be an arbitrary null state. Here, α_Y are some coefficients, and we have introduced the abbreviations

$$\begin{aligned} Y &= \{r_1, r_2, \ldots, r_k\} \\ |Y| &= r_1 + r_2 + \ldots + r_k \\ L_{-Y} &= L_{-r_1} L_{-r_2} \cdots L_{-r_k} \end{aligned} \tag{14.33}$$

with $1 \leq r_1 \leq r_2 \leq \cdots \leq r_k$. A correlation function involving χ must vanish (since we have in fact set $\chi = 0$), and so

$$\langle \chi(w) X \rangle = \sum_{Y,|Y|=N} \alpha_Y \mathscr{L}_{-Y}(w) \langle \phi(w) X \rangle = 0 \tag{14.34}$$

Solving this Nth order linear differential equation is a very useful practical means of computing the four-point correlation functions of a given CFT, provided that the level of degeneracy N is not too large. Indeed, since the coordinate dependence is through a single anharmonic ratio η, one has simply an ordinary linear differential equation.

Moreover, requiring consistency with (14.25) places restrictions on the primaries that can occur on the right-hand side of the OPE. One can then study the conditions under which this so-called *fusion algebra* closes over a finite number of primaries. The end result is that the minimal models are given by

$$c = 1 - \frac{6(m-m')^2}{mm'}$$
$$h_{r,s} = \frac{(mr-m's)^2-(m-m')^2}{4mm'} \tag{14.35}$$

with $m,m',r,s \in \mathbb{Z}$, and the allowed values of (r,s) are restricted by $1 \le r < m'$ and $1 \le s < m$. The corresponding $h_{r,s}$ are referred to as the *Kac table* of conformal weights. The corresponding fusion algebra reads (for clarity we omit scaling factors, structure constants, and descendents):

$$\phi_{(r_1,s_1)}\phi_{(r_2,s_2)} = \sum_{r,s} \phi_{(r,s)} \tag{14.36}$$

where r runs from $1+|r_1-r_2|$ to $\min(r_1+r_2-1, 2m'-1-r_1-r_2)$ in steps of 2, and s runs from $1+|s_1-s_2|$ to $\min(s_1+s_2-1, 2m-1-s_1-s_2)$ in steps of 2.

The Kac table (14.35) is the starting point for elucidating the structure of the reducible Verma modules $\mathscr{V}_{r,s}$ for minimal models, and for constructing the proper irreducible modules $\mathscr{M}_{r,s}$. The fundamental observation is that

$$h_{r,s} + rs = h_{r,-s}\,. \tag{14.37}$$

Using the symmetry property $h_{r,s} = h_{m'-r,m-s}$ and the periodicity property $h_{r,s} = h_{r+m',s+m}$ it is seen that $h_{r,s}+rs = h_{m'+r,m-s}$ and that $h_{r,s}+(m'-r)(m-s) = h_{r,2m-s}$. This means that $\mathscr{V}_{r,s}$ contains two submodules, $\mathscr{V}_{m'+r,m-s}$ and $\mathscr{V}_{r,2m-s}$, at levels rs and $(m'-r)(m-s)$ respectively, and these must correspond to null vectors. To construct the irreducible module $\mathscr{M}_{r,s}$ one might at first think that it suffices to quotient out these two submodules. However, iterating the above observations, the two submodules are seen to share two sub-submodules, and so on. So $\mathscr{M}_{r,s}$ is constructed from $\mathscr{V}_{r,s}$ by an infinite series of inclusions-exclusions of pairs of submodules. This allows us in particular to compute the irreducible characters of minimal models as

$$\chi_{(r,s)}(\tau) = K_{r,s}^{(m,m')}(q) - K_{r,-s}^{(m,m')}(q)\,, \tag{14.38}$$

where the infinite addition-subtraction scheme has been tucked away in the functions

$$K_{r,s}^{(m,m')}(q) = \frac{q^{-1/24}}{P(q)} \sum_{n\in\mathbb{Z}} q^{(2mm'n+mr-m's)^2/4mm'}\,. \tag{14.39}$$

This should be compared with the generic character (14.28). Note also the similarity between (14.37) and (14.38) on the level of the indices.

It is truly remarkable that the above classification of minimal models has been achieved without ever writing down the action S appearing in (14.2). In fact, an effective Landau-Ginzburg Lagrangian description for the unitary minimal models ($m' = m+1$) has been suggested a posteriori by Zamolodchikov [28]. It suggests that the minimal models can be interpreted physically as an infinite series of multicritical versions of the Ising model. Indeed, the Ising model can be identified with the first

non-trivial member in the series, $m = 3$, and the following, $m = 4$, with the tricritical Ising model.

To finish this section, we comment on the relation with SAP's. In section 14.3 we shall see that these (to be precise, the dilute O($n \to 0$) model) can be identified with the minimal model $m = 2$, $m' = 3$. Note that this is *not* a unitary theory. The central charge is $c = 0$, and the only field in the Kac table—modulo the symmetry property given after (14.37)—is the identity operator with conformal weight $h_{1,1} = 0$. Seemingly we have learnt nothing more than the trivial statement $Z = 1$. However, the operators of interest are of a *non-local* nature, and it is a pleasant surprise to find that their dimensions fit perfectly well into the Kac formula, although they are situated *outside* the "allowed" range of (r,s) values, and sometimes require the indices r,s to be half-integer. So the Kac formula, and the surrounding theoretical framework, is still a most useful tool for investigating these types of models.

14.2.7 Modular Invariance

In section 14.2.3 we have seen that conformal symmetry makes the stress tensor decouple into its holomorphic and antiholomorphic components, $T(z)$ and $\bar{T}(\bar{z})$, implying in particular that the corresponding mode operators, L_n and $\bar{L}_n$, form two non-interacting Virasoro algebras (14.20). As a consequence, the key results of section 14.2.6 could be derived by considering only the holomorphic sector of the CFT. There are however constraints on the ways in which the two sectors may ultimately couple, the diagonal coupling (14.26) being just the simplest example in the context of minimal models. As first pointed out by Cardy [23], a powerful tool for examining which couplings are allowed—and for placing constraints on the operator content and the conformal weights—is obtained by defining the CFT on a torus and imposing the constraint of *modular invariance*.

In this section we expose the principles of modular invariance and apply them to a CFT known as the *compactified boson*, which is going to play a central role in the Coulomb gas approach of section 14.3. Many other applications, including a detailed study of the minimal models, can be found in Ref. [15].

Let $\omega_1, \omega_2 \in \mathbb{C} \setminus \{0\}$ such that $\tau \equiv \omega_2/\omega_1 \notin \mathbb{R}$. A torus is then defined as $\mathbb{C}/(\omega_1\mathbb{Z} + \omega_2\mathbb{Z})$, i.e., by identifying points in the complex plane that differ by an element in the lattice spanned by ω_1, ω_2. The numbers ω_1, ω_2 are called the *periods* of the lattice, and τ the *modular parameter*. Without loss of generality we can assume $\omega_1 \in \mathbb{R}$ and $\Im\tau > 0$.

Instead of using the radial quantisation scheme of section 14.2.5 we now define the time (resp. space) direction to be the imaginary (resp. real) axis in $\mathbb{C}$. The partition function on the torus may then be written $Z(\tau) = \mathrm{Tr}\exp[-(\Im\omega_2)\mathscr{H} - (\Re\omega_2)\mathscr{P}]$, where $\mathscr{H} = (2\pi/\omega_1)(L_0 + \bar{L}_0 - c/12)$ is the Hamiltonian and $\mathscr{P} = (2\pi/i\omega_1)(L_0 - \bar{L}_0 - c/12)$ the momentum operator. This gives

$$Z(\tau) = \mathrm{Tr}\left(q^{L_0 - c/24}\bar{q}^{\bar{L}_0 - c/24}\right), \tag{14.40}$$

where we have defined $q = \exp(2\pi i\tau)$. Comparing with (14.26)–(14.27) we have also

$$Z(\tau) = \sum_{h,\bar{h}} n_{h,\bar{h}} \chi_{(c,h)}(\tau)\bar{\chi}_{(c,\bar{h})}(\tau) . \tag{14.41}$$

An explicit computation of $Z(\tau)$ will therefore give information on the coupling $n_{h,\bar{h}}$ between the holomorphic and antiholomorphic sectors. In many cases, but not all, the coupling turns out to be simply diagonal, $n_{h,\bar{h}} = \delta_{h,\bar{h}}$.

The fundamental remark is now that $Z(\tau)$ is invariant upon making a different choice ω_1', ω_2' of the periods, inasmuch as they span the same lattice as ω_1, ω_2. Any two set of equivalent periods must therefore be related by $\omega_i' = \sum_j a_{ij}\omega_j$, where $\{a_{ij}\} \in \mathrm{Mat}(2,\mathbb{Z})$ with $\det a_{ij} = 1$. Moreover, an overall sign change, $a_{ij} \to -a_{ij}$ is immaterial, so the relevant symmetry group is the so-called *modular group* $\mathrm{SL}(2,\mathbb{Z})/\mathbb{Z}_2 \simeq \mathrm{PSL}(2,\mathbb{Z})$.

The remainder of this section is concerned with the construction of modular invariant partition functions for certain bosonic systems on the torus. As a warmup we consider the free boson, defined by the action

$$S[\phi] = \frac{g}{2}\int \mathrm{d}^2\mathbf{x}\,(\nabla\phi)^2 \tag{14.42}$$

and $\phi(\mathbf{x}) \in \mathbb{R}$. Comparing (14.40) with (14.27)–(14.29), and bearing in mind that $c = 1$, we would expect the corresponding partition function to be of the form $Z_0(\tau) \propto 1/|\eta(\tau)|^2$. Fixing the proportionality constant is somewhat tricky [29]. In a first step, ϕ is decomposed on the normalised eigenfunctions of the Laplacian, and $Z_0(\tau)$ is expressed as a product over the eigenvalues. This product however diverges, due to the presence of a zero-mode, and must be regularised. A sensible result is obtained by a shrewd analytic continuation, the so-called ζ-function regularisation technique [29]:

$$Z_0(\tau) = \frac{\sqrt{4\pi g}}{\sqrt{\Im\tau}\,|\eta(\tau)|^2} \tag{14.43}$$

The CFT which is of main interest for the CG technique is the so-called *compactified boson* in which $\phi(\mathbf{x}) \in \mathbb{R}/(2\pi aR\mathbb{Z})$. In other words, the field lives on a circle of radius aR (the reason for the appearance of *two* parameters, a and R, will become clear shortly). In this context, suitable periodic boundary conditions are specified by a pair of numbers, $m, m' \in a\mathbb{Z}$, so that for any $k, k' \in \mathbb{Z}$

$$\phi(z + k\omega_1 + k'\omega_2) = \phi(z) + 2\pi R(km + k'm') \tag{14.44}$$

It is convenient to decompose $\phi = \phi_{m,m'} + \phi_0$, where

$$\phi_{m,m'} = \frac{2\pi R}{\bar{\tau} - \tau}\left[\frac{z}{\omega_1}(m\bar{\tau} - m') - \frac{\bar{z}}{\bar{\omega}_1}(m\tau - m')\right] \tag{14.45}$$

is the classical solution satisfying the topological constraint, and ϕ_0 represents the quantum fluctuations, i.e., is a standard free boson satisfying standard periodic boundary conditions.

Integrating over ϕ_0 as before, and keeping m, m' fixed, gives the partition function

$$Z_{m,m'}(\tau) = Z_0(\tau) \exp\left(-2\pi^2 g R^2 \frac{|m\tau - m'|^2}{\Im\tau}\right). \tag{14.46}$$

It is easy to see that this is not modular invariant. A modular invariant is however obtained by summing over all possible values of m, m':

$$Z(\tau) \equiv \frac{R}{\sqrt{2}} Z_0(\tau) \sum_{m,m' \in a\mathbb{Z}} \exp\left(-2\pi^2 g R^2 \frac{|m\tau - m'|^2}{\Im\tau}\right) \tag{14.47}$$

The prefactor $R/\sqrt{2}$ is again a subtle effect of the zero-mode integration. It is actually most easily justified a posteriori by requiring the correct normalisation of the identity operator in (14.48) below.

A more useful, and more physically revealing, form of (14.47) is obtained by using the Poisson resummation formula to replace the sum over $m' \in a\mathbb{Z}$ by a sum over the dual variable $e \in \mathbb{Z}/a$. The result is

$$Z(\tau) = \frac{1}{|\eta(\tau)|^2} \sum_{e \in \mathbb{Z}/a,\ m \in a\mathbb{Z}} q^{h_{e,m}} \bar{q}^{\bar{h}_{e,m}}, \tag{14.48}$$

with

$$h_{e,m} = \frac{1}{2}\left(\frac{e}{R\sqrt{4\pi g}} + \frac{mR}{2}\sqrt{4\pi g}\right)^2, \qquad \bar{h}_{e,m} = \frac{1}{2}\left(\frac{e}{R\sqrt{4\pi g}} - \frac{mR}{2}\sqrt{4\pi g}\right)^2. \tag{14.49}$$

Comparing now with (14.40) and (14.27)–(14.29) we see that (14.49) is nothing else than the conformal weights of the CFT at hand.

The requirement of modular invariance has therefore completely specified the operator content of the compactified boson system. An operator is characterised by two numbers, $e \in \mathbb{Z}/a$ and $m \in a\mathbb{Z}$, living on mutually dual lattices. A physical interpretation will be furnished by the CG formalism of section 14.3: e is the "electric" charge of a vertex operator (spin wave), and m is the "magnetic" charge of a topological defect (screw dislocation in the field ϕ). Let us write for later reference the corresponding scaling dimension and spin:

$$\Delta_{e,m} = \frac{e^2}{4\pi g R^2} + m^2 \pi g R^2, \qquad s_{e,m} = em \tag{14.50}$$

Observe in particular that the spin is integer, as expected for a bosonic system.

The reader will notice that the three constants R, a and g are related by the fact that they always appear in the dimensionless combination $R^2 a^2 g$. Field-theoretic literature often makes the choice $a = 1$ and $g = 1/4\pi$ in order to simplify formulae

such as (14.49). In the CG approach—the subject of section 14.3—one starts from a geometrical construction (mapping to a height model) in which a convention for a must be chosen. The compactification radius aR then follows from a "geometrical" computation (identification of the ideal state lattice), and the correct coupling constant g is only fixed in the end by a field-theoretic argument (marginality requirement of the Liouville potential). Needless to say, the results, such as (14.50) for the dimensions of physical operators, need (and will) be independent of the initial choice made for a.

To conclude, note that the roles of e and m in (14.49) are interchanged under the transformation $Ra\sqrt{2\pi g} \to (Ra\sqrt{2\pi g})^{-1}$, which leaves (14.48) invariant. This is another manifestation of the electro-magnetic duality. Ultimately, the distinction between e and m comes down to the choice of transfer direction. In the geometry of the torus this choice is immaterial, of course. In sections 14.3.4–14.3.5 we shall compare the geometries of the cylinder and the annulus; these are related by interchanging the space and time directions, and accordingly the electric and magnetic charges switch role when going from one to the other.

14.2.8 Boundary CFT

The aspects of CFT exposed to this point pertain to unbounded geometries, either that of the infinite plane (Riemann sphere) or, in section 14.2.7, that of the torus (which is really a finite geometry made unbounded through the periodic boundary conditions). In contrast, boundary conformal field theory (BCFT) describes surface critical behaviour, i.e., a critical system confined to a bounded geometry. The simplest such geometry, and probably the most relevant from the point of view of polymer physics, is that of the upper half plane $\{z \,|\, \Im z \geq 0\}$, where the real axis $\mathbb{R}$ acts as the boundary (one-dimensional "surface").

The foundations of BCFT were set by Cardy [22] who also initiated many of the subsequent developments and applications (see [15, 30] for reviews). A useful review of the status of boundary critical phenomena before the advent of CFT was given by Binder [31].

To convey an idea of which phase transitions may result from the interplay between bulk and boundary degrees of freedom, and what may be the corresponding boundary conditions, we begin by a qualitative discussion of a simple magnetic spin system. We denote the local order parameter (magnetisation) by ϕ. When the boundary spins enjoy free boundary conditions, they interact more weekly than the bulk spins, since microscopically they are coupled to fewer neighbouring spins. Upon lowering the temperature, the bulk will therefore order before the surface: this is the so-called *ordinary transition*. Now consider placing the system slightly below the bulk critical temperature. Then ϕ is non-zero deep inside the bulk, and will decrease upon approaching the boundary. One can argue that in the continuum limit ϕ will vanish exactly on the boundary. Thus, the Dirichlet boundary condition $\phi|_{\mathbb{R}} = 0$ is the appropriate choice for describing the ordinary transition.

Let us now introduce a coupling J_s between nearest-neighbour spins on the boundary which may be different from the usual bulk coupling constant J. Taking $J_s > J$ one may "help" the boundary to order more easily.[2] When J_s takes a certain critical value we are at the *special transition*, at which the bulk and the boundary order simultaneously. Finally, when $J_s \to \infty$ the boundary spins are always completely ordered[3], a fact which changes the nature of the ordering transition of the bulk, now referred to as the *extraordinary transition*. This corresponds to the Dirichlet boundary condition $\phi|_{\mathbb{R}} = \infty$ in the continuum limit. Note that in the application of boundary CFT to loop models (see section 14.6) the meaning of J_s is to give a specific fugacity to monomers on the boundary.

The control parameter J_s can be thought of in a renormalisation group sense, and is readily seen to be irrelevant at the ordinary and extraordinary transitions. Accordingly we expect a boundary RG flow to go from the special to either of the two other transitions. (In the case of the Ising model, the special and extraordinary transitions actually coincide.)

In our subsequent application to loop models (see section 14.6) we rather think of ϕ as a height field which is dual to the system of oriented loops (this is the so-called Coulomb gas approach, see section 14.3). In other words, the loops are level lines of ϕ. Dirichlet boundary conditions then describe a situation in which loops are reflected off the boundary, and adjoining two different Dirichlet conditions forces one or more "loop ends" to emanate from the boundary. One may also impose Neumann boundary conditions, $\partial\phi/\partial y|_{\mathbb{R}} = 0$, meaning that the "loops" coming close to the boundary must in fact terminate perpendicular to it. Clearly the non-local aspects of these situations call for a more detailed discussion, which will be postponed to section 14.6.

The allowed conformal mappings in BCFT must keep invariant both the boundary itself and the boundary conditions imposed along it. For the global conformal transformations (14.6) the invariance of the real axis forces $a_{ij} \in \mathbb{R}$, i.e., they form the group $\mathrm{SL}(2,\mathbb{R})$ and the number of parameters is halved from 6 to 3. For an infinitesimal local conformal transformation $z \to w(z) = z + \varepsilon(z)$ the requirement reads $\varepsilon(\bar{z}) = \bar{\varepsilon}(z)$. This property can be used to eliminate the $\bar{\varepsilon}(z)$ part altogether, since it is just the analytic continuation of $\varepsilon(\bar{z})$ into the lower half plane. It follows that $\bar{L}_n = L_{-n}$, and so one half of the conformal generators has been eliminated.

At the level of the stress tensor, the requirement is $T(\bar{z}) = \bar{T}(z)$. In Cartesian coordinates this reads $T_{xy} = 0$ on the real axis, the so-called *conformal boundary conditions*. Its physical meaning is that there is no energy-momentum flow across $\mathbb{R}$. This has important consequences on the conformal Ward identity (14.9) where $T(z)$ is applied to a product of primary fields $X = \prod_j \phi_j(z_j, \bar{z}_j)$ situated in the upper half plane. The contour C surrounding all z_j can then be taken as a large semicircle with the diameter parallel to the real axis. However, writing the same identity for

[2] A similar effect could be obtained by adding a surface magnetic field, but here we do not wish to break the symmetry of the model [typically $O(n)$ in applications to loop models].

[3] This should not (as is sometimes seen in the literature) be confused with imposing *fixed* boundary conditions, which would rather correspond to an infinite symmetry-breaking field applied on the boundary.

$\bar{T}(\bar{z})$ yields another Ward identity involving the conjugate semicircle contour $\bar{C}$, and since $\bar{T} = T$ when $z \in \mathbb{R}$, the two contours can be fused into a complete circle surrounding both z_j and $\bar{z}_j$. The end result, cf. (14.10), is thus

$$T(z)X = \sum_j \left(\frac{h_j}{(z-z_j)^2} + \frac{\partial_{z_j}}{z-z_j} + \frac{\bar{h}_j}{(\bar{z}-\bar{z}_j)^2} + \frac{\partial_{\bar{z}_j}}{\bar{z}-\bar{z}_j} \right) X \,. \tag{14.51}$$

In conclusion, everything happens as if each primary field in the upper half plane were accompanied by a mirror field in the lower half plane. This means that computations in the BCFT can be done using a *method of images* similar to that used in electrostatics when solving the Laplace equation with boundary conditions. Correlation functions are computed as if the theory were defined on the whole complex plane, and governed by a single Virasoro algebra (14.20): the physical fields are then situated in the upper half plane, and their unphysical mirror images in the lower half plane. The simplification of getting rid of $\bar{L}_n$ has thus been achieved at the price of doubling the number of points in correlation functions. In practice, the former simplification largely outweighs the latter complication.

In particular, the n-point boundary correlation functions satisfy the very same differential equations (14.34) as $2n$-point bulk correlation functions, but with different boundary conditions. The most interesting cases are $n = 1$ and $n = 2$, both tractable in the bulk picture in several situations of practical importance. As examples of the physical information which can be extracted from these cases we should mention, for $n = 1$, the probability profile of finding a monomer of a loop at a certain distance from the boundary, and for $n = 2$, the probability that a polymer comes close to the boundary at two prescribed points [32]. A particularly celebrated application of the $n = 2$ case is Cardy's computation [33] of the *crossing probability* that a percolation cluster traverses a large rectangle, as a function of the aspect ration of the latter.

The radial quantisation scheme of section 14.2.5 still makes sense in BCFT. The associated conformal mapping

$$w(z) = \frac{L}{\pi} \log z \tag{14.52}$$

transforms the upper half plane into a semi-infinite strip of width L with non-periodic transverse boundary conditions. The two rims of the strip are then the images of the positive and the negative real axis, and the time (resp. space) direction is parallel (resp. perpendicular) to the axis of the strip. The dilatation operator reads $\mathscr{D} = L_0$ and the Hamiltonian $\mathscr{H} = (\pi/L)(L_0 - c/24)$. Non-trivial eigenstates of $\mathscr{H}$ are formed by a *boundary operator* $\phi_j(0)$ acting on the vacuum state, $|h\rangle = \phi_j(0)|0\rangle$.

In general, we expect boundary operators to have different scaling dimensions than bulk operators. This can be understood from the method of images: when a primary field approaches the boundary it interacts with its mirror image and, by the OPE (14.25), produces a series of other primaries which then describe the boundary critical behaviour.

Likewise, a field $\phi_{(r,s)}$ with a given interpretation in the bulk will typically have a different interpretation when situated on the boundary. Examples pertinent to loop models will be given in section 14.6.

The finite-size formulae (14.15) and (14.17) can be adapted to the case of a strip of width L. For this, one uses the method of images and the mapping (14.52). The end results read:

$$f_0(L) = f_0(\infty) + \frac{f_0^{\mathrm{S}}}{L} - \frac{\pi c}{24L^2} + o(L^{-2}),$$
$$f_\phi(L) - f_0(L) = \frac{f_\phi^{\mathrm{S}} - f_0^{\mathrm{S}}}{L} + \frac{\pi\Delta}{L^2} + o(L^{-2}). \tag{14.53}$$

where there is now a non-universal $1/L$ dependence due to the presence of surface free energies f^{S}. For some (but not all) choices of excited levels $f_\phi(L)$ it can be argued that $f_\phi^{\mathrm{S}} = f_0^{\mathrm{S}}$, thus simplifying the second of these formulae.

Note that (14.7) applied to a boundary operator is the reason why we have not discussed *finite* Dirichlet boundary conditions at the beginning of this section. More generally, any uniform boundary condition is expected to flow under the renormalisation group towards a *conformally invariant boundary condition*. It is one of the goals of BCFT to classify such boundary conditions. One of the main results obtained is the following [30]: For diagonal models (i.e., $n_{h,\bar{h}} = \delta_{h,\bar{h}}$ in (14.26)) there is a bijection between the primary fields in the bulk CFT and the conformally invariant boundary conditions in the BCFT. For example, for the Ising model ($m = 3$ and $m' = 4$ in (14.35)) the three different bulk primary operators (the identity $I = \phi_{(1,1)}$, the spin $\sigma = \phi_{(1,2)}$, and the energy $\varepsilon = \phi_{(2,1)}$) correspond to three types of uniform boundary conditions in the lattice model of spins (fixed $s = +1$ and $s = -1$, and free boundary conditions).

To this point we have discussed only uniform boundary conditions. It is important to realise that the radial quantisation picture with a boundary operator $\phi_j(0)$ situated at the origin is compatible also with mixed boundary conditions, i.e., one boundary condition on the negative real half-axis and another on the positive half-axis. In this case, $\phi_j(0)$ is called a *boundary condition changing operator*. One then needs a second operator $\phi_j(\infty)$ situated at infinity to change back the boundary condition. A more symmetric picture is obtained by mapping the upper half plane to the strip, through (14.52). There are then different boundary conditions on the two sides of the strip, and a boundary condition changing operators is located at either end of the strip. More generally, one may study a BCFT on any simply connected domain with a variety of different boundary conditions along the boundary, each separated by a boundary condition changing operator.

For bulk CFT, crucial insight was gained by considering the theory on a torus. The analogous tool for BCFT is to consider the theory on an annulus.[4] In analogy

[4] It makes sense to think of this in the radial quantisation, or transfer matrix, picture. The theories are initially considered on a semi-infinite cylinder (resp. a strip) with specified transverse boundary conditions (periodic, resp. non-periodic) and unspecified longitudinal boundary conditions. This gives access to the transfer matrix eigenvalues. To access the fine structure, such as amplitudes of

with the torus case, we denote by $\omega_1 \in \mathbb{R}$ the width of the annulus and by $\omega_2 \in i\mathbb{R}$ its length (in the periodic direction), defining $\tau = \omega_2/\omega_1 \in i\mathbb{R}$. The boundary conditions on the two rims are denoted, symbolically, a and b. Then

$$Z_{ab}(\tau) = \mathrm{Tr}\left(q^{L_0 - c/24}\right) \tag{14.54}$$

with $q = \exp(\pi i \tau)$. This should be compared with (14.40). The analogue of (14.41),

$$Z_{ab}(\tau) = \sum_h n_h^{(ab)} \chi_{(c,h)}(\tau)\,, \tag{14.55}$$

then becomes linear in the characters. Equivalently, one might exchange the space and time direction and view the annulus as a cylinder of circumference ω_2 and finite length ω_1, with boundary conditions a (resp. b) in the initial (resp. final) state. This leads to

$$Z_{ab}(\tau) = \left\langle b \left| \mathrm{e}^{\tau^{-1}\mathscr{H}_{\mathrm{bulk}}} \right| a \right\rangle\,, \tag{14.56}$$

where now $\mathscr{H}_{\mathrm{bulk}}$ is the Hamiltonian of the *bulk* CFT propagating between boundary states $|a\rangle$ and $\langle b|$. The links between bulk and boundary CFT result from a detailed study of the equivalence between (14.54) and (14.56).

14.3 Coulomb Gas Construction

It has been known since the 1970's [34] that the critical point of many two-dimensional models of statistical physics can be identified with a Gaussian free-field theory. A general framework for the computation of critical exponents was first given in 1977 by José et al. in the so-called spin wave picture [9]. This was further elaborated in the early 1980's by den Nijs [10] and Nienhuis [11] into what has become known as the Coulomb gas (CG) construction. These developments have been reviewed by Nienhuis [35].

The CG approach is particularly suited to deal with the continuum limit of lattice models of closed loops, in which each loop carries a Boltzmann weight n. Such *loop models* arise as the diagrammatic expansion of spin systems in which the spins take values in $\mathbb{R}^n$ and the interactions possess an O(n) symmetry. Depending on the normalisation constraint imposed on the spins, and on the underlying lattice structure, the loops may or may not admit self-intersections. The former case can be treated by supersymmetric techniques [36], within the framework of the non-linear sigma model, but does not admit a CG representation. In the present review we are however only concerned with cases without self-intersections, for which the CG approach does apply. A particularly elegant and useful example was given by Nienhuis [37]. Another important model, the Q-state Potts model, can be formulated

the eigenvalues, one must impose periodic longitudinal boundary conditions and take the length of the cylinder (resp. strip) to be *finite*.

as a model of self-avoiding loops with $n = \sqrt{Q}$, as first shown by Baxter, Kelland and Wu [38]. We shall review the relevant mappings in section 14.3.1.

The marriage between the CG and conformal field theory (CFT) happened in 1986–87, when Di Francesco, Saleur and Zuber [39, 40] made the loop model $\leftrightarrow$ CG correspondence more precise and showed how the ideas of modular invariance [23, 29] can be put to good use in the study of loop models (see section 14.7 below). At the same time, Duplantier and Saleur developed a range of applications to SAW's and SAP's (see in particular [14]).

In section 14.3.2 we show how the loop models can be transformed into height models with local (albeit complex) Boltzmann weights. It is the continuum limit of this height which acts as the conformally invariant free field. The underlying lattice model implies that this height field is compactified, thus making contact with the modular invariance results of section 14.2.7.

The naive free field action however needs to be modified with extra terms, traditionally known as background and screening electric charges [35]. The resulting CFT, known as a Liouville field theory, is written down in section 14.3.3.

The requirement that the Liouville potential be RG marginal determines the coupling constant of the free field as a function of n, as first pointed out by Kondev [17]. This is an important ingredient, since otherwise one would have to rely on an independent exact solution to fix the coupling. The analogous marginality requirement for the case of surface critical behaviour has been established recently by Cardy [18]. We discuss these developments in sections 14.3.4–14.3.5.

14.3.1 From Potts and O(n) Models to Loops

In this section we show how to transform the Q-state Potts model and the O(n) model into loop models. There are several mappings of this type, depending on the lattice structure, the types of (local) interactions, and so on, but for simplicity we shall concentrate here on the simplest cases in which the Potts model is defined on a square lattice [38] and the O(n) model on a hexagonal lattice [37].

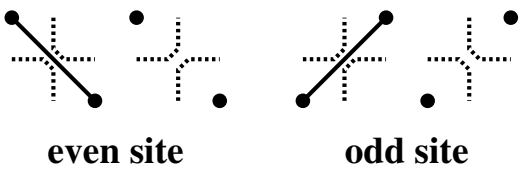

Fig. 14.1 Relation between the clusters E' (solid lines) on $\mathscr{L}$ (filled circles) and the transition system $T(E')$ (broken lines) on $S_{\mathscr{L}}$. Note that the rules differ for the two sublattices of $S_{\mathscr{L}}$.

Consider first the Potts model, defined initially by assigning spins $\sigma_i = 1, 2, \ldots, Q$ to each of the vertices of the square lattice $\mathscr{L}$. A pair of nearest-neighbour spins has

the interaction energy $-K\delta_{\sigma_i,\sigma_j}$, and we set $J = K/k_{\mathrm{B}}T$. The partition function then becomes that of the so-called random cluster model [41]:

$$Z = \sum_{\{\sigma\}} \prod_{(ij)\in E} \mathrm{e}^{J\delta_{\sigma_i,\sigma_j}} = \sum_{E'\subseteq E} (\mathrm{e}^J - 1)^{|E'|} Q^{c(E')}, \tag{14.57}$$

where E is the set of lattice edges, E' runs through all $2^{|E|}$ subsets thereof, and $c(E')$ is the number of connected components in the graph induced by E'. Define now the surrounding lattice $S_{\mathscr{L}}$ with vertices which are the midpoints of edges in $\mathscr{L}$, here a rotated square lattice. On $S_{\mathscr{L}}$ we define for each $E' \subseteq E$ a transition system $T(E')$ system according to the rule in Fig. 14.1; then $T(E')$ constitutes a set of cycles (loops[5]) that separate the connected components in the edge set E' from those dual to the complement $E \setminus E'$. (In other words, the loops form the boundaries of connected components in either set.) Using the Euler relation for a *planar* lattice with N vertices this results in

$$Z = Q^{N/2} \sum_{E'\subseteq E} \left(\frac{\mathrm{e}^J - 1}{\sqrt{Q}}\right)^{|E'|} Q^{l(T(E'))/2}, \tag{14.58}$$

where $l(T(E'))$ is the number of loops in the transition system $T(E')$. On a non-planar graph, (14.58) would be slightly modified (see section 14.7 below).

The local weights of the transition system in (14.58) are in general inhomogeneous, due to the first factor inside the sum, since vertices on the even (resp. odd) sublattice of $S_{\mathscr{L}}$ stand on horizontal (resp. vertical) edges of $\mathscr{L}$. This inhomogeneity can be directly read off from Fig. 14.1. Even though critical (and even integrable) points of the inhomogeneous model do exist [42, 43] we are here interested in homogeneous solutions only. Indeed, for $\mathrm{e}^J - 1 = \pm\sqrt{Q}$ and $0 \le Q \le 4$ the Potts model (14.57) is at its self-dual critical point [44, 45]. With the plus sign, (14.58) then becomes simply

$$Z = Q^{N/2} \sum_{E'\subseteq E} n^{l(T(E'))} \tag{14.59}$$

with $n \equiv \sqrt{Q}$. With the minus sign, (14.59) still holds true provided we take the other determination of the square root, $n = -\sqrt{Q}$, since $N + |E'| + l(T(E'))$ is even for any E'. In conclusion, (14.59) describes a selfdual critical $Q = n^2$ state Potts model for $-2 \le n \le 2$, and it takes the form of a simple *loop model* in which each loop carries the weight n.

The limit $n \to 0$ is of special interest here. The dominant contribution to (14.59) is such that each E' in the sum represents an (unrooted) spanning tree, and its contour is a so-called *osculating SAP*.

We now turn to the O(n) model, which is defined initially by assigning vector spins $\mathbf{S}_i \in \mathbb{R}^n$ to each of the vertices of the hexagonal lattice $\mathscr{L}$. A pair of nearest-neighbour spins has the interaction energy $-J\,\mathbf{S}_i \cdot \mathbf{S}_j$. The integration measure is

[5] The use of the word *loop* as a synonym of cycle is common in the physics literature, and should not be confused with its different meaning in graph theory.

defined such that $\int \mathrm{d}\mathbf{S}_i \mathrm{d}\mathbf{S}_j S_i^\alpha S_j^\beta = \delta_{\alpha,\beta}$ and odd moments of $\mathbf{S}_i$ vanish by the symmetry $\mathbf{S}_i \to -\mathbf{S}_i$. Expanding out the Boltzmann weights $\tilde{w}_{ij} = \exp(J\mathbf{S}_i \cdot \mathbf{S}_j / k_\mathrm{B}T)$ and forming the partition function, the contributing configurations are in bijection with systems of loops for which each loop carries a weight n. These loops are in general rather complicated. Namely, on a general lattice containing vertices of degree ≥ 4 the loops may cross; and for any lattice they may cover each edge more than once. The choice of the hexagonal lattice overcomes the first complication. To overcome the second we follow Nienhuis [37] and redefine the weights as $w_{ij} \equiv 1 + K\mathbf{S}_i \cdot \mathbf{S}_j$, i.e, by truncating the formal high-temperature expansion of the original weights. The effect of these simplifications on the critical behaviour may be judged a posteriori, in section 14.4.

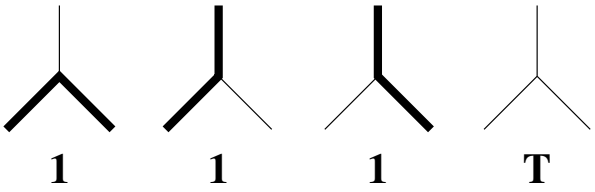

Fig. 14.2 Vertices in the O(n) loop model at temperature $T = 1/K$.

The partition function then reads

$$Z = \sum_{\mathscr{G}} K^{|\mathscr{G}|} n^{l(\mathscr{G})}, \tag{14.60}$$

where $\mathscr{G}$ are edge subsets of $\mathscr{L}$ with the property that every vertex is adjacent to an even number (zero or two) of edges in $\mathscr{G}$, as shown in Fig. 14.2. So $\mathscr{G}$ forms a system of $l(\mathscr{G})$ self-avoiding, mutually avoiding loops drawn on $\mathscr{L}$. Nienhuis [37] has argued that the loop model (14.60) is critical for $-2 \leq n \leq 2$ and

$$1/K^2 = 2 \pm \sqrt{2-n}. \tag{14.61}$$

The high-temperature solution [plus sign in (14.61)] is supposed to correctly describe the critical point of the original O(n) model. The loops described by it are commonly referred to as *dilute*, as they fill a vanishing fraction of the lattice in the thermodynamic limit. The low-temperature solution [minus sign in (14.61)] describes *dense loops* which cover a finite fraction of the lattice. One would expect these to be intimately related to the osculating SAP's of the Potts model, and this is indeed the case. Their critical behaviour is however not coincident with that of the original, unmodified O(n) model. These remarks will be clarified further below, and in section 14.4.

14.3.2 Transformation to a Height Model

In the definition of the Q-state Potts and the O(n) models, the parameters Q and n were originally positive integers. However, in the corresponding loop models, (14.59) and (14.60), they appear as formal parameters and may thus take arbitrary complex values. The price to pay for this generalisation is the appearance of a non-locally defined quantity, the number of loops l. The locality of the models may be recovered (though not completely, see section 14.3.3) by transforming them to height models with complex Boltzmann weights [38], as we now show.

In a first step, each loop is independently decorated by a global orientation $s = \pm 1$, which by planarity and self-avoidance can be described as either counter-clockwise ($s = 1$) or clockwise ($s = -1$). Each oriented loop must be given a weight $w(s)$, so that $n = \sum_s w(s)$. An obvious possibility, sometimes referred to as the *real loop ensemble*, is $w(1) = w(-1) = n/2$. This can be interpreted as an O($n/2$) model of complex spins.

We are however more interested in the *complex loop ensemble* with $w(s) = \mathrm{e}^{is\gamma}$. Note that in the expected critical regime,

$$n = 2\cos\gamma \in [-2, 2]\,, \tag{14.62}$$

the parameter $\gamma \in [0, \pi]$ is real. Locality is retrieved by remarking that the weights $w(\pm 1)$ are equivalent to assigning a local weight $w(\alpha/2\pi)$ to each vertex where a loop turns an angle α (counted positive for left turns). If a vertex is traversed by more than one loop, it gets weighted by the product of $w(\alpha/2\pi)$ over all traversals.

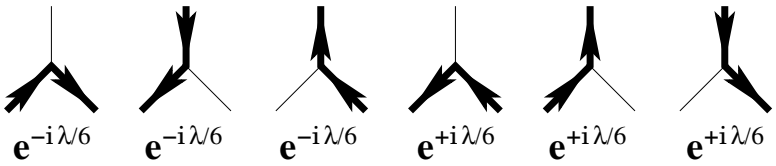

Fig. 14.3 Local redistribution of the loop weight n in the O(n) loop model on the hexagonal lattice.

The models (14.59) and (14.60) are now transformed into *local vertex models* by assigning to each edge traversed by a loop the orientation of that loop. An edge not traversed by any loop is assigned no orientation. The total vertex weight is determined from the configuration of its incident oriented edges, as the above local loop weights summed over the oriented transition systems compatible with edge orientations; this is illustrated for the hexagonal-lattice O(n) model in Fig. 14.3. In addition, one must multiply this by any loop-independent local weights, such as K in (14.60).

As a result, (14.59) is transformed into a six-vertex model on the square lattice, each vertex being incident on two outgoing and two ingoing edges [44], as shown in Fig. 14.4. The weights ω_i (resp. ω_i') on the even (resp. odd) sublattice read explicitly

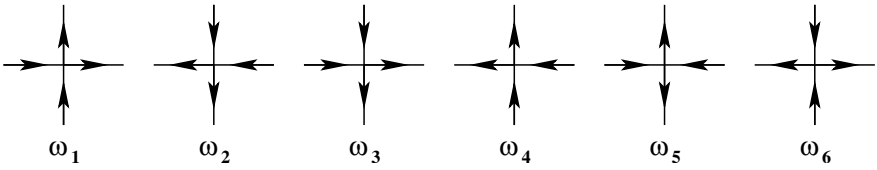

Fig. 14.4 Weights in the six-vertex model.

$$\omega_1,\ldots,\omega_6 = 1,1,x,x,\mathrm{e}^{i\gamma/2}+x\mathrm{e}^{-i\gamma/2},\mathrm{e}^{-i\gamma/2}+x\mathrm{e}^{i\gamma/2} \tag{14.63}$$

$$\omega'_1,\ldots,\omega'_6 = x,x,1,1,\mathrm{e}^{-i\gamma/2}+x\mathrm{e}^{i\gamma/2},\mathrm{e}^{i\gamma/2}+x\mathrm{e}^{-i\gamma/2} \tag{14.64}$$

where we have defined $x = (\mathrm{e}^J - 1)/\sqrt{Q}$. Note that the anisotropy parameter $\Delta = -\cos\gamma$ of the equivalent XXZ spin chain is independent of x and of the sublattice.

Similarly, (14.60) becomes a seven-vertex model on the hexagonal lattice, each vertex being either empty, or incident on one outgoing, one ingoing, and one empty edge. The six non-empty vertices are shown in Fig. 14.3.

Finally, the vertex models are turned into *height models*. For this, assign a scalar variable $h(\mathbf{x})$ to each lattice face $\mathbf{x}$ (i.e., to each vertex of the lattice *dual* to the one on which the loop model has been defined), so that h increases (resp. decreases) by a each time one traverses a left-going (resp. right-going) edge. This definition of the height h is consistent, since each vertex is incident on as many ingoing as outgoing edges. Since this defines only height differences, one may imagine fixing h completely by arbitrarily fixing $h(\mathbf{0}) = 0$.

In the continuum limit, we expect the local height field h to converge to a free bosonic field $\phi(\mathbf{x})$, whose entropic fluctuations are described by an action of the form (14.42), with coupling $g = g(n)$ which is a monotonically increasing function of n. In particular, for $n \to \infty$ the lattice model is dominated by the configuration where loops of the minimal possible length cover the lattice densely; the height field is then flat, $\phi(\mathbf{x}) = \text{constant}$, and the correlation length ξ is of the order of the lattice spacing. For finite but large n, ϕ will start fluctuating, loop lengths will be exponentially distributed, and ξ will be of the order of the linear size of the largest loop. When $n \to n_{\mathrm{c}}^+$, for some critical n_{c} (we shall see that $n_{\mathrm{c}} = 2$), this size will diverge, and for $n \le n_{\mathrm{c}}$ the loop model will be conformally invariant with critical exponents that depend on $g(n)$. The interface described by $\phi(\mathbf{x})$ is then in a *rough* phase. The remainder of this section is devoted to making this intuitive picture more precise, and to refine the free bosonic description of the critical phase.

As a first step towards greater precision, we now argue that $\phi(\mathbf{x})$ is in fact a *compactified boson*, cf. section 14.2.7. To see this, it is convenient to consider the *oriented* loop configurations that give rise to a maximally flat microscopic height h; following Henley and Kondev [61] we shall refer to them as *ideal states*. For the Potts model (14.59), an ideal state is a dense packing of length-four loops, all having the same orientation. There are four such states, corresponding to two choices of orientation and two choices of the sublattice of lattice faces surrounded by the loops. An ideal state can be gradually changed into another by means of $\sim N$ local changes

of the transition system and/or the edge orientations. As a result, the mean height will change, $\phi \to \phi \pm a$. Iterating this, one sees that one may return to the initial ideal state whilst having $\phi \to \phi \pm 2a$. For consistency, we must therefore require $\phi(\mathbf{x}) \in \mathbb{R}/(2a\mathbb{Z})$, i.e., the field is compactified with radius $R = 1/\pi$, cf. (14.44).

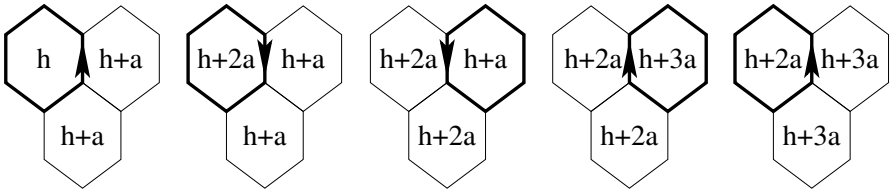

Fig. 14.5 Ideal states of the O(n) model on the hexagonal lattice. For each of the five panels, the state of the complete infinite lattice is obtained by tiling the plane with three faces shown, while respecting the three-sublattice structure. The different panels are related, from left to right, by the construction explained in the main text, under which one ideal state is gradually changed into another. The leftmost and rightmost panels represent the same ideal state, but with a global height change $\phi \to \phi + 2a$ that determines the compactification radius.

The same construction applied to the O(n) model (14.61) yields six ideal states of oriented length-six loops (resulting from a choice of three sublattices and two orientations). Changing the ideal state in four steps, as shown in Fig. 14.5, produces the initial state but with a height change of $\pm 2a$. So one has the same compactification radius, $\phi(\mathbf{x}) \in \mathbb{R}/(2a\mathbb{Z})$, as in the case of the Potts model.

Before we go on, a few remarks are in order:

1. In section 14.2.7 we have seen in detail that the normalisation constant a drops out from the final physical results. We shall therefore follow standard conventions and set $a = \pi$ in what follows.
2. While the complex loop ensemble is geometrically appealing, it is difficult to make quite rigorous a setup which is based on complex Boltzmann weights.
3. We may already suspect—and we shall see below in more detail—that the O(n) model in the dense phase and the Q-state Potts model give identical critical theories in the continuum limit, for $n = \sqrt{Q}$. However, the correspondence between operators in the microscopic model and the continuum limit is not necessarily identical, leading to subtle differences. For instance, the energy operators of the two models become different objects in the continuum limit (see section 14.4).

14.3.3 Liouville Field Theory

The essence of the above discussion is that the critical properties of the loop models under consideration can be described by a continuum-limit partition function that takes the form of a functional integral

$$Z = \int \mathscr{D}\phi(\mathbf{x}) \exp\left(-S[\phi(\mathbf{x})]\right) . \tag{14.65}$$

Here $S[\phi(\mathbf{x})]$ is the Euclidean action of the compactified scalar field $\phi(\mathbf{x}) \in \mathbb{R}/(2\pi\mathbb{Z})$. The hypothesis that the critical phase is described by bounded elastic fluctuations around the ideal states means that S must contain a term

$$S_{\mathrm{E}} = \frac{g}{4\pi} \int \mathrm{d}^2\mathbf{x} \, (\nabla\phi)^2 \tag{14.66}$$

with coupling constant $g > 0$. Higher derivative terms that one may think of adding to (14.66) can be ruled out by the $\phi \to -\phi$ symmetry, or by arguing a posteriori that they are RG irrelevant in the full field theory that we are about to construct.

Note that the partition function (14.65) does not purport to coincide with (14.59) or (14.60) on the scale of the lattice constant. (A similar remark holds true for the correlation functions that one may similarly write down.) We do however claim that their long-distance properties are the same. In that sense, the CG approach is an exact, albeit by no means rigorous, method for computing critical exponents and related quantities. A more precise equivalence between discrete and continuum-limit partition functions can however be achieved on a torus; see section 14.7.

The action (14.66) coincides with (14.42) for the compactified boson. To obtain the full physics of the loop model one however needs to add two more terms to the action, as we now shall see.

To proceed, we consider the underlying lattice model as being defined on a cylinder, $\mathbf{x} = (x,t)$. This has the advantage of making direct contact with the radial quantisation formalism of section 14.2.5 used in both numerical (transfer matrix) and analytical (Bethe Ansatz) studies. The boundary conditions are thus periodic in the space direction, $x = x + L$, and free in the time (t) direction. Ultimately, the results obtained on the cylinder can always be transformed into other geometries by means of a conformal mapping.

With this geometry, the equivalence between the loop model and a local height model with complex weights, established in section 14.3.2, must be revisited. While loops homotopic to a point still acquire their correct global weight n from the local angle-dependent weights $w(\alpha/2\pi)$, this is no longer true for loops that wind around the cylinder. Summing over loop orientations, their weight would be $\overline{n} = 1 + 1 = 2$. Consider now adding a term

$$S_{\mathrm{B}} = \frac{ie_0}{4\pi} \int \mathrm{d}^2\mathbf{x} \, \phi(\mathbf{x}) \mathscr{R}(\mathbf{x}) \tag{14.67}$$

to the effective action S, where $\mathscr{R}$ is the scalar curvature[6] of the space $\mathbf{x}$. The parameter e_0 is known in CG language as the *background electric charge*. On the cylinder, one has simply $S_{\mathrm{B}} = ie_0 \left(\phi(x,\infty) - \phi(x,-\infty)\right)$, meaning that in the partition function (14.65) an oriented loop with winding number $q = 0, \pm 1$ (all other winding numbers are forbidden by the self-avoidance of the loops) can equivalently be assigned an ex-

[6] We consider the scalar curvature in a generalised sense, so that delta function contributions may be located at the boundaries. Implicitly, we are just applying the Gauss-Bonnet theorem.

tra weight of $\exp(i\pi q e_0)$. For non-winding loops ($q = 0$) this does not change the reasoning of section 14.3.2, whilst summing over the two orientations ($q = \pm 1$) of a winding loop produces the weight $\overline{n} \equiv 2\cos(\pi e_0)$. The choice $e_0 = \gamma/\pi$ will thus assign to a winding loop the same weight $\overline{n} = n$ [see (14.62)] as to a non-winding one (but note that other choices leading to $\overline{n} \neq n$ may be useful in some applications of the CG technique).

The object $\mathrm{e}^{ie\phi}$ (or more precisely, its normal ordered product $:\mathrm{e}^{ie\phi}:$) is known in field theory as a *vertex operator* of (electric) charge e. The boundary term (14.67) thus corresponds to the insertion of two oppositely charged vertex operators at either end of the cylinder.

At this stage two problems remain: the field theory does not yet take account of the weight n of contractible loops, and the coupling constant g has not yet been determined. These two problems are closely linked, and allow [17] us to fix exactly $g = g(n)$. The idea is to add a further *Liouville term*

$$S_{\mathrm{L}} = \int \mathrm{d}^2\mathbf{x}\, w[\phi(\mathbf{x})] \tag{14.68}$$

to the action, which then reads in full

$$S[\phi(\mathbf{x})] = S_{\mathrm{E}} + S_{\mathrm{B}} + S_{\mathrm{L}}\,. \tag{14.69}$$

In (14.68), $\mathrm{e}^{-w[\phi(\mathbf{x})]}$ is the scaling limit of the microscopic vertex weights w_i. To identify it we show the argument for the O(n) model, the Potts case being similar.

Due to the compactification, $S_L[\phi]$ is a periodic functional of the field, and as such it can be developed as a Fourier sum over vertex operators

$$w[\phi] = \sum_{e \in \mathscr{L}_w} \tilde{w}_e\, \mathrm{e}^{ie\phi}\,, \tag{14.70}$$

where $\mathscr{L}_w$ is some sublattice of $\mathscr{L}_0 \equiv \mathbb{Z}$. Note that $\mathscr{L}_w$ may be a proper sublattice of $\mathscr{L}_0$ if $w[\phi]$ has a higher periodicity than that trivially conferred by the compactification of ϕ. By inspecting Fig. 14.5 we see that this is indeed the case here: the (geometric) averages of the microscopic weights coincide on the first, third, and fifth panels, indicating that the correct choice is $\mathscr{L}_w = 2\mathscr{L}_0$. This intuitive derivation of $\mathscr{L}_w$ (which can easily be corroborated by considering more complicated microscopic configurations) demonstrates the utility of the ideal state construction.

Some important properties of the compactified boson with action S_{E} have already been derived in section 14.2.7. In particular, its central charge is $c = 1$ and the dimension $\Delta_{e,m}$ of an operator with electromagnetic charge (e,m) is given by (14.50). Having now identified the electric charge e with that of the vertex operator $\mathrm{e}^{ie\phi}$, one could alternatively rederive (14.50) by computing the two-point function $\left\langle \mathrm{e}^{ie\phi(\mathbf{x})}\mathrm{e}^{-ie\phi(\mathbf{y})} \right\rangle$ by standard Gaussian integration.

The physical interpretation of the magnetic charge m is already obvious from (14.44): it corresponds to dislocations in the height field ϕ due to the presence of

defect lines. In section 14.4 we shall see how to identify these defect lines with SAW's and compute the related critical exponents.

It remains to assess how the properties of the compactified boson are modified by the inclusion of the term $S_{\rm B}$. Physical reasoning consists in arguing that the vertex operators $\mathrm{e}^{\pm ie_0\phi}$ will create a "floating" electric charge of magnitude $2e_0$ that "screens" that of the other fields in any given correlation function. We infer that (14.50) must be changed into

$$\Delta_{e,m} = \frac{1}{2}\left[\frac{e(e-2e_0)}{g} + gm^2\right]. \tag{14.71}$$

Note that to obtain (14.71) we have changed our normalisation so that both e and m are integers. This is consistent with the normalisation (14.66) of the coupling constant, rather than (14.42), which is the standard choice in the CG literature.

14.3.4 Marginality Requirement

Following Kondev [17] we now claim that the Liouville potential S_L must be exactly marginal. This follows from the fact that all loops carry the same weight n, independently of their size, and so the term S_L in the action that enforces the loop weight must not renormalise under a scale transformation. The most relevant vertex operator appearing in (14.70) has charge $e_w = 2\pi/a = 2$, and so $\Delta_{e_w,0} = 2$. Using (14.71), this fixes the coupling constant as $g = 1 - e_0$. In other words, the loop weight has been related to the CG coupling as

$$n = \pm\sqrt{Q} = -2\cos(\pi g) \tag{14.72}$$

with $0 < g \leq 1$ for the Potts model or the dense O(n) model.

The term S_B shifts the ground state energy with respect to the $c = 1$ theory described by S_E alone. The corrected central charge is then $c = 1 + 12\Delta_{e_0,0}$, where the factor of 12 comes from comparing (14.15) and (14.17). This gives

$$c = 1 - \frac{6(1-g)^2}{g}. \tag{14.73}$$

It should be noted that the choice $e_w = 2$ is not the only one possible. Namely, the coefficient $\tilde{w}_{e_w}$ of the corresponding vertex operator in (14.70) may be made to vanish, either by tuning the temperature T in the O(n) model, or by introducing non-magnetic vacancies in the Potts model. The former case corresponds to taking the high-temperature solution [plus sign] in (14.61), while the latter amounts to being at the tricritical point of the Potts model. The next-most relevant choice is then $\tilde{e}_w = -2$, and going through the same steps as above we see that one can simply maintain (14.72), but take the coupling in the interval $1 \leq g \leq 2$ for the dilute O(n) model or the tricritical Potts model.

The electric charge e_w whose vertex operator is required to be exactly marginal is known as the *screening charge* in standard CG terminology.

The central charge (14.73) can now be formally identified with that of the Kac table (14.35), with $m' = m+1$. The result is a formal relation between the minimal model index m and the CG coupling g, valid for integer m. We have

$$m = \begin{cases} \frac{g}{1-g} & \text{for the dense O}(n)\text{ model, or the critical Potts model} \\ \frac{1}{g-1} & \text{for the dilute O}(n)\text{ model} \end{cases} \tag{14.74}$$

The special cases $n \to 0$ are related to self-avoiding walks and polygons. This gives $g = 1/2$ for dense polymers (with $c = -2$ and $m = 1$), and $g = 3/2$ for dilute ones (with $c = 0$ and $m = 2$).

14.3.5 Annular Geometry

Consider now instead the loop model defined on an annulus which we shall take as an $L \times M$ rectangle with coordinates $x \in [0,L]$ and $y \in [0,M]$. The boundary conditions are free (f) in the x-direction and periodic in the y-direction. Very recently, Cardy [18] has shown how to impose the correct marginality requirement for this geometry.

Consider first the continuum-limit partition function $Z = Z_{\mathrm{ff}}(\tau)$ from (14.54) in the limit $M/L \gg 1$ of a very long and narrow annulus. The modular parameters $\tau = iM/L$ and $q = \exp(i\pi\tau) = \exp(-\pi M/L)$. We expect in this limit that only the identity operator contributes to Z, and so

$$Z \sim q^{-c/24} \sim \exp\left(\frac{\pi c M}{24 L}\right). \tag{14.75}$$

The central charge c is (14.73) from the bulk theory, and in particular is known to vary with the coupling constant g.

The question then arises how (14.75) is compatible with the continuum-limit action (14.66). According to Cardy [18] the answer is that there is a background magnetic flux m_0, a sort of electromagnetic dual of the background electric charge e_0 present in the cylinder geometry. Thus, in the continuum limit there is effectively a number (in general fractional) m_0 of oriented loops running along the rims of the annulus, giving rise to a height difference between the left and the right rim. Accepting this hypothesis, we can write

$$\phi(x,y) = \tilde{\phi}(x,y) + \frac{\pi m_0 x}{L} \tag{14.76}$$

where $\tilde{\phi}$ is a "gauged" height field that still contains the elastic fluctuations but obeys identical Dirichlet boundary conditions on both rims, say $\tilde{\phi}(0,y) = \tilde{\phi}(L,y) = 0$.

According to the functional integrations in section 14.2.7, the field $\tilde{\phi}$ contributes $q^{-1/24}$ to Z, corresponding to $c = 1$. The last term in (14.76) modifies the action (14.66) by $\Delta S = \frac{g}{4\pi}(\pi m_0)^2 \frac{M}{L}$ and thus multiplies Z by a factor $\mathrm{e}^{-\Delta S} = q^{gm_0^2/4}$, which correctly reproduces the contribution of the last term in (14.73) to (14.75) provided that we set

$$m_0 = \pm \frac{(1-g)}{\pi g}\,. \tag{14.77}$$

This value of m_0 can be retrieved from a marginality requirement which has the double advantage of being more physically appealing and of not invoking the formula (14.73) for c. Indeed, if m_0 is too large a pair of oriented loop strands will shed from the rims, corresponding to a vortex pair of strength $m = \pm 2$ situated at the top and the bottom of the annulus. This vortex pair can then annihilate in order to reduce the free energy. And if m_0 is too small the opposite will occur. The equilibrium requirement is then that inserting such a vortex pair must be an exactly marginal perturbation in the RG sense, i.e., the corresponding *boundary* scaling dimension is $\Delta_{\mathrm{v}} = 1$.

The free energy increase for creating the vortex pair is, by the same gauge argument as before,

$$\Delta S = \frac{g}{4\pi}\left((m_0+2)^2 - m_0^2\right)\left(\frac{\pi}{L}\right)^2 ML \tag{14.78}$$

and noting the factor of 24 between c and the scaling dimension Δ_{v} in (14.53), we now have $\mathrm{e}^{-\Delta S} = q^{-\Delta_{\mathrm{v}}}$ from (14.75), so that

$$\Delta_{\mathrm{v}} = \frac{g}{4}\left((m_0+2)^2 - m_0^2\right) = 1 \tag{14.79}$$

and we recover (14.77).

14.4 Bulk Critical Exponents

We shall now see how to use the Coulomb gas (CG) technology of section 14.3 to compute a variety of critical exponents in loop models.

The watermelon exponents were derived by Nienhuis [35] and by Duplantier and Saleur (see [14] and references therein). The issues of their relation to the standard exponents of polymer physics [46], and to the Kac table (14.31), were discussed in [14].

Although the watermelon exponents are essentially magnetic-type exponents in the CG, they do not produce the standard magnetic exponent of the Potts model. The latter was derived by den Nijs [10], but we present here a somewhat different argument.

We have seen above that the dense O(n) model and the critical Potts model coincide on the level of the central charge, but their thermal exponents are different.

These are electric-type exponents in the CG, and were first computed by Nienhuis [37] and den Nijs [10].

Duplantier and Saleur have developed a range of geometrical applications of the exponents mentioned above. In [47, 14] they have generalised the configurational exponent γ to arbitrary polymer network conformations. From these a family of physically relevant contact exponents can be derived. They have also obtained the probability distribution of the winding angle of a SAW around one of its end points [48]. Finally, they have derived the exponents for a polymer at the collapse transition (theta point) from a specific model [19].

14.4.1 Watermelon Exponents

An important object in loop models is the operator $\mathscr{O}_\ell(\mathbf{x}_1)$ that inserts ℓ oriented lines at a given point $\mathbf{x}_1$. Microscopically, this can be achieved by violating the arrow conservation constraint at $\mathbf{x}_1$. For instance, in the O(n) model one can allow a vertex which is adjacent to one outgoing and two empty edges. Doing so at ℓ vertices in a small region around $\mathbf{x}_1$ yields a microscopic realisation of the composite operator $\mathscr{O}_\ell(\mathbf{x}_1)$.

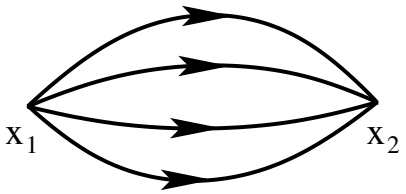

Fig. 14.6 Watermelon configuration with $\ell = 4$ legs.

If one had strict arrow conservation at all other vertices, the insertion of $\mathscr{O}_\ell(\mathbf{x}_1)$ would not lead to a consistent configuration. However, also inserting $\mathscr{O}_{-\ell}(\mathbf{x}_2)$, the operator that absorbs ℓ oriented lines in a small region around $\mathbf{y}$, will lead to consistent configurations (see Fig. 14.6) in which ℓ defect lines propagate from $\mathbf{x}_1$ to $\mathbf{x}_2$. Let $Z_\ell(\mathbf{x}_1,\mathbf{x}_2)$ be the corresponding constrained partition function. One then expects

$$\langle \mathscr{O}_\ell(\mathbf{x}_1)\mathscr{O}_{-\ell}(\mathbf{x}_2)\rangle \equiv \frac{Z_\ell(\mathbf{x}_1,\mathbf{x}_2)}{Z} \sim \frac{1}{|\mathbf{x}_1-\mathbf{x}_2|^{2\Delta_\ell}} \text{ for } |\mathbf{x}_1-\mathbf{x}_2| \gg 1\,. \tag{14.80}$$

The corresponding critical exponents Δ_ℓ are known as watermelon (or *fuseau*, or ℓ-leg) exponents. To compute them we first notice that the sum of the height differences around a closed contour encircling $\mathbf{x}_1$ but not $\mathbf{x}_2$ will be $a\ell$. Equivalently, one could place the two defects at the extremities of a cylinder [i.e., taking $\mathbf{x}_1 = (x,-\infty)$ and $\mathbf{x}_2 = (x,\infty)$], and the height difference would be picked up by any

non-contractible loop separating $\mathbf{x}_1$ and $\mathbf{x}_2$. This latter formulation makes contact with the defect lines (14.44) introduced when studying the compactified boson, the equivalent magnetic charge being $m_\ell = \frac{\ell a}{2\pi} = \frac{\ell}{2}$.

A little care is needed to interpret the configurations of $Z_\ell(\mathbf{x}_1, \mathbf{x}_2)$ in the model of un-oriented loops. The fact that all ℓ lines are oriented away from $\mathbf{x}_1$ prevents them from annihilating at any other vertex than $\mathbf{x}_2$. One should therefore like to think about them as ℓ marked lines linking $\mathbf{x}_1$ and $\mathbf{x}_2$, where each line carries the Boltzmann weight 1. This is consistent with not summing over the orientations of the defect lines in the oriented loop model. However, each oriented line can also pick up spurious phase factors $w(\alpha/2\pi)$, due to the local redistribution of loop weights, whenever it turns around the end points $\mathbf{x}_1$ and $\mathbf{x}_2$. These factors are however exactly cancelled if we insert in addition a vertex operator $\mathrm{e}^{ie_0\phi}$ (resp. $\mathrm{e}^{-ie_0\phi}$) at $\mathbf{x}_1$ (resp. $\mathbf{x}_2$) [11]. Note that these vertex operators do not modify the weighting of closed loops, since these must encircle either none of both of $\mathbf{x}_1, \mathbf{x}_2$. We conclude that $\Delta_\ell = \Delta_{e_0, m_\ell}$, and using (14.71) this gives

$$\Delta_\ell = \frac{1}{8} g \ell^2 - \frac{(1-g)^2}{2g} \,. \tag{14.81}$$

Interestingly, these exponents can be attributed to the Kac table under the identification (14.74). One has

$$\Delta_\ell = \begin{cases} 2h_{0,\ell/2} \text{ for the dense O}(n) \text{ model} \\ 2h_{\ell/2,0} \text{ for the dilute O}(n) \text{ model} \end{cases} \tag{14.82}$$

The appearance of half-integer indices [12, 14] is somewhat puzzling, whereas the fact that these exponents are located outside the fundamental domain of the Kac table reflects the non-local nature of the watermelon operators.

It should be noticed [49] that Δ_4 is irrelevant (resp. relevant) in the dilute (resp. dense) phase of the O(n) model, i.e., for $1 < g < 2$ (resp. $0 < g < 1$). This means that on lattices with vertices of degree ≥ 4, loop self-intersections are irrelevant in the dilute phase. On the other hand, for the dense phase such self-intersections are relevant and will induce a flow to a supersymmetric Goldstone phase [49] that is not described by the CG approach. In other words, Nienhuis' original approximation of the true O(n) model that led to (14.60) is exact in the continuum limit, but only in the dilute phase.

14.4.2 Standard Exponents of Polymer Physics

The relation of the standard exponents of critical phenomena (usually denoted α, β, γ, δ, ν, and η) to polymer physics has been discussed in details by de Gennes [46]. The end-to-end distance R of a SAW (and also the radius of gyration of a SAP) of chain length $l \gg 1$ behaves as

$$R^2 \sim l^{2\nu} \tag{14.83}$$

whereas the number of such objects in d dimensions (here both are supposed to have one monomer attached to a fixed point) scales like

$$\begin{aligned} \mathcal{N}_{\mathrm{SAW}} &\sim \mu^l l^{\gamma-1} \\ \mathcal{N}_{\mathrm{SAP}} &\sim \mu^l l^{-\nu d} \end{aligned} \tag{14.84}$$

where the connectivity constant μ can be related to the inverse of the critical temperature. There is a more detailed relation where the end-to-end distance R of the SAW has been fixed, valid for $R \gg 1$:

$$\frac{\mathcal{N}_{\mathrm{SAW}}(R)}{\mathcal{N}_{\mathrm{SAP}}} = R^{(\gamma-1)/\nu} H\left(\frac{R}{l^\nu}\right) \tag{14.85}$$

defining the scaling function $H(u)$, which obeys $H(u) \to \text{const}$ as $u \to 0$.

Standard scaling theory applied to the O(n) model then leads to the exponent relations

$$\begin{aligned} \Delta_1 &= 1 - \frac{\gamma}{2\nu} \\ \Delta_2 &= 2 - \frac{1}{\nu} \end{aligned} \tag{14.86}$$

In view of (14.81) this gives $\nu = \frac{1}{2}$, $\gamma = \frac{19}{16}$ for dense polymers ($g = \frac{1}{2}$) and $\nu = \frac{3}{4}$, $\gamma = \frac{43}{32}$ for dilute ones ($g = \frac{3}{2}$). The remaining critical exponents follow from standard scaling relations.

14.4.3 Magnetic Exponent in the Potts Model

The watermelon exponents can be said to be of the "magnetic" type, since they induce a magnetic type defect charge m_ℓ in the CG. The standard magnetic exponent, describing the decay of the spin-spin correlation function in the Potts model, is however not of the watermelon type. It can nevertheless be inferred from (14.71) as follows:

The probability that two spins situated at $\mathbf{x}_1$ and $\mathbf{x}_2$ are in the same Potts state is proportional, in the random cluster picture, to the probability that they belong to the same cluster. In the cylinder geometry this means that no winding loop separates $\mathbf{x}_1$ from $\mathbf{x}_2$. This can be attained in the CG by giving a weight $\bar{n} = 0$ to such loops. We have seen that inserting a pair of vertex operators with charge $\pm e$ at $\mathbf{x}_1$ and $\mathbf{x}_2$ leads exactly to this situation with $\bar{n} = 2\cos(\pi e)$, and so we need $e = \frac{1}{2}$. The scaling dimension of this excitation, with respect to the ground state which has $e = e_0$, is then

$$\Delta_{\mathrm{m}} = \Delta_{\frac{1}{2},0} - \Delta_{e_0,0} = \frac{1 - 4(1-g)^2}{8g}\,. \tag{14.87}$$

In particular we verify that for the Ising model, $g = \frac{3}{4}$, this yields $\Delta_{\rm m} = \frac{1}{8}$ as it should.

The location in the Kac table (14.31), using (14.74), is

$$\Delta_{\rm m} = 2h_{1/2,0}\,. \tag{14.88}$$

Note that this differs from the lowest possible watermelon excitation $\Delta_1 = 2h_{0,1/2}$, corresponding to one loop strand propagating along the length direction of the cylinder.[7] Indeed, the dominant configurations participating in the magnetic correlation function have *no* propagating strands, since the cluster containing $\mathbf{x}_1$ and $\mathbf{x}_2$ will typically wrap around the cylinder.

14.4.4 Thermal Exponents

As discussed in section 14.3.1, the Potts model at the critical temperature can be identified with the loop model (14.59) with homogeneous weights, $(\mathrm{e}^J - 1)/\sqrt{Q} = 1$. A deviation from the critical temperature will make the weights inhomogeneous, i.e., give different weights to the two possible states of the transition system in Fig. 14.1. Comparing this observation with the discussion of the marginality requirement in section 14.3.4, we see that the result is the appearance of electric charges $e = \pm 1$. Determining the correct sign of the charge requires a more careful microscopic analysis, which was first carried out by den Nijs [10] (see also [11, 35]). The end result for the thermal exponent is then

$$\Delta_{\rm t}^{\rm Potts} = \Delta_{-1,0} = \frac{3}{2g} - 1 \tag{14.89}$$

where we have used (14.71).

Under the identification (14.74), the location of this operator in terms of the Kac table (14.31) becomes [50]

$$\Delta_{\rm t}^{\rm Potts} = 2h_{2,1} = \frac{m+3}{2m}\,. \tag{14.90}$$

Note that this is an RG relevant operator for $m > 1$ [i.e., for coupling $\frac{1}{2} < g \leq 1$, or loop weight $0 < \sqrt{Q} \leq 2$], meaning that the critical point is unstable to a deviation from the critical temperature. On the other hand, for $0 < m < 1$ [i.e., for coupling $0 < g < \frac{1}{2}$, or loop weight $-2 < \sqrt{Q} < 0$] the thermal operator is irrelevant, implying the existence of a Berker-Kadanoff phase [51].

For the O(n) model, the microscopic derivation of the CG is different (see section 14.3.1), and by construction the sublattice symmetry can no longer be broken. Ac-

[7] Naively, the relation to the six-vertex model shows that in the Potts model these strands necessarily come in *pairs*, but this can be arranged by a suitable generalisation of the periodic boundary conditions, such that the six-vertex model is defined on an *odd* number of strands.

cordingly, a deviation in K from the critical values (14.61) must now couple to the next most relevant electrical charges $e = \pm 2$. Of these two, $e = 2$ has already been used for the marginality requirement $\Delta_{2,0} = 2$, and we expect in contrast a thermal exponent that depends on g. We are therefore led to

$$\Delta_{\mathrm{t}} = \Delta_{-2,0} = \frac{4}{g} - 2 \,. \tag{14.91}$$

A detailed derivation was first given by Nienhuis [37]. Note that the thermal operator is relevant for the dilute case ($1 < g < 2$), and irrelevant for the dense case ($0 < g < 1$). The entire low-temperature phase of the O(n) model will therefore renormalise towards the dense case. Exactly at zero temperature, a new critical theory emerges (see section 14.5).

The identification of Δ_{t} with the Kac table (14.31), via (14.74), is now

$$\Delta_{\mathrm{t}} = \begin{cases} 2h_{3,1} & \text{for the dense O}(n) \text{ model} \\ 2h_{1,3} & \text{for the dilute O}(n) \text{ model} \end{cases} \tag{14.92}$$

As a check, note that the critical Ising model is a special case of both the Potts model ($Q = 2$, or $g = \frac{3}{4}$) and of the O(n) model (dilute $n = 1$, or $g = \frac{4}{3}$). In both cases, the above formulae give $\Delta_{\mathrm{t}} = 1$ as they should.

14.4.5 Network Exponents

Duplantier and Saleur [47, 14] have shown how to generalise the exponent γ of (14.84) to more complicated network geometries. In the notation of section 14.4.1, consider a multi-point correlation function

$$\mathscr{C}_{\mathscr{G}} = \left\langle \mathscr{O}_{\ell_1}(\mathbf{x}_1) \mathscr{O}_{\ell_2}(\mathbf{x}_2) \cdots \mathscr{O}_{\ell_{\mathscr{V}}}(\mathbf{x}_{\mathscr{V}}) \right\rangle \tag{14.93}$$

involving $\mathscr{V}$ watermelon operators, where the k'th operator inserts an ℓ_k leg vertex at position $\mathbf{x}_k$. The orientations of the loop segments inserted do not matter in the following discussion, but must be chosen so that $\mathscr{C}_{\mathscr{G}}$ describes a well-defined network $\mathscr{G}$ (see Fig. 14.7). Accordingly we can assume that the indices ℓ_k are all positive.

Let n_ℓ be the number of ℓ-leg operators in $\mathscr{G}$, and let $\mathscr{E}$ be the total number of edges in $\mathscr{G}$. We then have the topological relations $\sum_\ell n_\ell \ell = 2\mathscr{E}$ and $\sum_\ell n_\ell = \mathscr{V}$.

Consider the case of a monodisperse network, where each of the $\mathscr{E}$ edges is constrained to have the same length l (with $l \gg 1$). Laplace transform and some scaling analysis then generalises (14.84) into

$$\frac{\mathscr{N}_{\mathscr{G}}}{\mathscr{N}_{\mathrm{SAP}}} \sim l^{\gamma_{\mathscr{G}} - 1 + \nu d} \tag{14.94}$$

with the network exponent

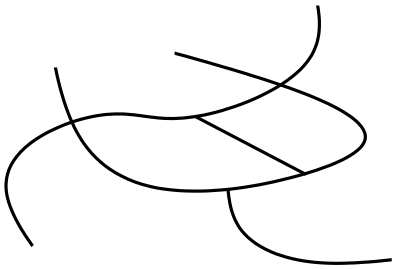

Fig. 14.7 A network $\mathscr{G}$ made of $\mathscr{E} = 10$ chains and $\mathscr{V} = 9$ vertices, with $n_1 = 5$, $n_3 = 3$, and $n_4 = 2$.

$$\gamma_{\mathscr{G}} = \nu \left[2(\mathscr{V} - 1) - \sum_{\ell} n_\ell \Delta_L \right] - (\mathscr{E} - 1) \tag{14.95}$$

Note that for the ordinary SAW topology ($n_\ell = 2\delta_{\ell,1}$), we retrieve $\gamma_{\mathscr{G}} = 2\nu(1 - \Delta_1)$, in agreement with (14.86).

For a polydisperse network, the total length l is freely distributed among the $\mathscr{E}$ edges in the network, and so one has simply to omit the last term $(\mathscr{E} - 1)$ in (14.95).

Special cases of (14.95) yield contact exponents, describing e.g. the probability that one of the end points of a SAW comes close to the midpoint of the walk.

14.4.6 Winding Angle Distribution

In section 14.4.1 we have seen that when computing the conformal weights of the watermelon operators, it was necessary to insert vertex operators $\mathrm{e}^{\pm i e_0 \phi}$ at the chain ends in order to cancel the spurious phase factors that occur in the oriented loop model due to the winding of the SAW around its end points. By a generalisation of this argument, Duplantier and Saleur [48] have shown how to actually compute the winding angle distribution of a SAW.

Consider an O(n) model with an arbitrary number of closed loops, each of fugacity

$$n = 2\cos(\pi e_0) = -2\cos(\pi g)\,, \tag{14.96}$$

and a single open walk (the SAW, for $n \to 0$) with end points $\mathbf{x}_1$ and $\mathbf{x}_2$. In the oriented loop picture, the walk is taken to be oriented from $\mathbf{x}_1$ to $\mathbf{x}_2$. To count precisely its number of windings around each $\mathbf{x}_i$, these two points are connected to infinity through parallel half lines $\mathscr{L}_i$, as shown in Fig. 14.8. Then let the winding number n_i be the signed number of times the walk crosses $\mathscr{L}_i$, the sign being positive for an anti-clockwise crossing. In the scaling limit we expect $n_i \gg 1$, and so even though n_i has been defined as an integer it can be used to deduce the winding angle.

One now compares on one hand the correlation function $\left\langle \exp(i\pi e_1 n_1 + i\pi e_2 n_2) \right\rangle$ in the O(n) model, and on the other hand $\left\langle \exp(i e'_1 \phi(\mathbf{x}_1) + i e'_2 \phi(\mathbf{x}_2)) \right\rangle$ in the equiva-

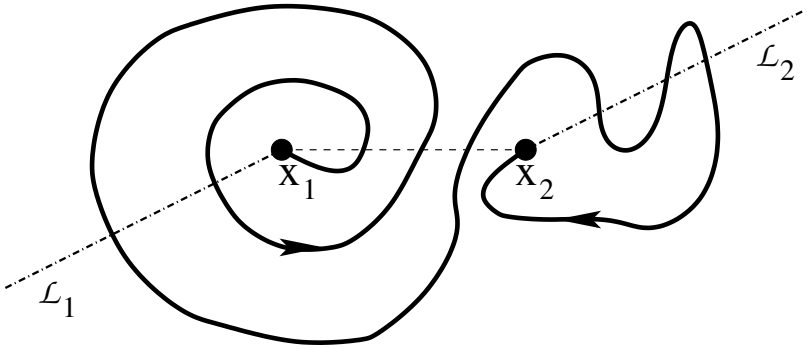

Fig. 14.8 SAW oriented from $\mathbf{x}_1$ to $\mathbf{x}_2$ with winding numbers $n_1 = 2$ and $n_2 = -1$.

lent height model, where we recall that ϕ is the height function. These will in general give incorrect weights (i.e., $\neq n$) to loops that surround both $\mathbf{x}_1$ and $\mathbf{x}_2$. A careful study of the complex phase factors arising in these correlators, and in the oriented loop/height model shows that the two correlators are identical, and the surrounding loops are weighted correctly, provided that we satisfy the conditions

$$e_1' = e_1 - e_0, \qquad e_2' = e_2 - e_0, \qquad e_1 + e_2 = 0 \text{ or } 2e_0\,. \tag{14.97}$$

We shall take $e_1 = -e_2 \equiv e$ in the last condition.

This deals with the electric charges in the CG picture. The magnetic charges needed to insert the walk are $m_1 = -m_2 \equiv m$ with $m = 1$ as usual. The joint value of the correlators is then, from (14.50),

$$\sim |\mathbf{x}_1 - \mathbf{x}_2|^{-2\Delta(e)} \qquad \text{with } \Delta(e) = \frac{1}{2}\left(\frac{e^2}{2g} + g\right) \tag{14.98}$$

valid in the scaling limit $|\mathbf{x}_1 - \mathbf{x}_2| \gg 1$. This result can be written

$$\left\langle \mathrm{e}^{i\pi e(n_1 - n_2)} \right\rangle = \mathrm{e}^{-\frac{e^2}{g}\log|\mathbf{x}_1 - \mathbf{x}_2|} \tag{14.99}$$

where we have normalised with respect to the same correlator with $e = 0$ (but still $m = 1$). Noting that this is Gaussian in e, the distribution of the winding angle $\theta = \theta_1 - \theta_2 = 2\pi(n_1 - n_2)$ itself is also Gaussian, and after a Fourier transformation we obtain finally the normalised distribution

$$P(\theta) = \left(\frac{16\pi \log|\mathbf{x}_1 - \mathbf{x}_2|}{g}\right)^{-1/2} \exp\left(-\frac{g\theta^2}{16\log|\mathbf{x}_1 - \mathbf{x}_2|}\right) \tag{14.100}$$

Usually we are interested in the fixed-length rather than the fixed-extremities ensemble, in which case it suffices to replace $|\mathbf{x}_1 - \mathbf{x}_2|$ by l^ν in (14.100), for a walk of length l. Another remark is that the winding numbers n_1 and n_2 can be argued to

be independent in the scaling limit, and so if one is interested in just one of them it suffices to replace (14.100) by a distribution of half the width.

The above argument was shown for a SAW (as in [48]), but can easily be adapted to the windings of a SAP constrained to go through two fixed points $\mathbf{x}_1$ and $\mathbf{x}_2$. The relevant magnetic charge is then $m = 2$, but the remainder of the argument is essentially unchanged.

The issue of winding angle distribution for a SAW, and its relation with that of Brownian walks, was studied further by Saleur [52].

14.4.7 Polymer Collapse: the Theta Point

The dilute SAW is a model of a polymer in a good solvent. When this assumption fails, e.g., upon lowering the temperature of the solvent, the effective attraction between the monomers increases, and eventually the polymer undergoes a collapse transition, first described by Flory [53]. The corresponding critical temperature is traditionally called Θ, or the theta point. It was argued by de Gennes [54, 46] that this is a tricritical point: intuitively this means that with respect to the critical, or dilute, SAW—obtained in our framework by tuning the monomer fugacity to a particular value—one additional parameter, viz. the effective monomer-monomer interaction, has to be adjusted to its critical value.

Duplantier and Saleur [19] have proposed a particularly simple model of the monomer-monomer interaction that is capable of capturing the physics of the theta point. Their argument shows that the corresponding universality class is that of the dense O($n = 1$) model, i.e., of critical percolation, and the exponents follow readily. The argument runs as follows.

Consider a SAW on the usual hexagonal lattice, but in the presence of annealed dilution. To be specific, each lattice face contains a "defective solvent" with probability p, and an "ideal solvent" with probability $1 - p$, independently for each face. The SAW is constrained to touch only lattice faces containing an ideal solvent, as shown in Fig. 14.9.

In the partition function, one may first sum over the configurations of the solvent consistent with a fixed configuration of the SAW, and then over those of the SAW itself. In the first sum, any face not touching the SAW contributes a trivial factor of one, whereas each of the remaining faces yields a weight $(1 - p)$. Let N_2 (resp. N_3) be the number of faces which are adjacent to two (resp. three) successions of monomers which are non-subsequent along the SAW. [In other words, let N_k be the number of hexagons having $2k$ occupied external legs.] The total face weight is then simply

$$(1 - p)^{l+1-N_2-2N_3} \tag{14.101}$$

where l is the length (number of edges) of the SAW. Clearly this is a kind of short-range attraction between the monomers in the SAW, albeit a somewhat peculiar one.

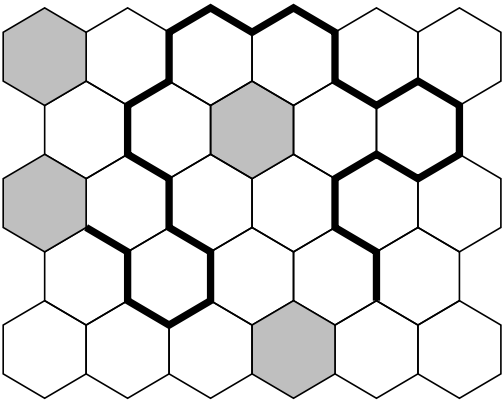

Fig. 14.9 Model of a polymer at the theta point. The SAW lives on a hexagonal lattice, but is not allowed to share an edge with any of the faces containing a defective solvent, here shown shaded in grey.

One now argues that the parameter p has a critical value p_c. If $p < p_c$ the system should renormalise towards the standard dilute SAW, and if $p > p_c$ the solvent deficiencies will percolate and the SAW will be in the dense phase. The threshold p_c must be that of site percolation on the triangular lattice, and so $p_c = \frac{1}{2}$ exactly. But exactly at p_c, defective and ideal faces are equiprobable and so form clusters which may equally well be described in terms of their contours, as an O(n) model of loops (14.60) with trivial parameters, $n = 1$ and $K = 1$. The latter value is precisely[8] the dense loop solution of (14.61).

We conclude that polymers at the theta point are described by the CG of the dense O($n = 1$) model, with coupling constant $g = \frac{2}{3}$. In particular, the watermelon exponents (14.81) read

$$\Delta_\ell = \frac{\ell^2 - 1}{12}\,. \tag{14.102}$$

The standard polymer exponents (14.84) describing the theta point are related to these through the scaling relations (14.86):

$$\eta = 2\Delta_1 = 0\,, \qquad \nu = \frac{1}{2 - \Delta_2} = \frac{4}{7}\,, \qquad \gamma = (2-\eta)\nu = \frac{8}{7}\,. \tag{14.103}$$

Finally, the thermal exponent ν' describing how the size of defective solvent clusters diverges, $\xi \sim |p - p_c|^{-\nu'}$ as $p \uparrow p_c$ is given by $\nu' = 1/(2 - \Delta_4) = \frac{4}{3}$, and so the so-called crossover exponent is

$$\phi = \frac{\nu}{\nu'} = \frac{3}{7}\,. \tag{14.104}$$

[8] Even if this had not precisely been the case, the outcome of the argument would be the same, since the dense loop solution of (14.61) is RG attractive in K by (14.91). This observation is certainly part of the explanation that the variant models explored in [55] yield unchanged critical exponents.

Although the theta point exponents (14.103)–(14.104) are in very good agreement with those of numerical simulations, and even experiments, the original paper [19] was subsequently challenged by a number of authors. Indeed, the interaction between monomers employed is quite peculiar—it corresponds to attractions between nearest neighbour vertices and a *subset* of the next-nearest neighbour vertices—and one may fear that the universality class described is not the required tricritical point, but an even higher multicritical point.

To meet this criticism, Duplantier and Saleur produced a second paper [55] in which they examined numerically a certain number of variant models, involving different local monomer interactions, anisotropy, and using different lattices. In all cases the exponents (14.103)–(14.104) were shown to be unchanged, and far from the values of any variant proposal. We can therefore conclude that in spite of its simplicity the original model captures the correct theta point physics and produces the exact values of the corresponding critical exponents.

14.5 Fully Packed Loop Models

In section 14.3 we have seen how to solve loop models by writing a Liouville field theory for their associated height model. We have discussed in detail two models, the Q-state Potts and the O(n) model. In both cases, we exploited a bijection between the configurations of oriented loops and those of a scalar (one-component) height variable $h(\mathbf{x})$ defined on the lattice faces $\mathbf{x}$. There does however exist geometric models whose microscopic formulation allows for the definition of a vector height $\mathbf{h}(\mathbf{x}) \in \mathbb{R}^D$ with $D > 1$. A necessary (but not sufficient) condition for this to happen seems to be that the objects (loops, tiles, colours, ...) be maximally packed on the lattice.

Tiling models are nice examples of statistical models possessing vector height mappings, provided that the shapes of the tiles and the lattice are chosen carefully. For example, one obtains $D = 2$ dimensional heights by tiling the square lattice with two different types of dimers [56], or by linear trimers [57], or by tiling the triangular lattice with triangular trimers [58]. In general, such models are either non-critical, or described in the continuum by D free bosons. For example, all of the tiling problems just mentioned have been shown (analytically and/or numerically) to have central charge $c = 2$.

In this section we are rather interested in models of fully packed loops (FPL) possessing a vector height. When critical, such models can be described in terms of a vectorial Coulomb gas (CG), generalising the working of section 14.3. In particular, the non-local nature of the loops allows for the existence of a background electric charge, and so one or more control parameters (typically the loop weights) permit one to change c and the critical exponents continuously. This amounts to a rather more interesting continuum limit than that of the tiling problems.

In section 14.5.1 we give some examples of FPL models and establish their height mappings. These models turn out to be highly non-universal, in the sense that D—

and hence ultimately the values of the critical exponents—depends on the underlying lattice. A necessary condition for the existence of a non-trivial continuum limit seems to be that the underlying lattice is bipartite [59].

The CG construction for these models is presented in some detail (see section 14.5.2), as it sheds further light both on the ideal state construction and on the marginality requirement. Bulk critical exponents are derived in section 14.5.3. We conclude by a few further remarks on the underlying quantum group symmetries of the FPL models, and the possibility of coupling them to two-dimensional quantum gravity.

14.5.1 Three Loop Models with a Vector Height Mapping

The loop model based on the Q-state Potts model is an example of an FPL model, since its loops jointly visit every vertex of the lattice (twice). But since its height mapping is one-dimensional (see section 14.3.2) this is not what were are interested in here.

Let us instead revisit the O(n) model (14.60) on the hexagonal lattice. The allowed vertices are shown in Fig. 14.2. It is easy to see that on a lattice with periodic boundary conditions respecting the three-sublattice structure of the lattice faces, the number of voids (of weight $T \equiv 1/K$) must be even, whence the model is symmetric under $T \to -T$. The fact (14.91) that the low-temperature branch of (14.61) is RG attractive in T then implies that the $T = 0$ manifold is a line of repulsive fixed points [60]. A numerical study [60] further reveals that these fixed points are critical for $|n| \leq 2$. For brevity we shall refer to this O(n) model at $T = 0$ simply as the FPL model in the remainder of this section. In the polymer limit $n \to 0$ it describes Hamiltonian circuits (SAP's) and paths (SAW's) on the hexagonal lattice.

In the oriented loop model corresponding to the FPL model there are three types of edges: A) empty edges, B) occupied edges pointing from an even to an odd vertex, and C) occupied edges pointing from odd to even. We shall often refer to these edge labels as colours. Denoting the height change when traversing any one of these edges by **A**, **B**, or **C**, occupied vertices lead to the consistency requirement

$$\mathbf{A} + \mathbf{B} + \mathbf{C} = \mathbf{0}, \tag{14.105}$$

whereas empty vertices require $\mathbf{A} = \mathbf{0}$. By symmetry, one must then choose $\mathbf{B} = +a$ and $\mathbf{C} = -a$ for some scalar a, as was indeed done in section 14.3.2. But if $T = 0$, empty vertices are forbidden, and the only requirement is (14.105). The height differences can then be taken as two-dimensional vectors pointing from the centre to the vertices of an equilateral triangle. Since we have shown carefully in section 14.2.7 that the normalisation of the heights drops out from the final results for the critical exponents, we henceforth adopt the choice

$$\mathbf{A} = \left(\frac{1}{\sqrt{3}}, 0\right), \qquad \mathbf{B} = \left(-\frac{1}{2\sqrt{3}}, \frac{1}{2}\right), \qquad \mathbf{C} = \left(-\frac{1}{2\sqrt{3}}, -\frac{1}{2}\right). \tag{14.106}$$

Kondev, de Gier and Nienhuis [20] used the height mapping (14.106) as the starting point for solving the FPL model exactly.

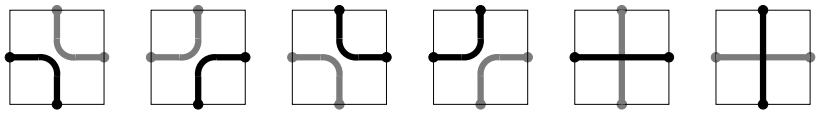

Fig. 14.10 The six vertices defining the FPL^2 model.

Another model that we shall consider is the so-called FPL^2 model on the square lattice, which was defined by Kondev and Henley [61] and solved by Jacobsen and Kondev [21]. This is a model of *two* different types of fully packed loops (whence the superscript in the denomination FPL^2), henceforth referred to as black and grey. The allowed vertices are shown in Fig. 14.10. The partition function is defined by assigning independent fugacities, n_{b} and n_{g}, to the two types of loops,

$$Z = \sum_{\mathscr{G}} n_{\mathrm{b}}^{N_{\mathrm{b}}} n_{\mathrm{g}}^{N_{\mathrm{g}}}, \tag{14.107}$$

where N_{b} (resp. N_{g}) is the number of black (resp. grey) loops, and $\mathscr{G}$ is the set of all allowed loop configurations.

A number of special cases of the FPL^2 model are of special interest: suffice it here to say that the limit $n_{\mathrm{g}} = 1$, $n_{\mathrm{b}} \to 0$ describes Hamiltonian circuits and paths on the square lattice.

The two types of loops can be oriented independently, giving rise to four types of edges: A) black edges oriented from the even to the odd sublattice, B) black edges oriented from the odd to the even sublattice, C) grey even-to-odd edges, and D) grey odd-to-even edges. These define the height differences for the height model on the dual lattice, with the consistency requirement

$$\mathbf{A} + \mathbf{B} + \mathbf{C} + \mathbf{D} = \mathbf{0} \tag{14.108}$$

that the total height change when encircling any vertex be zero. We have then a $D = 3$ dimensional height model, and by symmetry we can take the height differences to point from the centre to the vertices of a regular tetrahedron:

$$\mathbf{A} = (-1,1,1), \quad \mathbf{B} = (1,1,-1), \quad \mathbf{C} = (-1,-1,-1), \quad \mathbf{D} = (1,-1,1). \tag{14.109}$$

The last model to be discussed in this section is obtained from the FPL^2 model by attributing local vertex weights in addition to the loop weights. By rotational symmetry, it suffices to give a special weight w_{X} to the last two vertices in Fig. 14.10,

$$Z = \sum_{\mathscr{G}} n_{\mathrm{b}}^{N_{\mathrm{b}}} n_{\mathrm{g}}^{N_{\mathrm{g}}} w_{\mathrm{X}}^{V}, \tag{14.110}$$

where V is the number of vertices where the two types of loops cross, and $\mathscr{G}$ has the same meaning as in (14.107). We shall refer to this as the semi-flexible loop (SFL) model. It was first solved by Jacobsen and Kondev [62].

The polymer limit ($n_{\mathrm{g}} = 1$, $n_{\mathrm{b}} \to 0$) of the SFL model has been proposed as a model of protein melting by Flory half a century ago [63].

14.5.2 Coulomb Gas Construction

We now discuss how to dress the Coulomb gas (CG) for the three models of oriented loops (FPL, FPL^2, and SFL) just introduced. As in section 14.3 the CG will eventually take the form of a Liouville field theory, but with electromagnetic charges which are D-dimensional vectors. The construction for the FPL^2 and SFL models will only start differing when imposing the marginality requirement.

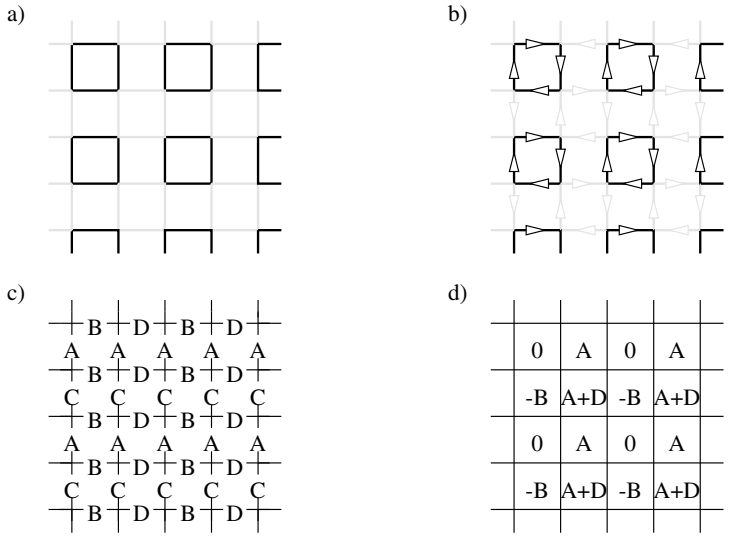

Fig. 14.11 An ideal state in the FPL^2 model shown in terms of a) loops, b) oriented loops, c) edge colourings, and d) the height mapping.

The first issue is to determine the analogue of the compactification radius, which now takes the form of a D-dimensional lattice. To this end, the ideal state construction [61] is a very convenient tool.

We define first the *ideal states* as periodic arrangements of the colours, such that the microscopic height is maximally flat. An example of an FPL^2 ideal state is shown in Fig. 14.11. In general, an ideal state is obtained by selecting a permutation of the edge labels around a fixed vertex; the arrangement is then extended to the whole lattice in such a way that alternations of any pair of colours form as many short

cycles as possible. For the FPL model there are 6 ideal states; in these all 3 colour pairs form short cycles (of length 6); and the colour pair BC defines the loops. In the FPL^2 model there are 24 ideal states; in these 4 out of 6 colour pairs form short cycles (of length 4); and the colour pairs AB and CD define black and grey loops respectively.

We construct next the *ideal state graph* $\mathscr{I}$. For this, we define a *transition* between two ideal states as a transposition of a colour pair forming a short cycle. To each transition we associate a vector in $\mathbb{R}^D$ equal to the difference between the average height in the two concerned ideal states. By definition, a transition changes only the heights on the faces surrounded by transposed short cycles. In $\mathscr{I}$, each vertex represents an ideal state, and each edge represents a transition. The graph $\mathscr{I}$ is embedded into $\mathbb{R}^D$ by letting each edge correspond to the vector associated with the transition between ideal states.

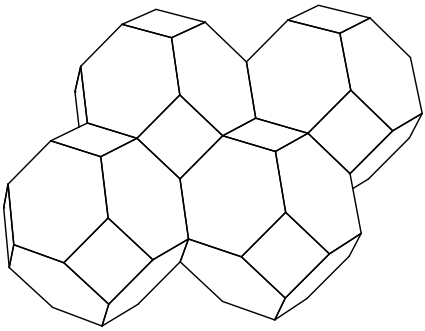

Fig. 14.12 The ideal state graph of the FPL^2 model.

For the FPL model, $\mathscr{I}$ turns out to be a hexagonal lattice [20], and for the FPL^2 model it is a tiling of $\mathbb{R}^3$ with truncated octahedra [61] (also known as the Wigner-Seitz cell of a body-centered cubic lattice). The latter $\mathscr{I}$ is shown in Fig. 14.12. Crucially, any *fixed* ideal state is represented infinitely many times in $\mathscr{I}$ and forms a lattice which we shall call the *repeat lattice* $\mathscr{R}$. It turns out that $\mathscr{R}$ is spanned by the vectors $\mathbf{A}-\mathbf{B}$, $\mathbf{B}-\mathbf{C}$ (and $\mathbf{C}-\mathbf{D}$ for the FPL^2 model). In other words, for the FPL model $\mathscr{R}$ is a triangular lattice of edge length 1 in the normalisation (14.105), and for the FPL^2 model $\mathscr{R}$ is a face-centered cubic lattice with a conventional cubic cell of edge length 4 in the normalisation (14.108).

In the CG construction, the height is then compactified with respect to $\mathscr{R}$, i.e.,

$$\mathbf{h}(\mathbf{x}) \in \mathbb{R}^D/\mathscr{R}. \tag{14.111}$$

In particular, the magnetic charges $\mathbf{m} \in \mathscr{R}$, and the electric charges $\mathbf{e} \in \mathscr{R}^*$, where $\mathscr{R}^*$ denotes the reciprocal lattice of $\mathscr{R}$.

The Liouville field theory is again described by the action (14.69), consisting of an elastic term $S_{\rm E}$, a boundary term $S_{\rm B}$, and the Liouville potential $S_{\rm L}$. We now describe these three terms in turn.

The *elastic term* is constrained by rotational invariance in real $d = 2$ dimensional space to take the form

$$S_{\rm E} = \frac{1}{2} \int {\rm d}^2{\bf x} \, K_{\alpha\beta} \, \partial h^\alpha \cdot \partial h^\beta \, , \tag{14.112}$$

where $\partial = (\partial_1, \partial_2)$ is the usual gradient. The D-dimensional tensor $K_{\alpha\beta}$ is further constrained by the loop reversal symmetries: $\mathbf{B} \leftrightarrow \mathbf{C}$ for the FPL model, while for the FPL^2 model one has both $\mathbf{A} \leftrightarrow \mathbf{B}$ and $\mathbf{C} \leftrightarrow \mathbf{D}$. The result for the FPL model is simply

$$S_{\rm E} = \frac{1}{2} \int {\rm d}^2{\bf x} \, g_\alpha (\partial h^\alpha)^2 \, . \tag{14.113}$$

with coupling constants $g_1 \equiv K_{11}$, $g_2 \equiv K_{22}$, and $g_1 = g_2$. For the FPL^2 model one obtains first a more complicated result

$$S_{\rm E} = \frac{1}{2} \int {\rm d}^2{\bf x} \left\{ K_{11} [(\partial h^1)^2 + (\partial h^3)^2] + 2 K_{13} (\partial h^1 \cdot \partial h^3) + K_{22} (\partial h^2)^2 \right\} , \tag{14.114}$$

which can however be diagonalised by a change of coordinates in height space,

$$\tilde{h}^1 = \frac{h^1 - h^3}{2} , \qquad \tilde{h}^2 = h^2 , \qquad \tilde{h}^3 = \frac{h^1 + h^3}{2} \tag{14.115}$$

yielding once again (14.113) for $\tilde{h}^\alpha$, but now with three *unrelated* coupling constants $g_1 \equiv 2(K_{11} - K_{13})$, $g_2 \equiv K_{22}$, and $g_3 \equiv 2(K_{11} + K_{13})$. Note that magnetic charges $\mathbf{m}$ transform as (14.115), whereas electric charges $\mathbf{e}$ transform according to the reciprocal transformation (swap tilded and untilded quantities). Henceforth we shall write everything in terms of the new heights $\tilde{h}^\alpha$ and electromagnetic charges $(\tilde{\mathbf{e}}, \tilde{\mathbf{m}})$, but drop the tildes to lighten the notation.[9]

Let us now parametrise the loop weights as

$$n = 2 \cos(\pi e_0) \tag{14.116}$$

for the FPL model, and

$$n_{\rm b} = 2 \cos(\pi e_{\rm b}) , \qquad n_{\rm g} = 2 \cos(\pi e_{\rm g}) \tag{14.117}$$

for the FPL^2 model. The *boundary term* $S_{\rm B}$ in (14.69) reads in vector notation

[9] It would seem tempting in a review like this to impose the transformation (14.115) right from the beginning and choose $\mathbf{A} = (-1,1,0)$, $\mathbf{B} = (1,1,0)$, $\mathbf{C} = (0,-1,-1)$, $\mathbf{D} = (0,-1,1)$ instead of (14.108). But note that (14.108) respects the full permutation symmetry of the four colours: the scalar product of any two vectors in (14.108) is -1. With (14.115) this symmetry is broken in a very particular way that could not have been guessed from the outset, and which reflects the choice of defining the loops from the colour pairs AB and CD.

$$S_{\mathrm{B}} = \frac{\mathrm{i}}{4\pi} \int \mathrm{d}^2\mathbf{x}\, (\mathbf{e}_0 \cdot \mathbf{h}) \mathscr{R}(\mathbf{x}) \tag{14.118}$$

and $\mathbf{e}_0$ is determined as in section 14.3 by requiring that wrapping loops of each type be weighted correctly. For instance, for the FPL^2 model we must have

$$\mathbf{e}_0 \cdot \mathbf{A} = \pi e_{\mathrm{b}}\,, \quad \mathbf{e}_0 \cdot \mathbf{B} = -\pi e_{\mathrm{b}}\,, \quad \mathbf{e}_0 \cdot \mathbf{C} = \pi e_{\mathrm{g}}\,, \quad \mathbf{e}_0 \cdot \mathbf{D} = -\pi e_{\mathrm{g}}\,, \tag{14.119}$$

which fixes the background electric charge as

$$\mathbf{e}_0 = -\pi(e_{\mathrm{b}}, 0, e_{\mathrm{g}}) \tag{14.120}$$

The analogous result for the FPL model is

$$\mathbf{e}_0 = 2\pi(0, e_0)\,. \tag{14.121}$$

The sceptical reader may object that the ideal state graph $\mathscr{I}$ is not really necessary to determine the repeat lattice $\mathscr{R}$. Indeed, it suffices to notice that the fundamental height dislocations (magnetic charges) allowed by the microscopic model is the difference between two of the colour vectors (14.105) or (14.108). However, the real use of $\mathscr{I}$ is for determining the *Liouville term*

$$S_{\mathrm{L}} = \int \mathrm{d}^2\mathbf{x}\, w[\mathbf{h}(\mathbf{x})]\,, \tag{14.122}$$

where $\exp(-w[\mathbf{h}(\mathbf{x})])$ is the scaling limit of the (complex) microscopic vertex weights in the oriented loop representation. To this end, we focus for a while on the FPL^2 model.

Denoting by $(\sigma_1, \sigma_2, \sigma_3, \sigma_4)$ the configuration of colours when going anticlockwise around an even vertex, the microscopic weights may be written compactly as

$$w(\mathbf{h}) = \frac{\mathrm{i}}{16}\, \mathbf{e}_0 \cdot [(\sigma_1 - \sigma_3) \times (\sigma_2 - \sigma_4)]\,. \tag{14.123}$$

Fourier analysing this formula, i.e., writing it as a sum of vertex operators, one arrives at

$$w(\mathbf{h}) = \sum_{\mathbf{e} \in \mathscr{R}^*_w} \tilde{w}_{\mathbf{e}} \exp(\mathrm{i}\mathbf{e} \cdot \mathbf{h})\,. \tag{14.124}$$

where $\mathscr{R}^*_w$ is a *proper* sublattice of $\mathscr{R}^*$ whose shortest vectors are the twelve next shortest vectors in the bcc-lattice $\mathscr{R}^*$.

Coming back to the FPL model one finds similarly that $\mathscr{R}^*_w$ is spanned by the next shortest vectors in $\mathscr{R}^*$.

To impose the *marginality requirement* and extract critical exponents we need to know the dimension of electromagnetic operators. In the basis where the coupling constant tensor g^α is diagonal, as in (14.113), this is a straightforward generalisation of the usual CG formula (14.71), which reads in the normalisation of the present section

$$\Delta_{\mathbf{e},\mathbf{m}} = \frac{1}{4\pi}\left[\frac{1}{g_\alpha} e_\alpha (e_\alpha - 2e_{0\alpha}) + g_\alpha (m^\alpha)^2\right]. \tag{14.125}$$

The FPL model is now solved by noting that $\mathbf{e}^{(0)} = (0, 4\pi)$ is the most relevant electric charge in $\mathscr{R}^*_w$. Solving the marginality requirement $\Delta_{\mathbf{e}^{(0)},\mathbf{0}} = 2$ then fixes the CG coupling in terms of the loop weight:

$$g = 2\pi(1 - e_0). \tag{14.126}$$

The case of the FPL^2 model is considerably more intricate. Moreover, determining the correct marginality requirement is the one and only point where the analysis differs from that of the SFL model. Referring to [21, 62] for a detailed discussion, the outcome is that the vectors

$$\mathbf{e}^{(1)} = (-2\pi, 0, 0), \qquad \mathbf{e}^{(2)} = (0, 0, -2\pi) \tag{14.127}$$

act as screening charges in both the FPL^2 and the SFL models, whereas an additional symmetry of the FPL^2 model implies that it possesses two extra screening charges

$$\mathbf{e}^{(3)} = (-\pi, \pi, -\pi), \qquad \mathbf{e}^{(4)} = (-\pi, \pi, -\pi). \tag{14.128}$$

The marginality requirement then fixes

$$g_1 = \frac{\pi}{2}(1 - e_{\mathrm{b}}), \qquad g_3 = \frac{\pi}{2}(1 - e_{\mathrm{g}}) \tag{14.129}$$

for both models. The extra screening charges in the FPL^2 model imply a third relation

$$\frac{1}{g_2} = \frac{1}{g_1} + \frac{1}{g_3}, \tag{14.130}$$

whereas in the SFL model g_2 remains a non-universal function of the parameter w_{X} appearing in (14.110).

In the critical regime $|n_{\mathrm{b}}|, |n_{\mathrm{g}}| \leq 2$ we have $g_1, g_3 \leq \frac{\pi}{2}$ from (14.129), and so $g_2 \leq \frac{\pi}{4}$ when $w_{\mathrm{X}} = 1$ (i.e., in the FPL^2 model). It is easy to see that increasing w_{X} will make the height interface stiffer in the 2-direction, and so will increase g_2. When $g_2 > \frac{\pi}{2}$ the operator that discretises the height in the 2-direction becomes relevant, and so the height profile becomes flat in the continuum limit, meaning that the model is no longer critical. We deduce that precisely at $g_2 = \frac{\pi}{2}$ the model stands at a Kosterlitz-Thouless transition; in the polymer limit this is the protein melting transition [62] that Flory [63] originally aimed at describing. Exact exponents can therefore be computed at this KT transition.

However, the CG method does not permit us to solve the SFL model for generic values of w_{X}, the relation to g_2 being unknown. However, note that all critical exponents can be expressed in terms of just one unknown parameter g_2. Furthermore, for any given values of n_{b}, n_{g} and w_{X}, numerical transfer matrix methods allow us to determine g_2 to very high precision [62].

14.5.3 Bulk Critical Exponents

In a D-dimensional CG the central charge is $c = D + 12\Delta_{\mathbf{e}_0,\mathbf{0}}$, giving

$$c = \begin{cases} 2 - \frac{6e_0^2}{1-e_0} & \text{for the FPL model} \\ 3 - 6\left(\frac{e_b^2}{1-e_b} + \frac{e_g^2}{1-e_g}\right) & \text{for the FPL}^2 \text{ and the SFL models.} \end{cases} \tag{14.131}$$

Watermelon configurations are obtained by violating the colouring constraint at two vertices $\mathbf{x}_1$ and $\mathbf{x}_2$. For example, in the FPL model a vertex whose adjacent edges are coloured $(\mathbf{A},\mathbf{A},\mathbf{B})$ will insert a 1-leg operator of magnetic charge $\mathbf{m}_1 = \mathbf{A} - \mathbf{C}$, whereas the vertex $(\mathbf{A},\mathbf{B},\mathbf{B})$ gives a 2-leg operator of charge $\mathbf{m}_2 = \mathbf{B} - \mathbf{C}$. Higher-leg operators are obtained by taking multiples of these basic charges. In all cases, a further electric charge $\mathbf{e}_0$ is needed to correct the spurious phase factors due to the polymer strands winding around their insertion point. The ℓ-leg watermelon exponents are then found from (14.125):

$$\Delta_\ell = \begin{cases} \frac{1}{8}g\ell^2 - \frac{(1-g)^2}{2g} & \text{for } \ell \text{ even} \\ \frac{1}{8}g\ell^2 - \frac{(1-g)^2}{2g} + \frac{3g}{8} & \text{for } \ell \text{ odd} \end{cases} \tag{14.132}$$

where we have set $g = 1 - e_0$ to facilitate the comparison with (14.81).

Similar results can be obtained for the FPL^2 [21] and SFL [62] models. Note that the watermelon strands can now be either black or grey, and the parity of the number of black strands must equal the parity of the number of grey strands. We here state the results only for the simplest case of the FPL^2 model where grey strands are ignored and grey loops are assigned a trivial fugacity, $n_g = 1$. This gives for the black ℓ-leg watermelon exponents

$$\Delta_\ell = \begin{cases} \frac{1}{8}g\ell^2 - \frac{(1-g)^2}{2g} & \text{for } \ell \text{ even} \\ \frac{1}{8}g\ell^2 - \frac{(1-g)^2}{2g} + \frac{g}{3g+2} & \text{for } \ell \text{ odd} \end{cases} \tag{14.133}$$

where again we have set $g = 1 - e_b$ for easy comparison.

With the watermelon exponents (14.132)–(14.133) many of the exponents discussed in section 14.4 (e.g., network and contact exponents) follow as before. We focus here on the *conformational exponents* for Hamiltonian circuits and paths on the hexagonal and square lattices, obtained from taking the polymer limit in the FPL and FPL^2 models and using the scaling relations (14.86). On both lattices $\nu = \frac{1}{2}$, a trivial result which however serves as a check of the above CG construction. More interestingly, we have

$$\gamma_{\text{hex}} = 1\,, \qquad \gamma_{\text{sq}} = \frac{117}{112}\,. \tag{14.134}$$

This means that the end points of a Hamiltonian SAW on the hexagonal lattice do not interact in the continuum limit, whereas they repel each other weakly on the square lattice.

Finally, one can compute the *thermal exponent* associated with breaking the $T = 0$ constraint that all lattice vertices be visited by a loop. For the FPL model the corresponding defect vertex is $(\mathbf{A},\mathbf{A},\mathbf{A})$ of magnetic charge $\mathbf{m}_{\mathrm{t}} = 3\mathbf{A}$, yielding

$$\Delta_{\mathrm{t}} = \Delta_{\mathbf{0},\mathbf{m}_{\mathrm{t}}} = \frac{3g}{2}\,. \tag{14.135}$$

Note that this is always RG relevant, confirming the result of section 14.5.1 that the $T = 0$ manifold is a line of repulsive fixed points.

For the FPL^2 model the defect $(\mathbf{C},\mathbf{D},\mathbf{C},\mathbf{D})$ of magnetic charge $\mathbf{m}_{\mathrm{t}} = 2(\mathbf{C}+\mathbf{D})$ excludes black loops from visiting the defect vertex. Again we specialise the general result [21] to the case where grey loops are weighted trivially ($n_{\mathrm{g}} = 1$):

$$\Delta_{\mathrm{t}} = \Delta_{\mathbf{0},\mathbf{m}_{\mathrm{t}}} = \frac{4g}{3g+2}\,. \tag{14.136}$$

Once again this is always RG relevant.

14.5.4 Further Remarks

We conclude this section with a few further remarks about the fully packed loop models.

The FPL model [64] and the FPL^2 model with equal fugacities $n_{\mathrm{b}} = n_{\mathrm{g}}$ [65] are also solvable by the Bethe Ansatz (BA) technique. The FPL^2 model with $n_{\mathrm{b}} \neq n_{\mathrm{g}}$, or the SFL model with $w_{\mathrm{X}} \neq 1$, do however not appear to be BA solvable. The critical exponents computed from the BA [64, 65, 66] confirm those of the CG, giving the above results a more rigorous status. Defining $n = q + q^{-1}$, there are even underlying quantum group symmetries, viz., $SU(3)_q$ for the FPL model [67] and $SU(4)_q$ for the equally weighted FPL^2 model [66]. The corresponding quantum group symmetry for the Potts and usual O(n) model discussed in section 14.3 is $SU(2)_q$ [68].

The FPL model has also been solved on random lattices using matrix integration techniques [69]. To be more precise, the loops in [69] were required to live on planar random graphs where each vertex is adjacent to three edges. However, while the loops on the regular hexagonal lattice automatically have even length (due to the bipartiteness), this restriction was not imposed in [69]. Since this is crucial for constructing the two-dimensional height model, the critical exponents on such unrestricted random lattices are not directly related to those on a regular lattice [20] by means of the KPZ equation.

A slightly modified version of the FPL^2 model [70] coupled to two-dimensional quantum gravity provides the exact asymptotic behaviour of meanders [71] and their multi-component generalisation [72].

Research on the surface critical behaviour of the fully packed loop models discussed in this section appears to have begun only very recently. This issue will be further discussed in section 14.6.5.

14.6 Surface Critical Behaviour

14.6.1 Ordinary, Special and Extraordinary Surface Transitions

The O(n) model with suitably modified surface couplings permits one to realise the ordinary, special, and extraordinary surface transitions described qualitatively in section 14.2.8. To this end, one studies the model defined in the annular geometry of section 14.3.5.

To be precise, the special transition requires the loops to be in the dilute phase, and so we shall assume this to be the case throughout section 14.6.1. The results for the ordinary and extraordinary transitions hold true in the dense phase as well.

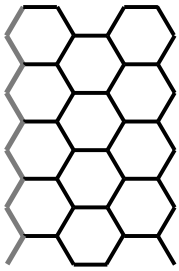

Fig. 14.13 Hexagonal lattice in an annular geometry. The top and the bottom of the figure are identified. Boundary edges on the left are shown in grey.

A well-studied case is the hexagonal-lattice loop model (14.60). The lattice is oriented such that one third of the lattice bonds are parallel to the x-axis, as shown in Fig. 14.13. The fugacity of a monomer is still denoted K in the bulk, but we now take a different weight $K_{\rm s}$ for a monomer touching the *left* rim of the annulus, $x = 0$. In contrast, the right rim of the annulus, $x = L$, enjoys free boundary conditions, meaning that its surface monomers still carry the usual weight K.

In this section we wish to limit the discussion to the case where only the left boundary sustains particular ($\neq$ free) boundary conditions; this is sometimes referred to as *mixed* boundary conditions. The case where both boundaries are distinguished is also of interest and will be discussed in section 14.6.8.

The loop model described above has been thoroughly studied by Batchelor and coworkers [73, 74, 75, 76], in particular using Bethe Ansatz analysis. They find in particular that when $K_{\rm s} = K$ the model is integrable and belongs to the universality class of the *ordinary* transition, while for

$$K_{\rm s} = K_{\rm s}^{\rm S} \equiv (2-n)^{-1/4} \tag{14.137}$$

it is also integrable and describes the special transition. [10] This is consistent with a boundary RG scenario, where K_s^S is a repulsive fixed point that flows towards either of the attractive fixed points $K_s^O < K$ and $K_s^E = \infty$, the former (resp. latter) point describing the ordinary (resp. the extraordinary) transition.

This scenario is corroborated by a detailed analysis [76] showing that a perturbation to the fixed point K_s^E is RG irrelevant. Moreover, the operator conjugate to K_s is obviously the energy density on the boundary. At the special transition, this operator can be identified [77] with $\phi_{(1,3)}$ of weight $h_{1,3} = \frac{2}{g} - 1$, and so this is a relevant perturbation (i.e., $h_{1,3} < 1$) only for $g > 1$ (i.e., in the dilute phase). On the other hand, the surface energy density has weight $h = 2$ at the ordinary transition [78], and so is always irrelevant.

The flow between the ordinary and special transitions has been further studied by Fendley and Saleur [79], from the point of view of boundary S matrices.

14.6.2 Watermelon Exponents

Surface watermelon exponents can be defined as in section 14.4.1, the only difference being that the ℓ legs are inserted at the boundary. We shall denote these exponents by Δ_ℓ^O, Δ_ℓ^S, Δ_ℓ^E at the ordinary, special, extraordinary surface transition respectively. Whenever a result applies to any of these transitions, we use the generic notation Δ_ℓ', where the prime indicates a surface rather than a bulk exponent.

For the ordinary transition, Δ_ℓ^O can be derived by a slight refinement of the marginality argument given in section 14.3.5. First recall that in the continuum limit there is a background flux m_0 given by (14.77), corresponding to a (fractional) number of oriented loop strands running along the rims of the annulus. Suppose now that we wish to evaluate the scaling dimension Δ_ℓ^O corresponding to having $\ell > 0$ non-contractible oriented loop strands running around the periodic direction of the annulus. This can be done by evaluating the free energy increase $\Delta S = S_\ell - S_0$ due to these strands, as in (14.78)

$$\Delta S = \frac{g}{4\pi}\left((\ell + m_0)^2 - m_0^2\right)\left(\frac{\pi}{L}\right)^2 ML \tag{14.138}$$

and using $e^{-\Delta S} = q^{-\Delta_\ell^O}$ from (14.75).

The question now arises which sign for m_0 to pick in (14.77). With the plus sign we would have $\Delta_2 = 1$ independently of g, in clear contradiction with numerical results [47]. Taking therefore the minus sign leads to the result

$$\Delta_\ell^O = \frac{1}{4}g\ell^2 - \frac{1}{2}(1-g)\ell\,. \tag{14.139}$$

[10] Technically speaking this is the mixed ordinary-special transition, but we have simplified the terminology according to the above remarks.

The derivation just presented follows the argument of Cardy [18], but in fact (14.139) was found a long time before by other means. Duplantier and Saleur [47] were the first to propose (14.139) for any ℓ, by noting that their numerical transfer matrix results were in excellent agreement with the following locations in the Kac table (14.31)

$$\Delta_\ell^{\mathrm{O}} = \begin{cases} h_{1,1+\ell} \text{ for the dense O}(n) \text{ model} \\ h_{1+\ell,1} \text{ for the dilute O}(n) \text{ model} \end{cases} \tag{14.140}$$

from which (14.139) follows by the identification (14.74). On a more rigorous level, (14.139) has been established by Bethe Ansatz (BA) techniques [80, 73, 74].

For the special transition, Δ_ℓ^{S} does not seem to permit a CG derivation. It is however known from the BA analysis [75, 74] that one has

$$\begin{aligned} \Delta_\ell^{\mathrm{S}} &= \frac{1}{4}g(1+\ell)^2 - (1+\ell) + \frac{4-(1-g)^2}{4g} \\ &= h_{1+\ell,2} \text{ for the dilute O}(n) \text{ model} \end{aligned} \tag{14.141}$$

in this case.

Alternatively, one may imagine producing the special ℓ-leg operator $\mathscr{O}_\ell^{\mathrm{S}}$ by fusion of the ordinary ℓ-leg operator $\mathscr{O}_\ell^{\mathrm{O}}$ and an ordinary-to-special boundary condition changing operator ϕ_{OS}. The scaling dimension (14.141) pertains to the insertion of this composite operator at either strip end. Comparing the Kac indices in (14.140) and (14.141), and using the CFT fusion rules (14.36), immediately leads to the identification $\phi_{\mathrm{OS}} = \phi_{1,2}$. If one wants special boundary conditions on both the left and the right rim, two insertions of ϕ_{OS} are needed (to change from special to ordinary and back again). One would then expect $h_{1+\ell,3}$, as is indeed confirmed by the BA analysis [75, 74].

Finally, the extraordinary transition is rather trivially related to the ordinary transition. Indeed, for $K_{\mathrm{s}} = \infty$ the entire left rim of the annulus will be coated by a straight polymer strand, so that the remaining system (of width $L-1$) effectively sees free boundary conditions—this is dubbed the *teflon effect* in [76]. Thus, for $\ell = 0$ the coating strand will be the left half of a long stretched-out loop, whose right half will act as a one-leg operator, and one effectively observes the exponent Δ_1^{O}. For $\ell > 0$, one of the legs will act as the coating strand, and one observes $\Delta_{\ell-1}^{\mathrm{O}}$.

14.6.3 Network Exponents

The network exponents discussed in section 14.4.5 can be generalised [81] to the case where at least one vertex of the network $\mathscr{G}$ is constrained to stay close to the surface. Let $\mathscr{G}$ consist of n_ℓ (resp. n'_ℓ) bulk (resp. surface) ℓ-leg vertices, $\mathscr{E}$ edges, and let $\mathscr{V} = \sum_\ell n_\ell$ (resp. $\mathscr{V}' = \sum_\ell n'_\ell$) be the total number of bulk (resp. surface) vertices. The derivation then goes through with straightforward modifications.

For the case of a monodisperse network, where each of the $\mathscr{E}$ edges is constrained to have the same length l (with $l \gg 1$), the end result for the network exponent is

$$\gamma_{\mathscr{G}} = \nu \left[2\mathscr{V} + \mathscr{V}' - 1 - \sum_{\ell} (n_\ell \Delta_L + n'_\ell \Delta'_\ell) \right] - (\mathscr{E} - 1) . \tag{14.142}$$

For a polydisperse network of total length l, the last term $(\mathscr{E}-1)$ has to be omitted as before.

Note that (14.142) does not reduce to (14.95) upon setting all $n'_\ell = 0$ (there is one excess ν). This is because of the initial hypothesis that at least one vertex of $\mathscr{G}$ is attached to the surface.

Instead of having $\mathscr{G}$ grafted to a linear surface, one may consider tying the network in a wedge of opening angle $\alpha \neq \pi$ by means of an extra $\hat{\ell}$-leg vertex. Since the wedge can be transformed back on the half plane through the conformal mapping $w(z) = z^{\pi/\alpha}$ [22], this geometry leads only to a minor modification [81] of the previous result (14.142):

$$\gamma_{\mathscr{G}}(\alpha) = \gamma_{\mathscr{G}}(\pi) - \nu \left(\frac{\pi}{\alpha} - 1 \right) \Delta'_{\hat{\ell}} \tag{14.143}$$

Special cases of these formulae were obtained prior to [81] by Cardy [22], and yet others were conjectured by Guttmann and Torrie [82].

14.6.4 Standard Exponents of Polymer Physics

Standard exponents describing surface critical behaviour can be defined in analogy with those valid in the bulk. However, these can all be derived from the watermelon exponents (14.139) by using the network relation (14.142) and standard scaling relations. We focus here on the ordinary transition.

Consider as an example the exponent $\eta_{\|}$ describing the decay of the spin-spin correlation function along the surface. This is related to the conformational exponent γ_1 of a chain with one extremity tied to the surface and the other belonging to the bulk, through the scaling relation [31]

$$2\gamma_1 = \gamma + \nu(2 - \eta_{\|}) \tag{14.144}$$

Now, γ_1 is a special case of (14.142) with $n_\ell = n'_\ell = \delta_{\ell,1}$, giving $\gamma_1 = \nu(2 - \Delta_1 - \Delta'_1)$. Isolating $\eta_{\|}$ reveals that it belongs to the Kac table:

$$\eta_{\|} = \begin{cases} 2h_{1,2} \text{ for the dense O}(n) \text{ model} \\ 2h_{2,1} \text{ for the dilute O}(n) \text{ model} \\ 2h_{1,3} \text{ for the Potts model} \end{cases} \tag{14.145}$$

as first conjectured by Cardy [22].

14.6.5 Ordinary Transition in Fully Packed Loop Models

As mentioned in section 14.6.1, the special surface transition is absent in the dense O(n) model. This agrees with physical intuition: since each edge has a finite probability of being covered by a monomer, it is redundant to try to attract the loops to the surface by enhancing the fugacity of surface monomers. In analogy, one would expect that fully packed loops are unable to sustain a special transition.

On the other hand, the ordinary transition for fully packed loop models does exist. It can be investigated [83] by adapting the Coulomb gas analysis of sections 14.3.5 and 14.6.2 to the vectorial setup of section 14.5. To this end, we focus on the FPL model on the hexagonal lattice and the FPL^2 model on the square lattice.

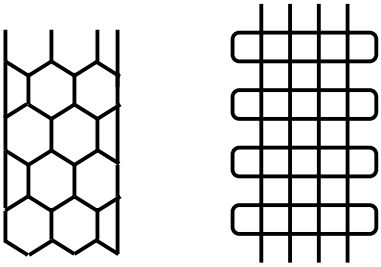

Fig. 14.14 Appropriate modifications of the hexagonal (left panel) and square (right panel) lattices for the definition of the surface versions of the FPL and FPL^2 models. The top and bottom of the figures are identified to make an annular geometry.

The vectorial Coulomb gas treatment of section 14.5 depended crucially on the lattice being bipartite and of constant coordination number. These features must therefore be maintained when defining the surface geometry of the FPL and FPL^2 models. In particular, the FPL model cannot be defined on the lattice shown in Fig. 14.13. The appropriate choices of lattices are shown in Fig. 14.14. Note that in both cases, the corresponding transfer matrix adds two rows of vertices at a time.

For simplicity, we henceforth limit the discussion to the boundary FPL^2 model, defined on an annulus of *even* width L. The case $L = 4$ is shown in Fig. 14.14.

Note that if the vertical edges of a given time-slice are labelled alternatingly as even and odd, the following quantity is strictly conserved by the transfer matrix:

$$Q = \frac{1}{2}\left[(\mathrm{even_b} - \mathrm{odd_b}) - (\mathrm{even_g} - \mathrm{odd_g})\right] \tag{14.146}$$

where, e.g., $\mathrm{even_b}$ means the number of even-labelled vertical edges covered by black loops. Accordingly, critical exponents are labelled by three indices, viz., Q and the number of watermelon strands of each colour (ℓ_b and ℓ_g). For L even, all three indices must have the same parity (even or odd).

Using again the argument of section 14.3.5, the spontaneous vector magnetic flux $\mathbf{m}_0$ is obtained by matching the known central charge (14.131) to (14.75). After the change of basis (14.115) which makes the action diagonal, the result reads

$$\widetilde{\mathbf{m}}_0 = \left(\frac{e_\mathrm{b}}{1-e_\mathrm{b}}, 0, \frac{e_\mathrm{g}}{1-e_\mathrm{g}} \right) \tag{14.147}$$

where we have used the usual parameterisation (14.117).

Consider first the case $Q=0$ and $\ell_\mathrm{b}, \ell_\mathrm{g}$ even. Then the flux is increased by the magnetic charges of the watermelon strands

$$\mathbf{m}_{\ell_\mathrm{b},\ell_\mathrm{g}} = \frac{\ell_\mathrm{b}}{2}(\mathbf{A}-\mathbf{B}) + \frac{\ell_\mathrm{g}}{2}(\mathbf{C}-\mathbf{D}) \tag{14.148}$$

which reads in coordinates $\widetilde{\mathbf{m}}_{\ell_\mathrm{b},\ell_\mathrm{g}} = (-\ell_\mathrm{b}, 0, -\ell_\mathrm{g})$. This excitation multiplies the partition function by $q^{-\Delta c/24}$ and we can identify the critical exponent $\Delta_{\ell_\mathrm{b},\ell_\mathrm{g};0} = -\frac{\Delta c}{24}$. Recalling the one-colour boundary exponents Δ^O_ℓ of (14.139), this result can be expressed as

$$\Delta_{\ell_\mathrm{b},\ell_\mathrm{g};0}(e_\mathrm{b}, e_\mathrm{g}) = \Delta^\mathrm{O}_{\ell_\mathrm{b}}(e_\mathrm{b}) + \Delta^\mathrm{O}_{\ell_\mathrm{g}}(e_\mathrm{g}) \,. \tag{14.149}$$

Thus, in this sector the two loop species do not interact in the continuum limit.

Consider next the case $Q=1$ and $\ell_\mathrm{b}, \ell_\mathrm{g}$ odd. The defect magnetic charge is now

$$\mathbf{m}_{\ell_\mathrm{b},\ell_\mathrm{g}} = \frac{\ell_\mathrm{b}-1}{2}(\mathbf{A}-\mathbf{B}) + \frac{\ell_\mathrm{g}-1}{2}(\mathbf{C}-\mathbf{D}) + (\mathbf{C}-\mathbf{B}) \tag{14.150}$$

which reads in coordinates $\widetilde{\mathbf{m}}_{\ell_\mathrm{b},\ell_\mathrm{g}} = (-\ell_\mathrm{b}, -2, -\ell_\mathrm{g})$. The critical exponent is then

$$\Delta_{\ell_\mathrm{b},\ell_\mathrm{g};1}(e_\mathrm{b}, e_\mathrm{g}) = \Delta^\mathrm{O}_{\ell_\mathrm{b}}(e_\mathrm{b}) + \Delta^\mathrm{O}_{\ell_\mathrm{g}}(e_\mathrm{g}) + \delta(e_\mathrm{b}, e_\mathrm{g}) \tag{14.151}$$

where the additional contribution

$$\delta(e_\mathrm{b}, e_\mathrm{g}) = \frac{2g_2}{\pi} = \frac{(1-e_\mathrm{b})(1-e_\mathrm{g})}{(1-e_\mathrm{b})+(1-e_\mathrm{g})} \tag{14.152}$$

comes from the second height component.

To settle the general case, we note that to obtain sectors with higher charge, Q can be increased by two units by a succession of four consecutive vertical edges with alternating loop colors. This corresponds to a height defect $\mathbf{m} = -2(\mathbf{A}+\mathbf{B}) = (0,-4,0) = \widetilde{\mathbf{m}}$, and in general for even Q $\mathbf{m}_Q = \widetilde{\mathbf{m}}_Q = (0,-2Q,0)$. The final result for any values of $(s_1, s_2; Q)$ can thus be written succintly as

$$\Delta_{\ell_\mathrm{b},\ell_\mathrm{g};Q}(e_\mathrm{b}, e_\mathrm{g}) = \Delta^\mathrm{O}_{\ell_\mathrm{b}}(e_\mathrm{b}) + \Delta^\mathrm{O}_{\ell_\mathrm{g}}(e_\mathrm{g}) + Q^2\delta(e_\mathrm{b}, e_\mathrm{g}) \,. \tag{14.153}$$

This expression has been checked numerically to a very good precision [83].

Finally, let us consider the special case where grey strands are ignored and grey loops are assigned a trivial fugacity, $n_\mathrm{g} = 1$. This gives for the black ℓ-leg boundary watermelon exponents (with $Q = \ell \bmod 2$)

$$\Delta_\ell = \begin{cases} \frac{1}{4}g\ell^2 - \frac{1}{2}(1-g)\ell & \text{for } \ell \text{ even} \\ \frac{1}{4}g\ell^2 - \frac{1}{2}(1-g)\ell + \frac{2g}{3g+2} & \text{for } \ell \text{ odd} \end{cases} \tag{14.154}$$

where $g = 1 - e_{\mathrm{b}}$. This should be compared with (14.133) and (14.139).

14.6.6 Conformal Boundary Loop Model

Very recently, Jacobsen and Saleur [84] have studied a so-called *conformal boundary loop* (CBL) model in which a continuous parameter n_1 permits one to vary the boundary condition. In sharp contrast with the model of section 14.6.1 this boundary condition remains conformal for any real value of n_1, i.e., any n_1 constitutes a boundary RG fixed point and gives rise to a distinct critical exponent of the associated boundary condition changing operator.

For definiteness, consider the loop model (14.59) based on the critical Potts model, with each loop having the fugacity n, and defined on the annulus. Now assign to each loop touching *at least once* the left rim a different fugacity n_1. Algebraically this situation is closely related to the so-called blob algebra—subsequently often known as the one-boundary Temperley-Lieb algebra—originally introduced by Martin and Saleur [85]. Obviously it is possible to apply this boundary condition also to other types of loop models.

Physically one can consider the CBL model as an O(n)-type model in which the bulk spins belong to $\mathbb{R}^n$, while the boundary spins have been constrained to live in a smaller space $\mathbb{R}^{n_1}$ (this makes sense also for $n_1 > n$, by analytic continuation). Alternatively, the same developments which led to (14.59) establish the equivalence with a Potts model in which bulk spins can take $Q = n^2$ states, and boundary spins $Q_1 = nn_1$ states.

One central claim of [84] is that the operator that changes the boundary conditions from free ($n = n_1$) to the CBL boundary conditions just described ($n \neq n_1$) has conformal weight h_{r_1,r_1}, where we have parameterised

$$\begin{aligned} n &= 2\cos\gamma \\ n_1 &= \frac{\sin[(r_1+1)\gamma]}{\sin(r_1\gamma)} \end{aligned} \tag{14.155}$$

and $\gamma = \frac{\pi}{m+1}$ defines the central charge and the conformal weights through (14.31). The parameter $r_1 \in (0, m+1)$ is in general a real number. When r_1 and m are integers, the above statement can be rigorously derived from the representation theory of the corresponding XXZ spin chain with boundary terms. Another check is when $Q_1 = 1$ (i.e., $n = 1/n_1$, or $r_1 = m-1$); indeed it is a well-known result by Cardy [33] that the operator that changes the Potts model boundary conditions from free to fixed is $\phi_{m-1,m-1} = \phi_{1,2}$. Finally, the statement for arbitrary r_1 and m has been subjected to extensive numerical tests in [84].

The above result can be generalised to the watermelon topology where ℓ non-contractible loops wrap around the periodic direction of the annulus. A careful study of the transfer matrix structure reveals that in this case one needs to distinguish two possible situations, or sectors: either the leftmost non-contractible loop is constrained to touch the left rim at least one (blobbed sector), or it is constrained to never touching it (unblobbed sector). The corresponding conformal weight is then

$$\Delta_\ell^{\mathrm{O}}(n,n_1) = h_{r_1,r_1\pm\ell} \tag{14.156}$$

where the upper (resp. lower) sign is for the blobbed (resp. unblobbed) sector.

The formula (14.156) has subsequently been derived for the O(n) model on random lattices by Kostov [86].

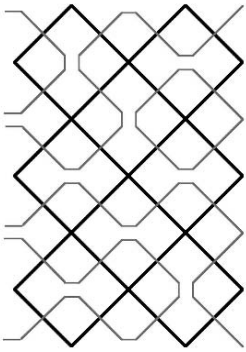

Fig. 14.15 Configuration of loops (in green) on the annulus, with Neumann (resp. Dirichlet) boundary conditions on the left (resp. right) rim. The original Potts spins and their duals live on the black lattice.

Obviously, the result (14.156) has many applications. One of these is to identify the operator that changes the O(n) model boundary condition from Dirichlet to Neumann. By definition, these names refer to the equivalent height model. Therefore, Dirichlet boundary conditions mean that loops are reflected off the boundary, while Neumann conditions mean that loop strands terminate perpendicularly on the boundary. A configuration with Neumann boundary conditions on the left rim of the annulus is shown in Fig. 14.15. Note that it involves half loops beginning and ending on the left rim, and by definition these must have unit weight. By connecting the termination points of these half loops two by two, it is seen that this situation is actually equivalent to the CBL model with parameter $n_1 = 1$. Thus, the required operator is $\phi_{\mathrm{DN}} = \phi_{m/2,m/2}$ of weight

$$h_{\mathrm{DN}} = h_{m/2,m/2} = \frac{m^2-4}{16m(m+1)}\,. \tag{14.157}$$

The result (14.156) holds true also for the hexagonal-lattice model (14.60), provided that one performs the usual swap of the indices when going from the dense to the dilute phase [87].

Note that when $n_1 = n$, we have $r_1 = 1$ from (14.155), and so (14.156) reproduces (14.140) for the ordinary transition, as it should.

14.6.7 Generalised Special Transition

The hexagonal-lattice loop model (14.60) that admitted us to access the special transition in section 14.6.1 can be modified in a natural way so as to accommodate the CBL type boundary conditions of section 14.6.6. To this end, we consider again the annular geometry of Fig. 14.13 with the left boundary being distinguished. A pair of consecutive boundary edges can be either empty, or carry a surface monomer, or carry a *marked* surface monomer.

Loops containing only bulk and surface monomers are called bulk loops, while loops containing at least one marked surface monomer are referred to as boundary loops. Note that this terminology differs slightly from that used in section 1.6.6, since it is now possible for a bulk loop to touch the surface, provided that it contains only unmarked surface monomers. While this may appear physically slightly unnatural, it is necessary in order to make contact with the relevant algebraic framework, viz., the *dilute* one-boundary Temperley-Lieb algebra.

The weight of a bulk (resp. boundary) loop is n (resp. n_1). An unmarked (resp. marked) surface monomer comes with a weight $K_{\rm s}$ (resp. $K_{\rm s,1}$). The physically natural situation, in which boundary loops are simply those that touch the surface, is recovered upon setting $K_{\rm s} = 0$. Depending on the parameters, this may renormalise towards any of the fixed points to be discussed below.

The following parameterisation turns out useful:

$$\begin{aligned} n &= -2\cos(4\varPhi) \\ n_1 &= -\frac{\sin[4(\kappa-1)\varPhi]}{\sin(4\kappa\varPhi)}. \end{aligned} \tag{14.158}$$

The dilute critical point (14.61) is then obtained by setting $1/K = 2\cos(\varPhi)$. One can show [88] that the model defined above admits two new integrable points, that we shall refer to as the *generalised ordinary* transition and the *generalised special* transition. For the former $(K_{\rm s}, K_{\rm s,1}) = (K_{\rm s}^{\rm O}, K_{\rm s,1}^{\rm O})$ with

$$(K_{\rm s}^{\rm O})^2 = \frac{\sin[(2\kappa-1)\varPhi]}{2\cos(\varPhi)\sin(2\kappa\varPhi)} \qquad (K_{\rm s,1}^{\rm O})^2 = \frac{\cos(2\kappa\varPhi)\tan(\varPhi)}{\sin(2\kappa\varPhi)}, \tag{14.159}$$

and for the latter $(K_{\rm s}, K_{\rm s,1}) = (K_{\rm s}^{\rm S}, K_{\rm s,1}^{\rm S})$ with

$$(K_{\rm s}^{\rm S})^2 = \frac{\cos[(2\kappa-1)\Phi]}{2\cos(\Phi)\cos(2\kappa\Phi)} \qquad (K_{\rm s,1}^{\rm S})^2 = -\frac{\sin(2\kappa\Phi)\tan(\Phi)}{\cos(2\kappa\Phi)}. \qquad (14.160)$$

It is interesting to examine a few special cases of (14.159)–(14.160). For $n_1 = n$, we have $\kappa = -1$, and boundary loops are indistinguishable from bulk loops. The weight of a pair of boundary monomers is therefore $y^2 \equiv (K_{\rm s})^2 + (K_{\rm s,1})^2$. Using (14.159) this gives $y^2 = K^2$, which is the usual ordinary transition. Meanwhile, (14.160) gives $y^2 = (2-n)^{-1/2}$ as in (14.137), which is the usual special transition.

The case $n_1 = 1$, or $\kappa = \frac{1}{2}$, corresponds to Neumann boundary conditions. Indeed, when boundary loops are weighted trivially, they might as well be transformed into half loops, as in Fig. 14.15. The generalised ordinary transition (14.159) then corresponds to $K_{\rm s}^{\rm O} = 0$ and $K_{\rm s,1}^{\rm O} = 1$, i.e., only boundary loops are allowed at the surface, and are weighted trivially.

Finally, for $n_1 = 0$, or $\kappa = 1$, boundary loops are forbidden, and the weight of marked surface monomers is therefore immaterial. As expected one has then $K_{\rm s}^{\rm O} = K$, and $K_{\rm s}^{\rm S} = (2-n)^{-1/4}$ in agreement with (14.137).

The critical exponents corresponding to these generalised surface transitions can be identified from numerical diagonalisation of the transfer matrix [88]. To state the results, it is convenient to go back to the parameterisation (14.155). For the ordinary case (14.159) one finds

$$\Delta_\ell^{\rm O}(n,n_1) = h_{r_1\pm\ell,r_1} \qquad (14.161)$$

where we recall that the upper (resp. lower) sign refers to the blobbed (resp. unblobbed) sector. This agrees as expected with (14.156) after swapping the indices (since we are here in the dilute phase of the O(n) model). For the special case (14.160) one finds instead

$$\Delta_\ell^{\rm S}(n,n_1) = h_{r_1\pm\ell,1+r_1} \qquad (14.162)$$

which is a nice generalisation of (14.141).

14.6.8 Two-Boundary CBL Model

The conformal boundary loop (CBL) model of section 14.6.6 can be generalised to the case where both boundaries of the annulus are distinguished. In this two-boundary CBL model, bulk loops have a weight n, while boundary loops touching only the left (resp. right) boundary have weight n_1 (resp. n_2), and loops touching both boundaries have weight n_{12}.

This model—which is related to the so-called two-boundary Temperley-Lieb algebra—has been the subject of several recent studies (see [89, 90, 91, 92] and references therein). It is equivalent to a Potts model in which bulk spins have $Q = n^2$ states, while spins on the left (resp. right) boundary are constrained to a smaller number $Q_1 = nn_1$ (resp. $Q_2 = nn_2$) of states, of which there are $Q_{12} = nn_{12}$ common states.

The following parameterisation turns out to be instrumental for further study:

$$\begin{aligned} n &= 2\cos\gamma \\ n_1 &= \frac{\sin[(r_1+1)\gamma]}{\sin(r_1\gamma)} \\ n_2 &= \frac{\sin[(r_2+1)\gamma]}{\sin(r_2\gamma)} \\ n_{12} &= \frac{\sin[(r_1+r_2+1-r_{12})\frac{\gamma}{2}]\sin[(r_1+r_2+1+r_{12})\frac{\gamma}{2}]}{\sin(r_1\gamma)\sin(r_2\gamma)} \end{aligned} \tag{14.163}$$

The full meaning of this parameterisation only becomes clear within the representation theory of the underlying algebra.

From a CFT point of view, distinguishing both rims of the annulus is expected to be described by the fusion (OPE) of the "free to one-boundary CBL" boundary condition changing operators which are responsible for the weights n_1 and n_2 on either rim. However, a detailed study [92] unravels a number of technical subtleties, mainly having to do with the possibility of a loop of weight n_{12} touching both rims.

Critical exponents $\Delta_\ell^{\alpha_1\alpha_2}$ depend on all the weights (14.163), on the number of non-contractible loops ℓ, and on the sector labels α_1 and α_2. The label $\alpha_1 = \mathrm{b}$ (resp. $\alpha_1 = \mathrm{u}$) if the leftmost non-contractible loop is constrained to touching (resp. to never touching) the left rim; these two possibilities are referred to as the blobbed (resp. unblobbed) sector. The label α_2 similarly constrains the behaviour of the rightmost non-contractible loop. Note that we have supposed that the system size L is even (and so the number of non-contractible loops is always even).

We give here only the final results for the leading critical exponents in each sector [92]:

$$\begin{aligned} \Delta_0 &= h_{r_{12},r_{12}} \\ \Delta_\ell^{\mathrm{bb}} &= h_{r_1+r_2-1,r_1+r_2-1+\ell} \\ \Delta_\ell^{\mathrm{bu}} &= h_{r_1-r_2-1,r_1-r_2-1+\ell} \\ \Delta_\ell^{\mathrm{ub}} &= h_{-r_1+r_2-1,-r_1+r_2-1+\ell} \\ \Delta_\ell^{\mathrm{uu}} &= h_{-r_1-r_2-1,-r_1-r_2-1+\ell} \end{aligned} \tag{14.164}$$

Note that changing the sector label α_k simply results in changing the sign of the parameter r_k (for $k = 1, 2$).

We refer the reader to [92] for details on how these expressions are derived.

14.7 Exact Partition Functions

Writing down exact partition functions Z in the continuum limit is a very strong tool for revealing the complete operator content of the underlying theory. This was first

pointed out by Cardy [23] who worked on the torus, where the possible forms of Z are very strongly constrained by modular invariance. Thus, for the three-state Potts model, Cardy was able to determine Z and the complete operator content from a prior knowledge of just the central charge and a few scaling dimensions.

Most of the early efforts [23, 29] concentrated on extending this approach to all the unitary minimal models, and an extensive set of modular invariant Z on the torus were unravelled. The question however soon arose how to adapt this approach to non-minimal models [39], and in particular how to make the connection [40] with the Potts and O(n) model in their loop model formulation, reviewed in section 14.3.

In section 14.2.7 we have already seen how a modular invariant Z of the free boson (14.42) is constructed by summing over all possible frustrations (magnetic charges) m. This led to the form (14.48) that revealed the electromagnetic operator content (14.50). However, this is valid only for a truly free field, with Gaussian action (14.42) and central charge $c = 1$. It does not apply to the Potts and O(n) models whose CG action (14.69) also contains the boundary term (14.67), linked to the background electric charge e_0 and the modification (14.73) of c.

In section 14.7.1 we show how to remedy this shortcoming on a torus, following the original work of Di Francesco, Saleur and Zuber [40], with a few subsequent improvements [93, 94]. We also present some applications to polymers, following Duplantier and Saleur [14].

Exact continuum limit partition functions on the annulus are given in section 14.7.2. Due to the two possible ways of orienting the annulus, these give access to both the bulk and the boundary operator content. The multiplicities with which the various terms appear in Z are derived from a combinatorial argument by Richard and Jacobsen [95], which has the advantage of being readily generalisable to more complicated geometries [94, 84, 91]. The applications to polymers are due to Cardy [18].

Finally, we treat the CBL model in section 14.7.3, its two-boundary extension in section 14.7.4, and the fully packed loop model FPL^2 in section 14.7.5.

14.7.1 Toroidal Geometry

Recall first the expression (14.46) for the free boson partition function $Z_{m,m'}(g)$ at coupling g and fixed frustrations m, m'. Summing this over frustrations which are multiples of $2\pi f$ defines the coulombic partition function

$$Z_{\mathrm{c}}[g,f] = f \sum_{m,m' \in f\mathbb{Z}} Z_{m,m'}(g) = \frac{1}{\eta\bar{\eta}} \sum_{e \in \mathbb{Z}/f,\ m \in f\mathbb{Z}} q^{\Delta_{e,m}} \bar{q}^{\bar{\Delta}_{e,m}} . \tag{14.165}$$

where we denote by $\Delta_{e,m}$ the conformal weights with respect to the $c = 1$ theory, i.e., without the correction coming from the background electric charge e_0:

$$\Delta_{e,m} + \bar{\Delta}_{e,m} = \frac{e^2}{2g} + \frac{g}{2}m^2$$
$$\Delta_{e,m} - \bar{\Delta}_{e,m} = em\,. \tag{14.166}$$

The free field admits a duality transformation that exchanges electric and magnetic charges

$$g \to \frac{4}{g}\,, \qquad e \to 2m\,, \qquad m \to \frac{e}{2} \tag{14.167}$$

leading to the following symmetries

$$Z_{\rm c}[g,f] = Z_{\rm c}[g^{-1},f^{-1}] = Z_{\rm c}[gf^2,1]\,. \tag{14.168}$$

Consider now the O(n) model on a torus in its formulation as an oriented loop model, or a height model. When n is distributed locally as complex Boltzmann weights in the usual way, the partition function is simply $Z_{\rm c}[g,1/2] = Z_{\rm c}[g/4,1]$. This however assigns a wrong weight $\bar{n} = 2$ to any loop which is non-homotopic to a point, since by self-avoidance each of its oriented versions makes as many left as right turns.

We therefore consider more carefully oriented loops of non-trivial homotopy. Let there be $\mathscr{N}$ such loops. Clearly, they all belong to the same homotopy class, up to the choice of their global orientation which can be described by a sign $\varepsilon_i = \pm 1$. The homotopy class can be defined by giving the (signed) winding numbers n_1 and n_2 with respect to the two principal cycles of the torus. One then has $|n_1| \wedge |n_2| = 1$. Using this and a trigonometric identity yields

$$\big(2\cos(\pi e_0)\big)^{\mathscr{N}} = \prod_i \sum_{\varepsilon_i=\pm 1} {\rm e}^{i\pi e_0 \varepsilon_i} = \sum_{\{\varepsilon_i=\pm 1\}} \cos\left(\pi e_0 \sum_i \varepsilon_i\right) \tag{14.169}$$

from which one deduces that the correctly weighted modular invariant partition function is

$$\hat{Z}[g,e_0] = \sum_{m,m'\in\mathbb{Z}} Z_{m,m'}\left(\frac{g}{4}\right) \cos(\pi e_0 m \wedge m')\,. \tag{14.170}$$

Computing this term by term in the m summation leads to the central result

$$\hat{Z}[g,e_0] = \frac{1}{\eta\bar{\eta}} \left\{ \sum_{p\in\mathbb{Z}} (q\bar{q})^{\Delta_{e_0+2p,0}} + \sum_{p\in\mathbb{Z}} \sum_{m>0} {\sum_{k>0}}' \Lambda(m,k) q^{\Delta_{2p/k,m/2}} \bar{q}^{\bar{\Delta}_{2p/k,m/2}} \right\} \tag{14.171}$$

where we have singled out the $m = 0$ term. The prime on the sum over k indicates the constraints $k|m$ and $p \wedge k = 1$. Note that (14.171) has the correct form to enable a physical interpretation. Clearly, m is the magnetic charge corresponding to the number of non-contractible polymer strands that propagate along the time direction. The indices k and p control how fast the strands wind around the space direction, and give access to subdominant operators. Finally, the coefficients $\Lambda(m,k)$ count the multiplicities of each operator with $m > 0$.

The original paper [40] provides an operational way of computing the $\Lambda(m,k)$ from the prime decomposition of m and k. Unfortunately, this is quite cumbersome to apply, even for moderately small values of m,k. An elegant closed-form expression which brings out the number theoretical content of $\Lambda(m,k)$ was derived much later by Read and Saleur [93]:

$$\Lambda(m,k) = 2 \sum_{d>0\,:\,d|m} \frac{\mu\left(\frac{k}{k\wedge d}\right)\phi\left(\frac{m}{d}\right)}{m\,\phi\left(\frac{k}{k\wedge d}\right)} \cos(2\pi d e_0) \; . \tag{14.172}$$

Here, $k\wedge d$ denotes the greatest common divisor of k and d, and μ and ϕ are respectively the Möbius and Euler's totient function. The Möbius function μ is defined by $\mu(x) = (-1)^r$, if x is an integer that is a product $x = \prod_{i=1}^r p_i$ of r *distinct* primes, $\mu(1) = 1$, and $\mu(x) = 0$ otherwise or if x is not an integer. Similarly, Euler's totient function $\phi(x)$ is defined for positive integers x as the number of integers x' such that $1 \le x' \le x$ and $x\wedge x' = 1$. Note that in (14.172) we may also write $\cos(2\pi d e_0) = T_{2d}(\bar{n})$, where T_ℓ is the ℓ'th order Chebyshev polynomial of the first kind, and $\bar{n}$ is the weight of a non-contractible loop as usual.

The expression (14.172) has been rederived by Richard and Jacobsen [94] following a completely different route. Indeed, these authors view $\Lambda(m,k)$ as eigenvalue amplitudes with respect to a suitably defined transfer matrix for the O(n) model on a torus of width and length which are a *finite* number of lattice spacings (but wide enough to accommodate m non-contractible strands), on an arbitrary regular lattice, and at an arbitrary temperature. By an intricate, but completely rigorous, combinatorial argument they arrive at the same formula (14.172). We shall illustrate their method for a much simpler case in section 14.7.2.

Very recently, a more concise and equally rigorous derivation of (14.172) was provided by Dubail et al. [92] through the construction of the Jones-Wenzl projectors of the periodic Temperley-Lieb algebra.

Note that the $\Delta(m,k)$ are not integers for general values of the loop fugacity n. This was to be expected in view of the non-minimality of the underlying CFT.

The operator content of (14.171) is readily extracted [40]. We state the results in terms of the true ($c < 1$) conformal weights

$$h = \Delta - \frac{e_0^2}{4g} = \Delta + \frac{c-1}{24} \tag{14.173}$$

and their Kac table values

$$h_{r,s} = \frac{(gr-s)^2 - (1-g)^2}{4g} \tag{14.174}$$

where we have taken the notation appropriate for the dilute phase of the O(n) model. The terms with $m = 0$ contain the thermal series

$$\Delta_{\rm t}(\ell) = 2h_{1,1+2\ell} = \frac{2\ell(\ell+1)}{g} - 2\ell \tag{14.175}$$

of which the principal member $\ell = 1$ is (14.91). Similarly, the terms with $m > 0$ contain precisely the ℓ-leg watermelon exponents (14.81).

Note also that (14.171) can be rewritten in the form (14.41). Once again, the coupling constants $n_{h,\bar{h}}$ need not be integers in general.

When g and/or e_0 is rational, (14.171) simplifies due to multiple cancellations, and one can in some cases derive simpler expressions. These can in turn be compared to those derived for the minimal models [23, 29].

Turning now to the Potts model, the derivation is almost identical, with one important modification. As we have already remarked in section 14.4.3 it may happen that Potts clusters wrap around (at least) *two* independent non-contractible cycles on the torus; this is closely linked to the magnetic exponent Δ_{m}. Care must be taken to give such clusters their correct weight Q, rather than 1. The result is simply that (14.171) must be replaced by

$$\hat{Z}[g, e_0] + \frac{1}{2}(Q-1)\hat{Z}\left[g, \frac{1}{2}\right] . \tag{14.176}$$

We end this subsection by giving some applications to polymers, following Duplantier and Saleur [14]. First note that (14.170) still permits one to distinguish the weights of contractible and non-contractible loops, which are respectively $n = -2\cos(\pi g)$ and $\bar{n} = 2\cos(\pi e_0)$. In other words, we need not take $e_0 = 1 - g$.

There are obviously several interesting ways of taking the polymer (SAP) limit. To obtain polymers of indeterminate homotopy, one first sets $\bar{n} = n$ and then lets $n \to 0$. To have contractible polymers only, one first sets $\bar{n} = 0$ and then lets $n \to 0$. Finally, to have non-contractible polymers only, one first sets $n = 0$ and then lets $\bar{n} \to 0$. In all cases, a derivative with respect to the fugacity is needed before taking the last limit, in order to single out configurations having a single loop—otherwise, the surviving configuration will have zero loops and give rise to a trivial partition function, just as in the discrete model (14.60).

To illustrate this, consider the case of contractible polymers. Setting $\bar{n} = 0$ in (14.170) gives

$$\hat{Z}\left[g, \frac{1}{2}\right] = 2 \sum_{m,m' \in 4\mathbb{Z}} Z_{m,m'}\left(\frac{g}{4}\right) - \sum_{m,m' \in 2\mathbb{Z}} Z_{m,m'}\left(\frac{g}{4}\right) = \frac{1}{2}\left(Z_{\mathrm{c}}[4g, 1] - Z_{\mathrm{c}}[g, 1]\right) , \tag{14.177}$$

where we have used (14.165) and (14.168). If we now set simply $n = 0$, one recovers in the dilute (resp. dense) case $g = \frac{3}{2}$ (resp. $g = \frac{1}{2}$), by using Euler's pentagonal identity (resp. (14.168))

$$\hat{Z}\left[\frac{3}{2}, \frac{1}{2}\right] = 1 , \qquad \hat{Z}\left[\frac{1}{2}, \frac{1}{2}\right] = 0 . \tag{14.178}$$

Both these results are trivial, as expected. By contrast, if one takes the derivative $\partial/\partial n$ before setting $n = 0$, a non-trivial result is obtained. For dense polymers this reads explicitly, after some algebra,

$$\frac{\partial}{\partial n}\hat{Z}\left[g,\frac{1}{2}\right]\Big|_{g=\frac{1}{2}} = -\frac{1}{4\pi}\eta^2(q)\eta^2(\bar{q})\log(q\bar{q})\,. \tag{14.179}$$

14.7.2 Annular Geometry

We now consider instead the geometry of an $L\times M$ annulus with free $\times$ periodic boundary conditions, as defined in section 14.3.5. Recall that in the preceding subsection we have constructed the continuum limit partition function Z starting from the explicit weights of the microscopic model—and invoking modular invariance—and extracted the operator content as a corollary at the end of the calculation. Let us instead now work the other way around, starting from the known operator content, viz., the watermelon exponents (14.139) at the ordinary surface transition.

According to (14.55) we have

$$Z \equiv Z_{\mathrm{ff}}(q) = \sum_h n_h \chi_{(c,h)}(q) \tag{14.180}$$

where the sum is over the boundary scaling dimensions h, $\chi_{(c,h)}(q)$ is the generic character (14.28), and the modular parameter $q=\exp(i\pi\tau)=\exp(-\pi M/L)$. The degeneracy factor n_h states how many times a given character appears in the partition function, and as usual for non-minimal theories it needs not in general be an integer. We omit in the following the subscript ff which reminds us that the boundary conditions on both rims of the annulus are free.

As the watermelon operators are indexed by their number of legs ℓ, we may replace the sum over h by one over ℓ. Below we shall give a combinatorial argument that the correct degeneracy factor is

$$n_\ell = \frac{\sin\big((1+\ell)\pi e_0\big)}{\sin(\pi e_0)} = U_\ell\left(\frac{\bar{n}}{2}\right), \tag{14.181}$$

where $U_\ell(x)$ is the ℓ'th order Chebyshev polynomial of the second kind. Note that n_ℓ depends only on the weight $\bar{n}=2\cos(\pi e_0)$ of a non-contractible loop, which may in general be different from that of a contractible loop, $n=-2\cos(\pi g)$.

Accepting for the moment (14.181), we then have the central result

$$Z[g,e_0] = \frac{q^{-c/24}}{P(q)}\sum_{\ell\in\mathbb{Z}}\frac{\sin\big((1+\ell)\pi e_0\big)}{\sin(\pi e_0)}q^{\frac{g\ell^2}{4}-\frac{(1-g)\ell}{2}} \tag{14.182}$$

which is the analogue of (14.171) on the torus. The attentive reader may object that 1) the expansion (14.180) should not be over generic characters, but the degenerate ones

$$K_{r,s} = \frac{q^{h_{r,s}}-q^{h_{r,-s}}}{q^{c/24}P(q)}\,, \tag{14.183}$$

and 2) the sum in (14.182) should be over $\ell \geq 0$ and not $\ell \in \mathbb{Z}$. While these observations are certainly correct, a little analysis shows that taking into account 1) and 2) leads to exactly the same result (14.182).

The expression (14.182) was first obtained by Saleur and Bauer [80], using techniques of integrability and quantum groups. It has later been rederived and discussed by Cardy from a Coulomb gas point of view [18].

We now turn to the derivation of (14.181). One line of reasoning is to invoke the correspondence between the oriented loop model and an $SU(2)$ spin chain Hamiltonian, as in [80]. The number of non-contractible loop strands ℓ is then the conserved spin S of the chain. For each value $S = \ell$ there is a degeneracy corresponding to the $(2\ell+1)$ corresponding values of S^z. To be more precise, the symmetry of the spin chain is not classical $SU(2)$ but the quantum algebra $SU(2)_q$, with deformation parameter[11] given by $\bar{n} = q + q^{-1}$. The degeneracy factor is therefore the q-deformed number $(2\ell+1)_q$, by definition equal to n_ℓ in (14.181).

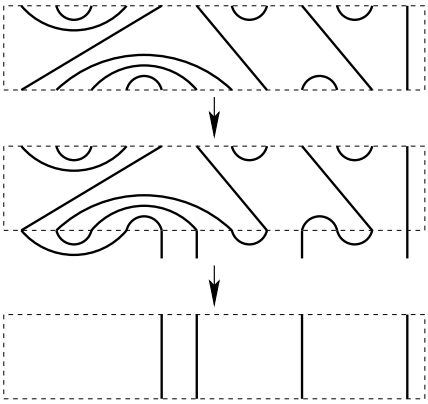

Fig. 14.16 Construction of compatible states (see text).

A very different argument was given by Richard and Jacobsen [95] who used elementary combinatorics. The lattice partition function can be constructed from a transfer matrix T that acts on connectivity states between two time slices at $t = 0$ and $t = t_0$. An example of a *state* is shown in Fig. 14.16.a; it consists of *arcs* that connect pairs of points within one time slice, and ℓ *strings* that connect one point on either time slice. Upon cutting all the strings, a state is transformed into a pair of *reduced states*. T transforms a state from time t_0 to $t_0 + 1$ by acting on the upper time slice. One may write

$$Z = \langle v|T^M|u\rangle = \sum_i n_i \lambda_i^M \tag{14.184}$$

[11] This q should not be confused with the modular parameter q used elsewhere in the text.

where $|u\rangle$ is an initial state that identifies the two time slices, and $\langle v|$ is a final state that reglues the two time slices and imposes the correct powers of n and $\bar{n}$ according to the loops thus formed. As Z is not a trace, each eigenvalue λ_i of T has a corresponding amplitude n_i.

Note that ℓ cannot increase under the action by T, whence T is upper block-triangular with respect to ℓ. Therefore, each eigenvalue of T is an eigenvalue of one of the blocks on the diagonal denoted T_ℓ. Furthermore, T cannot change the reduced state corresponding to the lower time slice, so each T_ℓ is block-diagonal with a number of identical blocks given by the number of reduced states with ℓ strings. In particular, $n_i = n_{\ell(i)}$ and the eigenvalues can be labeled by ℓ, so we may write

$$Z = \sum_{\ell=0}^{L} n_\ell \sum_k \lambda_{\ell,k}^M . \tag{14.185}$$

Define now $K_\ell = \mathrm{Tr}(T_\ell^M)$ as a trace over reduced states, and Z_j as the partition function constrained to having exactly j non-contractible loops. To determine n_ℓ we must determine how many times each K_ℓ contributes to Z. Consider instead the inverse problem

$$K_\ell = \sum_{j=\ell}^{L} n(j,\ell) Z_j \bar{n}^{-j} . \tag{14.186}$$

where $n(j,\ell)$ is the number of times a configuration with j non-contractible loops occurs in the trace K_ℓ. To determine it we depict a configuration contributing to Z_j as a state $\mathscr{S}_j$, i.e., we suppress all internal loops and empty sites in the time slices; see Fig. 14.16.a. Then $n(j,\ell)$ is the number of ℓ-string reduced states $\mathscr{R}_\ell$ that are *compatible* with $\mathscr{S}_j$, i.e., that are invariant when propagated through $\mathscr{S}_j$. A necessary condition is that $\mathscr{R}_\ell$ contains the same arcs as the upper time slice of $\mathscr{S}_j$; see Fig. 14.16.b. What remains is topologically equivalent to just j strings; see Fig. 14.16.c. To ensure compatibility, these must be linked up by arcs so as to leave exactly ℓ non-enclosed strings. This is an easy counting problem with solution

$$n(L,\ell) = \binom{L}{(L-\ell)/2} - \binom{L}{(L-\ell)/2-1} . \tag{14.187}$$

Finally inverting (14.186) gives the number of times K_ℓ appears in each Z_j, and since by definition each eigenvalue appears with unit amplitude in K_ℓ, we can sum this over j to obtain $n_\ell = U_\ell(\bar{n}/2)$ proving (14.181).

Once again, an alternative to this combinatorial method is furnished by the study of Jonez-Wenzl projectors of the Temperley-Lieb algebra. The degeneracy factors (or eigenvalue amplitudes) n_ℓ then appear as the Markov traces of the ℓ-strand projectors. The reader is referred to [92] for further details.

We now return to the result (14.182). It may be rewritten [18] in terms of the conjugate modulus $\tilde{q} = \exp(-2\pi L/M)$, giving

$$Z[g,e_0]=\sqrt{\frac{2}{g}}\frac{\tilde{q}^{-c/12}}{P(\tilde{q}^2)}\sum_{m\in\mathbb{Z}}\frac{\sin\left(\frac{\pi(e_0+2m)}{g}\right)}{\sin(\pi e_0)}\tilde{q}^{\frac{(e_0+2m)^2}{2g}-\frac{(1-g)^2}{2g}}\,. \tag{14.188}$$

Note that when going from q to $\tilde{q}$, the time and space directions have effectively been swapped, and so (14.188) pertains to a *cylinder* geometry (with free boundary conditions on the rims), meaning that the expansion is in terms of the *bulk* theory. More precisely, in view of the decomposition (14.41) for a *diagonal* theory, (14.180) is now replaced by

$$Z=\sum_h |b_h|^2\chi_{(c,h)}(\tilde{q}^2)\,, \tag{14.189}$$

where the sum is over the bulk conformal weights h, $\chi_{(c,h)}(q)$ is a bulk character, and b_h is a matrix element with the boundary state corresponding to free boundary conditions at the rim. Note that there is no multiplicity $\Lambda(m,k)$, as in the first term of (14.171), since the free boundary conditions do not allow loops to wrap around the system in the *time*-like direction.

In particular setting $h=0$ in (14.188) we can read off [18]

$$b_0^2=-\sqrt{\frac{2}{g}}\frac{\sin(\pi/g)}{\sin(\pi g)} \tag{14.190}$$

for $\bar{n}=n$, from which the boundary entropy [96] can be determined as $\log b_0$.

As in the toroidal case, we end by giving some applications to polymers, following Cardy [18]. For $\bar{n}=n$, simply setting $n=0$, one recovers in the dilute (resp. dense) case $g=\frac{3}{2}$ (resp. $g=\frac{1}{2}$), by using Euler's pentagonal identity (resp. simple algebra), that

$$Z\left[\frac{3}{2},\frac{1}{2}\right]=1\,,\qquad Z\left[\frac{1}{2},\frac{1}{2}\right]=0\,. \tag{14.191}$$

This should be compared with (14.178). Non-trivial results are obtained by singling out the $O(\bar{n})$ term, i.e., by taking a derivative before going to the limit. This gives for the dilute case

$$Z_1=\prod_{r=1}^{\infty}(1-q^r)^{-1}\sum_{k\in\mathbb{Z}}k(-1)^{k-1}q^{\frac{3}{2}k^2-k+\frac{1}{8}}\sim q^{5/8} \tag{14.192}$$

and since $Z=1$ this can be interpreted as the probability of having a single non-contractible loop. For the dense case the $O(\bar{n})$ term in Z is similarly

$$Z_1=q^{-1/24}\prod_{m=1}^{\infty}\left(1-q^{m-\frac{1}{2}}\right)^2\sim q^{-1/24}\,. \tag{14.193}$$

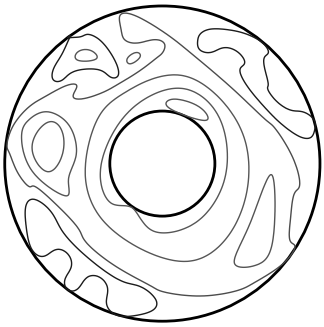

Fig. 14.17 Continuum-limit view of the four different types of loops in the CBL model. In this figure the annulus has been conformally mapped to the plane, and the "left rim" referred to in the text has become the outer rim.

14.7.3 Conformal Boundary Loop Model

Continuum limit partition functions for the CBL model defined in section 14.6.6 have been written down by Jacobsen and Saleur [84]. In this context it is convenient to define a more general model in which bulk loops have fugacity n or $\overline{n}$, and loops touching the left boundary have weight n_1 or $\overline{n_1}$, where in all cases the overline refers to non-contractible loops (i.e., loops that are not homotopic to a point). This is illustrated in Fig. 14.17.

We have seen above how the transfer matrix T of any loop model on the annulus can be decomposed into blocks T_ℓ labeled by the number of non-contractible loops ℓ. For the CBL model one may further decompose T_ℓ into the blobbed (resp. unblobbed) sector T_ℓ^{b} (resp. T_ℓ^{u}) in which the leftmost non-contractible loop is required (resp. forbidden) to touch the left rim of the annulus. Indeed, since a non-contractible loop is conserved by definition, once it has been blobbed (i.e., touched the boundary) it cannot subsequently be unblobbed. Therefore, T_ℓ is upper block-triangular in the basis $\{|\mathrm{b}\rangle, |\mathrm{u}\rangle\}$ and the previous argument applies mutatis mutandis.

The CBL model contains the ordinary O(n) loop model as the special case $n_1 = n$, but it is clear that its transfer matrix must contain many more states in order to produce the correct weights for $n_1 \neq n$. Therefore, the conformal towers must be more densely filled, and the spectrum generating functions must contain fewer degeneracies. Since the loop model characters (14.183) contain just one subtraction, it seems reasonable that the CBL characters for generic $n_1 \neq n$ will not involve any subtractions, i.e., they must be the generic characters (14.28). This is indeed confirmed by numerical diagonalisation of the transfer matrix [84]. Combining this with the result for the conformal weights (14.156), we conclude that the spectrum generating functions for the blobbed and unblobbed sectors read

$$Z_\ell^{\mathrm{b}} = \frac{q^{h_{r,r+\ell}-c/24}}{P(q)}, \qquad Z_\ell^{\mathrm{u}} = \frac{q^{h_{r,r-\ell}-c/24}}{P(q)}. \tag{14.194}$$

To find out how to combine these sectors to obtain the complete partition function Z, one needs to know the multiplicities (eigenvalue amplitudes) of each sector. These can be derived combinatorially [84], by using the line of reasoning [95, 94] that we illustrated in section 14.7.2 for a simpler case. Parametrising the weights of non-contractible loops as

$$\overline{n} = 2\cosh\alpha\,, \qquad \overline{n_1} = \frac{\sinh(\alpha+\beta)}{\sinh\beta} \tag{14.195}$$

the result reads

$$n_\ell^{\mathrm{b}} = \frac{\sinh(\ell\alpha+\beta)}{\sinh\beta}\,, \qquad n_\ell^{\mathrm{u}} = \frac{\sinh(\ell\alpha-\beta)}{\sinh(-\beta)}\,. \tag{14.196}$$

Supposing L is even, and setting $\ell = 2j$, the results (14.194) and (14.196) lead to

$$Z = q^{-c/24}\left[\sum_{j=0}^{\infty}\frac{\sinh(2j\alpha+\beta)}{\sinh\beta}\,\frac{q^{h_{r,r+2j}}}{P(q)} - \sum_{j=1}^{\infty}\frac{\sinh(2j\alpha-\beta)}{\sinh\beta}\,\frac{q^{h_{r,r-2j}}}{P(q)}\right] \tag{14.197}$$

If one further supposes $\beta = r\alpha$ with r integer this can be rewritten as

$$Z = \sum_{j=-\lfloor r/2\rfloor}^{\infty}\frac{\sinh(2j+r)\alpha}{\sinh r\alpha}\,K_{r,r+2j} \tag{14.198}$$

where $\lfloor\ldots\rfloor$ denotes the integer part, and $K_{r,s}$ is given by (14.183).

As an example of an application to dense polymers ($c=-2$), we consider the case $n=\overline{n}=0$ and $n_1=\overline{n_1}=1$ where only loops touching the boundary are allowed. Then (14.197) can be cast in the form

$$Z = \frac{q^{-1/24}}{P(q)}\sum_{j=-\infty}^{\infty}(-1)^j q^{(4j-1)^2/32}\,. \tag{14.199}$$

14.7.4 Two-Boundary CBL Model

The two-boundary extension of the CBL model was defined in section 14.6.8. In particular, we recall the four different weights (14.163) of contractible loops. Since we have constrained the width of the annulus L to be even, a non-contractible loop cannot touch both rims of the annulus. We thus need only the following additional three weights for non-contractible loops:

$$\begin{aligned}
\overline{n} &= 2\cos\chi \\
\overline{n_1} &= \frac{\sin[(u_1+1)\chi]}{\sin(u_1\chi)} \\
\overline{n_2} &= \frac{\sin[(u_2+1)\chi]}{\sin(u_2\chi)}
\end{aligned} \tag{14.200}$$

The exact continuum limit partition function, expressed in terms of all these seven weights, has been derived by Dubail et al. [92]:

$$\begin{aligned}
Z = {} & \frac{q^{-c/24}}{P(q)} \sum_{n\in Z} q^{h_{r_{12}-2n,r_{12}}} \\
& + \frac{q^{-c/24}}{P(q)} \sum_{j\geq 1} \sum_{n\geq 0} \frac{\sin[(u_1+u_2-1+2j)\chi]\sin\chi}{\sin(u_1\chi)\sin(u_2\chi)} q^{h_{r_1+r_2-1-2n,r_1+r_2-1+2j}} \\
& + \frac{q^{-c/24}}{P(q)} \sum_{j\geq 1} \sum_{n\geq 0} \frac{\sin[(-u_1+u_2-1+2j)\chi]\sin\chi}{\sin(-u_1\chi)\sin(u_2\chi)} q^{h_{-r_1+r_2-1-2n,-r_1+r_2-1+2j}} \\
& + \frac{q^{-c/24}}{P(q)} \sum_{j\geq 1} \sum_{n\geq 0} \frac{\sin[(u_1-u_2-1+2j)\chi]\sin\chi}{\sin(u_1\chi)\sin(-u_2\chi)} q^{h_{r_1-r_2-1-2n,r_1-r_2-1+2j}} \\
& + \frac{q^{-c/24}}{P(q)} \sum_{j\geq 1} \sum_{n\geq 0} \frac{\sin[(-u_1-u_2-1+2j)\chi]\sin\chi}{\sin(-u_1\chi)\sin(-u_2\chi)} q^{h_{-r_1-r_2-1-2n,-r_1-r_2-1+2j}}
\end{aligned} \tag{14.201}$$

The five-term structure of this expression mirrors that of the principal critical exponents (14.164). The trigonometric factors inside the four last terms are the eigenvalue amplitudes, which can be derived using combinatorial [91] or algebraic [92] means.

Obviously, an expression like (14.202) contains a wealth of exact probabilistic information, which can be extracted explicitly for any special case of interest (such as percolation). Moreover, it determines the complete operator content of the two-boundary model, and the precise fusion rules of two one-boundary CBL type boundary condition changing operators.

14.7.5 Fully Packed Loop Models

To write the exact continuum limit partition function of the FPL^2 model of section 14.5, we need the sector labels $(\ell_{\rm b},\ell_{\rm g};Q)$ identified in section 14.6.5 as well as the corresponding critical exponents $\Delta_{\ell_{\rm b},\ell_{\rm g};Q}(e_{\rm b},e_{\rm g})$ of (14.153). The remaining ingredients are the corresponding eigenvalue amplitudes $D_{\ell_{\rm b},\ell_{\rm g};Q}$ and the structure of descendent states within each sector.

These can be obtained by noting [83] that the two Temperley-Lieb like structures associated with each of the loop flavours (black and grey), with corresponding semi-conserved quantum numbers $\ell_{\rm b}$ and $\ell_{\rm g}$, decouple on the algebraic level. The last

field, related to the conserved quantum number Q, essentially behaves as a free boson. One has therefore a simple product form of (14.181)

$$D_{\ell_{\rm b},\ell_{\rm g};Q} = \frac{\sin[(1+\ell_{\rm b})\pi f_{\rm b}]}{\sin(\pi f_{\rm b})} \frac{\sin[(1+\ell_{\rm g})\pi f_{\rm g}]}{\sin(\pi f_{\rm g})} \tag{14.202}$$

independently of Q. We have here as usual given different weights to non-contractible loops:

$$\begin{aligned} \overline{n_{\rm b}} &= 2\cos(\pi f_{\rm b}) \\ \overline{n_{\rm g}} &= 2\cos(\pi f_{\rm g})\,. \end{aligned} \tag{14.203}$$

A further consequence of this algebraic decoupling is that the characters describing the structure of descendent states factorise. The factors corresponding to quantum numbers $\ell_{\rm b}$ and $\ell_{\rm g}$ are degenerate characters of the K type, while the last factor corresponding to quantum number Q is just that of a free boson.

Assembling all this information we thus arrive at

$$Z = \frac{q^{-c/24}}{P(q)^3} \sum_{Q=-\infty}^{\infty} \sum_{\ell_{\rm b}=0}^{\infty} \sum_{\ell_{\rm g}=0}^{\infty} D_{\ell_{\rm b},\ell_{\rm g};Q} (1-q^{\ell_{\rm b}+1})(1-q^{\ell_{\rm g}+1}) q^{\Delta_{\ell_{\rm b},\ell_{\rm g};Q}(e_{\rm b},e_{\rm g})} \tag{14.204}$$

where the sums over $\ell_{\rm b}$ and $\ell_{\rm g}$ are constrained so that all three labels $(\ell_{\rm b},\ell_{\rm g};Q)$ have the same parity.

It should be possible to endow one or both loop flavours of the FPL^2 model with (one- or two-boundary) CBL type boundary conditions, and work out the corresponding partition function using the methods of sections 14.7.3–14.7.4.

14.8 Epilogue

We hope to have convinced the reader that loop models are a useful tool for deriving exact results about two-dimensional self-avoiding polygons and walks, and that these models offer a fruitful testing ground for many, if not most, of the concepts developed in two-dimensional conformal field theory.

There are many relevant issues about loop models that we have omitted in order to keep this review to a reasonable length. Most importantly, we have focused here mainly on the application of the Coulomb gas approach, and only mentioned very briefly the results obtainable from integrability, combinatorics, quantum groups, etc. Also, several exact results—often due to Cardy—are known about universal amplitude ratios in loop models, such as the ratio between the mean area of a loop and its squared ratio of gyration [97]. Other issues have been omitted because we feel that they have not yet been sufficiently elucidated. This is the case for loop models in the presence of quenched disorder, and for certain aspects of surface critical behaviour in which the two sides of the annulus both sustain non-trivial boundary conditions.

Another promising field of future research is that of several coupled loop models (see [98] for an example).

Another limitation of this review resides of course in the number of loop models that we have treated. Roughly speaking, we have included here only models of *self-avoiding* loops whose bulk critical properties are more-or-less fully understood, and amenable to Coulomb gas analysis. Some interesting examples of loop models which fall outside this criterion have been discussed by Fendley [99]. One important model that we could actually have chosen to include is the dilute O(n) model on the square lattice [100], which is related to the integrable Izergin-Korepin model [101], and its two-loop generalisation, which is referred to as the DPL^2 model in [70].

In any case, despite the effort dedicated to understanding two-dimensional loop models, they remain a very active area of research to this date.

Acknowledgments

The author warmly thanks the Bannier family for hospitality at Les Loges where the present review was written. He is very much indebted to J.L. Cardy, J. Dubail, Y. Ikhlef, J. Kondev, B. Nienhuis, J.-F. Richard, H. Saleur, and P. Zinn-Justin who have helped shaping his understanding of the subject over the years. This work was supported through the European Community Network ENRAGE (grant MRTN-CT-2004-005616) and by the Agence Nationale de la Recherche (grant ANR-06-BLAN-0124-03).

References

1. L. Onsager, *Crystal statistics. I. A two-dimensional model with an order-disorder transition*, Phys. Rev. **65**, 117 (1944).
2. K.G. Wilson, *Non Lagrangian models of current algebra*, Phys. Rev. **179**, 1499 (1969).
3. K.G. Wilson and J. Kogut, *The renormalization group and the ε expansion*, Phys. Rep. C **12**, 75 (1974).
4. J. Zinn-Justin, *Quantum field theory and critical phenomena* (Oxford Science Publications, Oxford, 1989).
5. E.H. Lieb, *Residual entropy of square ice*, Phys. Rev. **162**, 162 (1967).
6. R.J. Baxter, *Eight-vertex model in lattice statistics*, Phys. Rev. Lett. **26**, 832 (1971).
7. A.A. Belavin, A.M. Polyakov and A.B. Zamolodchikov, *Infinite conformal symmetry in two-dimensional quantum field theory*, Nucl. Phys. B **241**, 333 (1984).
8. A.M. Polyakov, *Conformal symmetry of critical fluctuations*, JETP Lett. **12**, 381 (1970).
9. J.V. José, L.P. Kadanoff, S. Kirkpatrick and D.R. Nelson, *Renormalization, vortices, and symmetry-breaking perturbations in the two-dimensional planar model*, Phys. Rev. B **16**, 1217 (1977).
10. M. den Nijs, *Extended scaling relations for the magnetic critical exponents of the Potts model*, Phys. Rev. B **27**, 1674 (1983); *Extended scaling relations for the chiral and cubic crossover exponents*, J. Phys. A **17**, L295 (1984).
11. B. Nienhuis, *Critical behavior of two-dimensional spin models and charge asymmetry in the Coulomb gas*, J. Stat. Phys. **34**, 731 (1984).

12. Vl. S. Dotsenko and V. Fateev, *Conformal algebra and multipoint correlation functions in 2D statistical models*, Nucl. Phys. B **240**, 312 (1984).
13. Vl. S. Dotsenko and V. Fateev, *Four-point correlation functions and the operator algebra in 2D conformal invariant theories*, Nucl. Phys. B **251**, 691 (1985).
14. B. Duplantier and H. Saleur, *Exact critical properties of two-dimensioanl dense self-avoiding walks*, Nucl. Phys. B **290**, 291 (1987).
15. P. Di Francesco, P. Mathieu and D. Sénéchal, *Conformal field theory* (Springer Verlag, New York, 1987).
16. J.L. Cardy, *Conformal invariance and statistical mechanics*, and P. Ginsparg, *Applied conformal field theory*, both in *Fields, strings and critical phenomena* (Les Houches, session XLIX), eds. E. Brézin and J. Zinn-Justin (Elsevier, New York, 1989).
17. J. Kondev, *Liouville field theory of fluctuating loops*, Phys. Rev. Lett. **78**, 4320 (1997).
18. J. Cardy, *The O(n) model on the annulus*, J. Stat. Phys. **125**, 1 (2006).
19. B. Duplantier and H. Saleur, *Exact tricritical exponents for polymers at the Θ point in two dimensions*, Phys. Rev. Lett. **59**, 539 (1987).
20. J. Kondev, J. de Gier and B. Nienhuis, *Operator spectrum and exact exponents of the fully packed loop model*, J. Phys. A **29**, 6489 (1996).
21. J.L. Jacobsen and J. Kondev, *Field theory of compact polymers on the square lattice*, Nucl. Phys. B **532**, 635 (1998); *Conformational entropy of compact polymers*, Phys. Rev. Lett. **81**, 2922 (1998).
22. J.L. Cardy, *Conformal invariance and surface critical behavior*, Nucl. Phys. B **240**, 514 (1984).
23. J. Cardy, *Operator content of two-dimensional conformally invariant theories*, Nucl. Phys. B **270**, 186 (1986).
24. V.A. Fateev and A.B. Zamolodchikov, *Conformal quantum field theory models in two dimensions having Z_3 symmetry*, Nucl. Phys. B **280**, 644 (1987).
25. H.W.J. Blöte, J.L. Cardy and M.P. Nightingale, *Conformal invariance, the central charge, and universal finite-size amplitudes at criticality*, Phys. Rev. Lett. **56**, 742 (1986); I. Affleck, *Universal term in the free energy at a critical point and the conformal anomaly*, Phys. Rev. Lett. **56**, 746 (1986).
26. J.L. Cardy, *Conformal invariance and universality in finite-size scaling*, J. Phys. A **17**, L385 (1984).
27. D. Friedan, Z. Qiu and S. Shenker, *Conformal invariance, unitarity and critical exponents in two dimensions*, Phys. Rev. Lett. **52**, 1575 (1984).
28. A.B. Zamolodchikov, *Conformal symmetry and multicritical points in two-dimensional quantum field theory*, Sov. J. Nucl. Phys. **44**, 530 (1986).
29. C. Itzykson and J.-B. Zuber, *Two-dimensional conformal invariant theories on a torus*, Nucl. Phys. B **275**, 580 (1986).
30. J. Cardy, *Boundary conformal field theory*, in J.-P. Françoise, G. Naber and T.S. Tsun (eds.), *Encyclopedia of mathematical physics* (Elsevier, 2005).
31. K. Binder, *Critical behaviour at surfaces*, in C. Domb and J.L. Lebowitz (eds.), *Phase transitions and critical phenomena*, vol. 8, p. 1 (Academic Press, London, 1983).
32. T.W. Burkhardt and E. Eisenriegler, *Conformal theory of the two-dimensional O(N) model with ordinary, extraordinary, and special boundary conditions*, Nucl. Phys. B **424**, 487 (1994).
33. J.L. Cardy, *Critical percolation in finite geometries*, J. Phys. A **25**, L201 (1992).
34. A. Luther and I. Peschel, *Calculation of critical exponents in two dimensions from quantum field theory in one dimension*, Phys. Rev. B **12**, 3908 (1975); L.P. Kadanoff, *Lattice Coulomb gas representations of two-dimensional problems*, J. Phys. A **11**, 1399 (1978); L.P. Kadanoff and A.C. Brown, *Correlation functions on the critical lines of the Baxter and Ashkin-Teller models*, Ann. Phys. **121**, 318 (1979); H.J.F. Knops, *Renormalization connection between the eight-vertex model and the Gaussian model*, Ann. Phys. **128**, 448 (1981).
35. B. Nienhuis, *Coulomb gas formulations of two-dimensional phase transitions*, in C. Domb and J.L. Lebowitz (eds.), *Phase transitions and critical phenomena*, vol. 11, p. 1–53 (Academic Press, London, 1987).

36. G. Parisi and N. Sourlas, *Self avoiding walk and supersymmetry*, J. Physique Lett. **41**, L403 (1980).
37. B. Nienhuis, *Exact critical point and critical exponents of O(n) models in two dimensions*, Phys. Rev. Lett. **49**, 1062 (1982).
38. R.J. Baxter, S.B. Kelland and F.Y. Wu, *Equivalence of the Potts model or Whitney polynomial with an ice-type model*, J. Phys. A **9**, 397 (1975).
39. P. Di Francesco, H. Saleur and J.B. Zuber, *Modular invariance in non-minimal two-dimensional conformal theories*, Nucl. Phys. B **285**, 454 (1987).
40. P. Di Francesco, H. Saleur and J.B. Zuber, *Relations between the Coulomb gas picture and conformal invariance of two-dimensional critical models*, J. Stat. Phys. **49**, 57 (1987).
41. P. W. Kasteleyn et C. M. Fortuin, *Phase transitions in lattice systems with random local properties*, J. Phys. Soc. Jpn. **26** (suppl.), 11 (1969); C.M. Fortuin and P.W. Kasteleyn, *On the random-cluster model. I. Introduction and relation to other models*, Physica **57**, 536 (1972).
42. R.J. Baxter, *Critical antiferromagnetic square-lattice Potts model*, Proc. Roy. Soc. London Ser. A **383**, 43 (1982).
43. J.L. Jacobsen and H. Saleur, *The antiferromagnetic transition for the square-lattice Potts model*, Nucl. Phys. B **743**, 207 (2006); Y. Ikhlef, J.L. Jacobsen and H. Saleur, *A staggered six-vertex model with non-compact continuum limit*, Nucl. Phys. B **789**, 483–524 (2008).
44. R.J. Baxter, *Potts model at the critical temperature*, J. Phys. C **6** L445 (1973).
45. H. Saleur, *The antiferromagnetic Potts model in two dimensions: Berker-Kadanoff phase, antiferromagnetic transition, and the role of Beraha numbers*, Nucl. Phys. B **360**, 219 (1991).
46. P.-G. de Gennes, *Scaling concepts in polymer physics* (Cornell University Press, New York, 1979).
47. B. Duplantier and H. Saleur, *Exact surface and wedge exponents for polymers in two dimensions*, Phys. Rev. Lett. **57**, 3179 (1986).
48. B. Duplantier and H. Saleur, *Winding-angle distributions of two-dimensional self-avoiding walks from conformal invariance*, Phys. Rev. Lett. **60**, 2343 (1988).
49. J.L. Jacobsen, N. Read and H. Saleur, *Dense loops, supersymmetry, and Goldstone phases in two dimensions*, Phys. Rev. Lett. **90**, 090601 (2003).
50. Vl. S. Dotsenko, *Critical behaviour and associated conformal algebra of the Z_3 Potts model*, Nucl. Phys. B **235**, 54 (1984).
51. H. Saleur, *The antiferromagnetic Potts model in two dimensions: Berker-Kadanoff phase, antiferromagnetic transition, and the role of Beraha numbers*, Nucl. Phys. B **360**, 219 (1991).
52. H. Saleur, *Winding-angle distribution for Brownian and self-avoiding walks*, Phys. Rev. E **50**, 1123 (1994).
53. P.J. Flory, *The configuration of real polymer chains*, J. Chem. Phys. **17**, 303 (1949).
54. P.G. de Gennes, *Collapse of a polymer chain in poor solvents*, J. Physique Lett. **36**, 55 (1975).
55. B. Duplantier and H. Saleur, *Stability of the polymer Θ point in two dimensions*, Phys. Rev. Lett. **62**, 1368 (1989).
56. R. Raghavan, C.L. Henley and S.L. Arouh, *New two-color dimer models with critical ground states*, J. Stat. Phys. **86**, 517 (1997).
57. A. Ghosh, D. Dhar and J.L. Jacobsen, *Random trimer tilings*, Phys. Rev. E **75**, 011115 (2007).
58. A. Verberkmoes and B. Nienhuis, *Triangular trimers on the triangular lattice: An exact solution*, Phys. Rev. Lett. **83**, 3986 (1999).
59. J.L. Jacobsen, *On the universality of fully packed loop models*, J. Phys. A **32**, 5445 (1999).
60. H.W.J. Blöte and B. Nienhuis, *Fully packed loop model on the honeycomb lattice*, Phys. Rev. Lett. **72**, 1372 (1994).
61. J. Kondev and C.L. Henley, *Four-coloring model on the square lattice: A critical ground state*, Phys. Rev. B **52**, 6628 (1995).
62. J.L. Jacobsen and J. Kondev, *Conformal field theory of the Flory model of protein melting*, Phys. Rev. E **69**, 066108 (2004); *Continuous melting of compact polymers*, Phys. Rev. Lett. **92**, 210601 (2004).
63. P.J. Flory, *Statistical thermodynamics of semi-flexible chain molecules*, Proc. Roy. Soc. London A **234**, 60 (1956).

64. M.T. Batchelor, J. Suzuki and C.M. Yung, *Exact results for hamilton walks from the solution of the fully packed loop model on the honeycomb lattice*, Phys. Rev. Lett. **73**, 2646 (1994).
65. D. Dei Cont and B. Nienhuis, *The packing of two species of polygons on the square lattice*, J. Phys. A **37**, 3085 (2004); *Critical exponents for the FPL^2 model*, cond-mat/0412018.
66. J.L. Jacobsen and P. Zinn-Justin, *Algebraic Bethe Ansatz for the FPL^2 model*, J. Phys. A **37**, 7213 (2004).
67. N.Y. Reshetikhin, *A new exactly solvable case of an O(n) model on a hexagonal lattice*, J. Phys. A **24**, 2387 (1991).
68. V. Pasquier and H. Saleur, *Common structures between finite systems and conformal field theories through quantum groups*, Nucl. Phys. B **330**, 523 (1990).
69. B. Eynard, E. Guitter and C. Kristjansen, *Hamiltonian cycles on a random three-coordinate lattice*, Nucl. Phys. B **528**, 523 (1998).
70. J.L. Jacobsen and J. Kondev, *Transition from the compact to the dense phase of two-dimensional polymers*, J. Stat. Phys. **96**, 21 (1999).
71. P. Di Francesco, O. Golinelli and E. Guitter, *Meanders: Exact asymptotics*, Nucl. Phys. B **570**, 699 (2000).
72. P. Di Francesco, E. Guitter and J.L. Jacobsen, *Exact meander asymptotics: A numerical check*, Nucl. Phys. B **580**, 757 (2000).
73. M.T. Batchelor and J. Suzuki, *Exact solution and surface critical behaviour of an O(n) model on the honeycomb lattice*, J. Phys. A **26**, L729 (1993).
74. C.M. Yung and M.T. Batchelor, *O(n) model on the honeycomb lattice via reflection matrices: Surface critical behaviour*, Nucl. Phys. B **453**, 552 (1995).
75. M.T. Batchelor and C.M. Yung, *Exact results for the adsorption of a flexible self-avoiding polymer chain in two dimensions*, Phys. Rev. Lett. **74**, 2026 (1995).
76. M.T. Batchelor and J. Cardy, *Extraordinary transition in the two-dimensional O(n) model*, Nucl. Phys. B **506**, 553 (1997).
77. T.W. Burkhardt, E. Eisenriegler and I. Guim, *Conformal theory of energy correlations in the semi-infinite two-dimensional O(N) model*, Nucl. Phys. B **316**, 559 (1989).
78. T.W. Burkhardt and J.L. Cardy, *Surface critical behaviour and local operators with boundary-induced critical profiles*, J. Phys. A **20**, L233 (1987).
79. P. Fendley and H. Saleur, *Exact theory of polymer adsorption in analogy with the Kondo problem*, J. Phys. A **27**, L789 (1994).
80. H. Saleur and M. Bauer, *On some relations between local height probabilities and conformal invariance*, Nucl. Phys. B **320**, 591 (1989).
81. B. Duplantier and H. Saleur, *Exact surface and wedge exponents for polymers in two dimensions*, Phys. Rev. Lett. **57**, 3179 (1986).
82. A.J. Guttmann and G.M. Torrie, *Critical behaviour at an edge for the SAW and Ising model*, J. Phys. A **17**, 3539 (1984).
83. J.L. Jacobsen, *Surface critical behaviour of fully packed loop models*, in preparation (2008).
84. J.L. Jacobsen and H. Saleur, *Conformal boundary loop models*, Nucl. Phys. B **788**, 137–166 (2008).
85. P.P. Martin and H. Saleur, *The blob algebra and the periodic Temperley-Lieb algebra*, Lett. Math. Phys. **30**, 189 (1994).
86. I. Kostov, *Boundary loop models and 2D quantum gravity*, J. Stat. Mech. P08023 (2007).
87. J.L. Jacobsen and H. Saleur, unpublished (2007).
88. J. Dubail, J.L. Jacobsen and H. Saleur, *Generalised special surface transition in the two-dimensional O(n) model*, in preparation (2008).
89. A. Nichols, *The Temperley-Lieb algebra and its generalizations in the Potts and XXZ models*, J. Stat. Mech. P01003 (2006); *Structure of the two-boundary XXZ model with non-diagonal boundary terms*, J. Stat. Mech. L02004 (2006).
90. J. de Gier and A. Nichols, *The two-boundary Temperley-Lieb algebra*, math.RT/0703338.
91. J.L. Jacobsen and H. Saleur, *Combinatorial aspects of conformal boundary loop models*, J. Stat. Mech. P01021 (2008).

92. J. Dubail, J.L. Jacobsen and H. Saleur, *Conformal two-boundary loop model on the annulus*, Nucl. Phys. B **813**, 430 (2009); *Boundary extensions of the Temperley-Lieb algebra: representations, lattice models and BCFT*, in preparation (2008).
93. N. Read and H. Saleur, *Exact spectra of conformal supersymmetric nonlinear sigma models in two dimensions*, Nucl. Phys. B **613**, 409 (2001).
94. J.-F. Richard and J.L. Jacobsen, *Eigenvalue amplitudes of the Potts model on a torus*, Nucl. Phys. B **769**, 256 (2007).
95. J.-F. Richard and J.L. Jacobsen, *Character decomposition of Potts model partition functions, I: Cyclic geometry*, Nucl. Phys. B **750**, 250 (2006).
96. I. Affleck and A.W.W. Ludwig, *Universal noninteger "ground-state degeneracy" in critical quantum systems*, Phys. Rev. Lett. **67**, 161 (1991).
97. J.L. Cardy, *Mean area of self-avoiding loops*, Phys. Rev. Lett. **72**, 1580 (1994).
98. P. Fendley and J.L. Jacobsen, *Critical points in coupled Potts models and critical phases in coupled loop models*, J. Phys. A **41**, 215001 (2008).
99. P. Fendley, *Loop models and their critical points*, J. Phys. A **39**, 15445 (2006).
100. B. Nienhuis, *Critical spin-1 vertex models and O(n) models*, Int. J. Mod. Phys. B **4**, 929 (1990).
101. A.G. Izergin and V.E. Korepin, *The inverse scattering method approach to the quantum Shabat-Mikhailov model*, Comm. Math. Phys. **79**, 303 (1981).